An Aperture Synthesis Technique for Cylindrical Printed Lens / Transmitarray Antennas with Shaped Beams

by

Mahmud Biswas

A thesis submitted to the
Faculty of Graduate and Postdoctoral Studies
in partial fulfillment of the requirements for the degree of

Master of Applied Science
in Electrical & Computer Engineering

Ottawa-Carleton Institute for Electrical and Computer Engineering
School of Electrical Engineering and Computer Science
Faculty of Engineering
University of Ottawa

ABSTRACT

Printed lens antennas offer the possibility of realizing shaped beam patterns using no more complexity than is required for pencil beam patterns. Shaped beam patterns can be obtained by appropriately determining the complex transmission coefficient required for each cell (or element) of the printed lens, taking into account the varying feed field over the input surface of the lens. Certain ranges of transmission coefficient amplitude and phase are undesirable (eg. too low an amplitude implies a large reflection at the lens input surface). It would be preferable to constrain the range of values that the transmission coefficient can take as an integral part of the lens synthesis procedure, and thus the transmission coefficient itself needs to be the synthesis variable. In this thesis a synthesis technique for doing this is developed based on the method of generalized projections, modified to "operate" in the space of transmission coefficients. This makes it possible to immediately perceive what influence constraints on the actual transmission coefficients have on the possible radiation pattern performance. In addition, an approach that allows one to constrain the transmission coefficient to values that must be selected from an available database of transmission coefficients is incorporated into the synthesis technique.

Keywords:

Printed lens, transmitarray, aperture synthesis, shaped beams

ACKNOWLEDGEMENTS

I am very grateful for the guidance and support of my supervisor Dr. Derek McNamara, who kindly agreed to take me on when, mid-stream in my masters degree studies, my technical interests shifted to the antenna field. I am especially grateful for his allowing me to liberally garner material from his notes on array synthesis for the literature review in Chapter 2. I am extremely indebted to him for his personal attention and patience in meticulously sketching out the map of the research studies. Without his unwavering support and encouragement, this thesis wouldn't have come to a successful completion. One simply could not wish for a better or friendlier supervisor.

I would also like to thank the past and present members of the Antenna Research Group at the School of Electrical Engineering & Computer Science of the University of Ottawa. Special thanks go to Dr. Nicolas Gagnon of the Communication Research Centre Canada for permitting me to use his phase-shifting surface database in describing the "opportunistic" synthesis method.

A special appreciation goes to my colleague Mr. Mohan Bhardwaj at the Department of National Defence for his constant moral support and encouragement throughout this research work.

.

Last but not least, I would like to pay high regards to my parents and my sister for their sincere encouragement and inspiration throughout my research work and lifting me uphill during this phase of life. I owe everything to them.

TABLE OF CONTENTS

CHAPTER 3
Modified Method of Projections for Transmission Coefficient Synthesis of Cylindrical Printed Lens Antennas

List of Figures

CHAPTER 1
Introduction

1.1 SHAPED BEAM ANTENNAS

The need for antennas with shaped beam, as opposed to pencil beam, patterns arises in many applications, including satellite communications, terrestrial wireless networks, and radar systems [1,2,3]. In this thesis we confine attention to isoflux beams, cosecant beams, and sectoral beams (also called flat-topped beams). These are qualitatively illustrated in Fig.1.1-1 along with that of the usual pencil beam. Each of these pattern shapes is considered in turn in later sections of the thesis, and further quantitative detail will be given then (including derivations of their ideal pattern shapes), along with further comments on the applications for which such shaped beams are desirable. Full control of the shape of an antenna's radiation pattern can only be achieved if the amplitude and the phase of the antenna's aperture distribution can be independently controlled.

Earth-coverage or isoflux antennas (which are mounted on satellite payloads) are those that have a broad pattern that is shaped in a way that results in equal field strength at all points on the Earth within some defined field of view (FOV) of the satellite [4]. A variety of antenna types have been employed in efforts to obtain antennas with isoflux radiation patterns for both geostationary earth orbit (GEO) and low earth orbit (LEO) satellites. Horn antennas with rings at the aperture are described in [5-10]. As the satellite orbital height decreases it is increasingly difficult to obtain the desired wide beam width using such horn antennas; it is also difficult to excite an increasing number of outer rings. For example, the Globalstar satellites which had H = 1400 km and hence an edge of coverage (EOC) angle of 52.4° used horns for telemetry, tracking and command (TT&C) antennas, but achieved only "*near isoflux* type pattern performance" from nadir to 40° off of nadir" [9]. Other authors who have used ringed horns also considered cases for which the EOC was between 40° and 45° [6,7,8]. EOC angles larger than this require alternative antenna configurations. One antenna geometry that can achieve EOC angles as large as 65° consists of a shaped reflector with a rear-radiating feed [11]. They have excellent performance out to wide EOC angles, but near boresight they depart from the ideal isoflux pattern. A third configuration that has been used in an attempt to satisfy wide EOC requirements

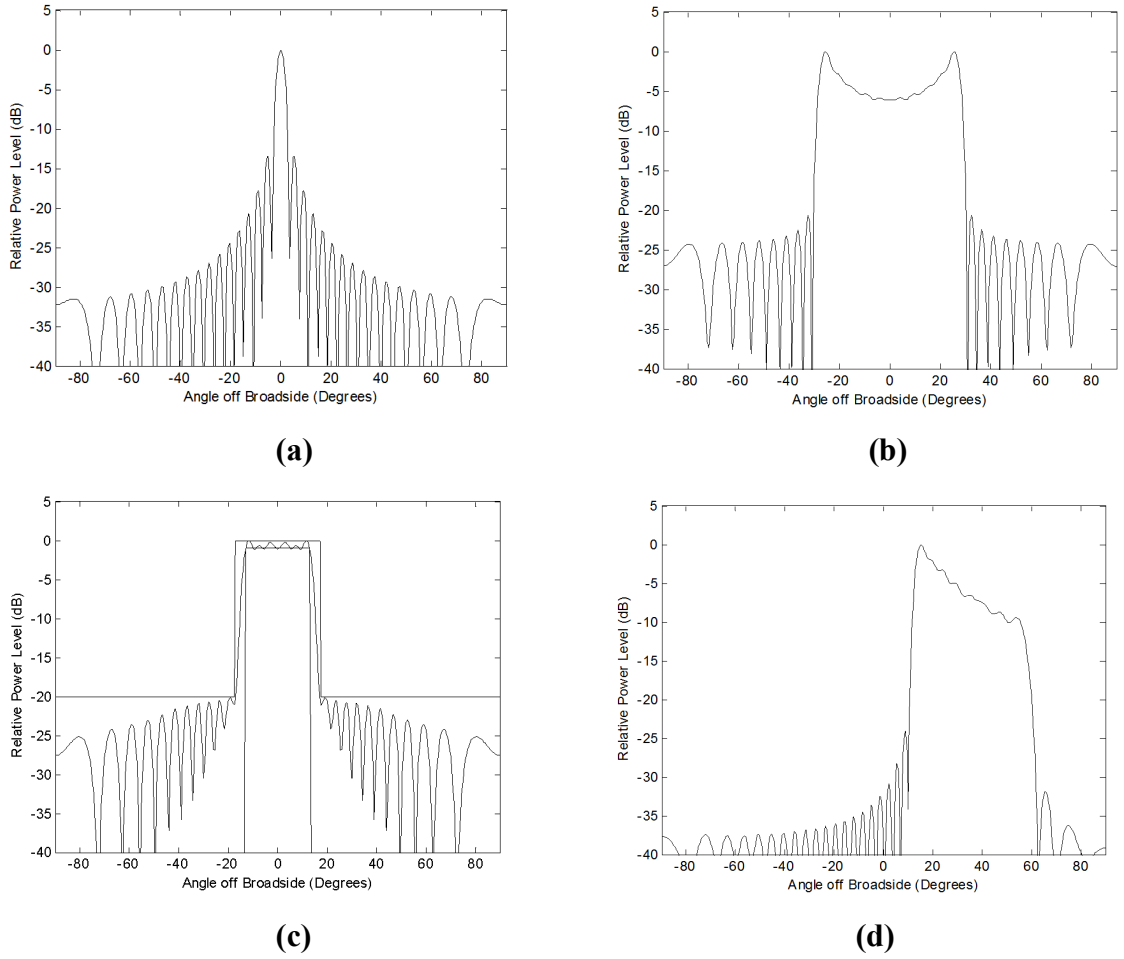

Fig.1.1-1 : Shaped beam radiation patterns compared to conventional pencil beam case.

(a). Pencil beam pattern

(b). Isoflux antenna pattern

(c). Flat-topped antenna pattern, showing the upper (say S_U) and lower (say S_L) masks

(d). Cosec-squared antenna pattern.

is a slot-fed biconical type antenna, identified by the acronym SOPERA in [12,13,14]. Quadrifilar helix antennas have also been used to approximate isoflux antenna beam shapes [15].

Cosecant beam antennas have been required for air surveillance radars [16,17] when there is a desire for the return signal level to be independent of the distance of a constant-height target over a range of radar-to-target distances. They have similarly been suggested for wireless basestation antennas [18] when the signal level at the mobile user is to be almost independent of the basestation-to-mobile distance within the cell sector being covered by the basestation. In radar applications, cosecant beam antennas have usually been realised using reflector antennas. The reflector antennas either have a single feed and their surfaces shaped (that is, no longer entirely

parabolic) to obtain the cosecant beam [19,20], or are parabolic but have several feeds (eg. twelve horns in the case of the German ASR-910 air surveillance radar) that allow the beam to be shaped in the vertical plane [21]. In wireless networks, arrays [22] are more common. Note that the usual situation for radar applications is that cosecant beams are wanted in the vertical plane and the usual pencil beam pattern in azimuth. In wireless networks, the cosecant pattern is also needed in the vertical plane but sectoral beams (discussed in the next paragraph) are normally required in the horizontal plane.

Flat-topped (or sectoral) beam patterns have been used in satellite communications systems and microcell wireless networks. This capability has been achieved using shaped and/or multi-feed reflectors [23] and conventional dielectric lenses [24,25,26], or arrays [27] with intricate beamforming networks.

1.2 PRINTED LENS / TRANSMITARRAY ANTENNAS

Whereas the various realizations of shaped beam antennas may have good resulting radiation pattern performance, they are all somewhat complex. In publications [28-30] printed free-standing phase shifting surfaces (PSSs) were devised, and their effectiveness in realizing transmitarray antennas with pencil beam radiation patterns, applications in which only phase correction over the aperture is required for very acceptable performance, was demonstrated. Such devices are in essence all-pass networks, because they are intended to maximize the transmission amplitude at all points over the aperture but implement phase control there. In order to allow for beam shaping, the PSS concept was extended [31] to include independent control of both the amplitude and phase, and referred to as a phase and amplitude shifting surface (PASS). It was applied to the realization of a transmitarray with a flat-topped beam. A significant advantage of this proposed method is that the beam shaping can be achieved easily with a simple technique that results in a relatively low-cost[1], light, thin and flat surface suitable for mass production. It is in principle no more difficult to design for shaped beams than pencil beams, and the resulting structure need be no more complicated either. However, while [31] demonstrated the proof of concept, the measured radiation patterns of the fabricated PASS transmitarray antenna showed lower directivity levels, much higher sidelobe levels, and a larger in-beam ripple, than was expected. The reasons were identified in [31] but, before we can discuss these, and how this

[1] Compared to the other shaped beam antenna configurations mentioned in Section 1.1.

thesis aims to contribute to an improved aperture distribution synthesis process that might circumvent some of these issues, the technical basics of the PSS printed lens / transmitarray antenna need to first be described.

The essence of the printed lens antenna is shown in Fig.1.1-2. The printed lens consists of layers of conducting shapes etched on multiple dielectric sheets. In other words, the resulting lens is made up of layers of conducting shapes separated by dielectric spacers, as illustrated in Fig.1.1-3. The conductor layers are divided into a lattice of cells, with a conducting shape in each cell. The cell size is kept to less than $\lambda/2$, and the thickness of the individual dielectric spacers is purposefully kept electrically small (on the order of $\lambda/20$) in order that it is possible to obtain good transmission phase control without significantly lowering the transmission amplitude. We may refer to the first and last layers of the lens as the input and the output surfaces, respectively. This assumes we will always consider the lens antenna as if it were being used as a transmitting antenna; reciprocity ensures that there is no loss of generality in doing so. A feed horn (or any other appropriate radiator) illuminates the input surface of the lens. There is thus an incident field distribution over the input surface that is not uniform in either amplitude or phase. The purpose of the lens structure is to correct this so that the field distribution over the output surface of the lens is what we need to provide a particular radiation pattern. The conducting shapes thus vary from cell to cell in order to provide a different transmission coefficient amplitude and phase at each cell to ensure the necessary transformation of the incident field at each cell. The feed plus the lens forms the printed lens / transmitarray antenna.

The output surface (that is, aperture) of a lens antenna is shown in Fig.1.1-4. This is for illustration purposes only. In practice the lens aperture would be divided into many more cells. The lens can clearly be thought of as a planar array of cells, each of size $d_x \times d_y$. The centre of the m-th cell is (x_m, y_m). Each cell acts as a radiating element in the array[2]. This is useful since it allows one to use array synthesis as a step in the lens antenna design process. If we desire that the lens antenna has a radiation pattern of some specified shape we can use array excitation synthesis to determine what the amplitude and phase must be at each cell, and then determine (using a pre-determined database) the dimensions of the conducting shapes in each cell needed to achieve this for a known feed incident field.

[2] More will be said about this in Section 2.3.

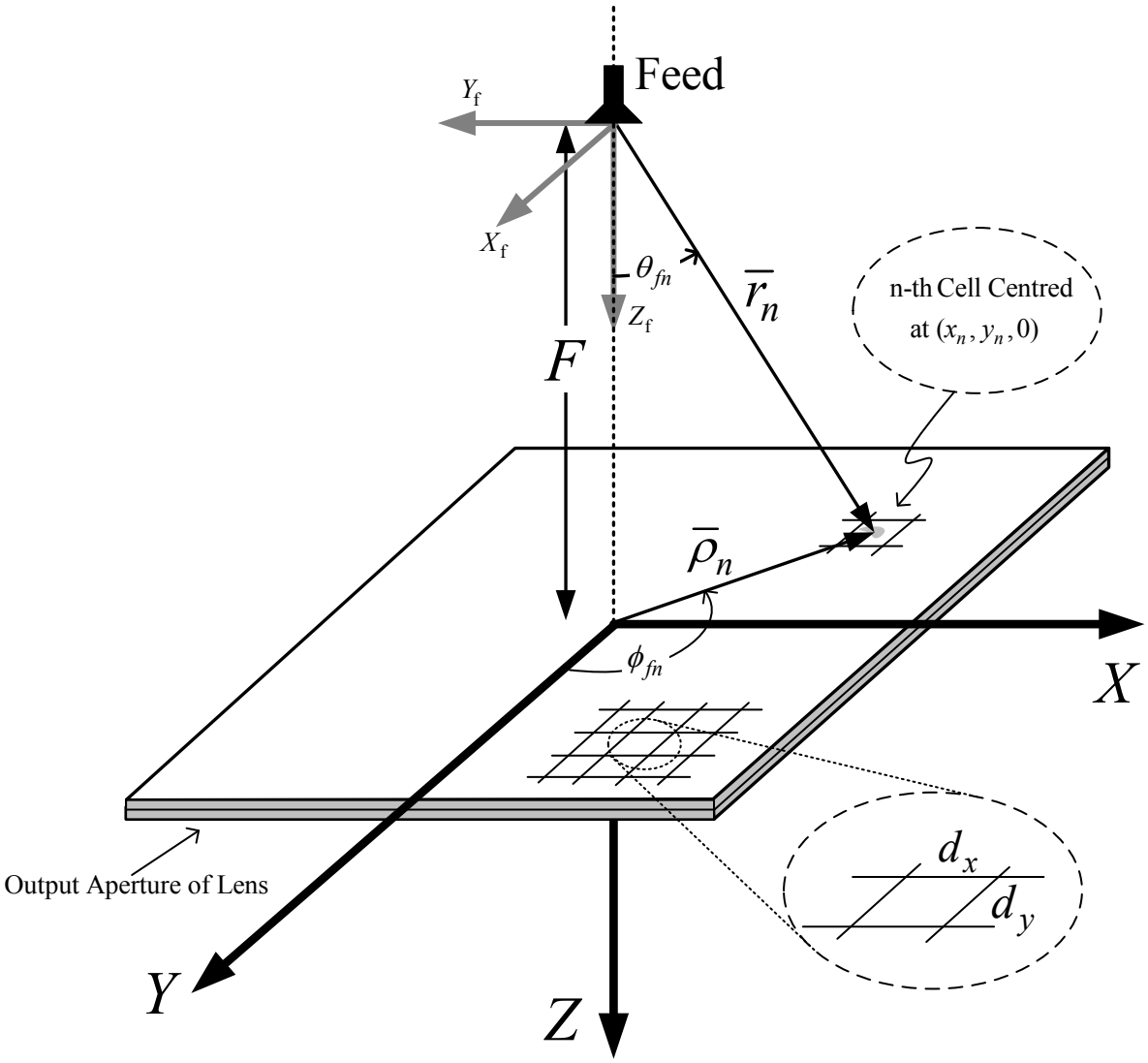

Fig.1.1-2 : Illustration of printed transmitarray antenna configuration.

(Courtesy of D.A.McNamara)

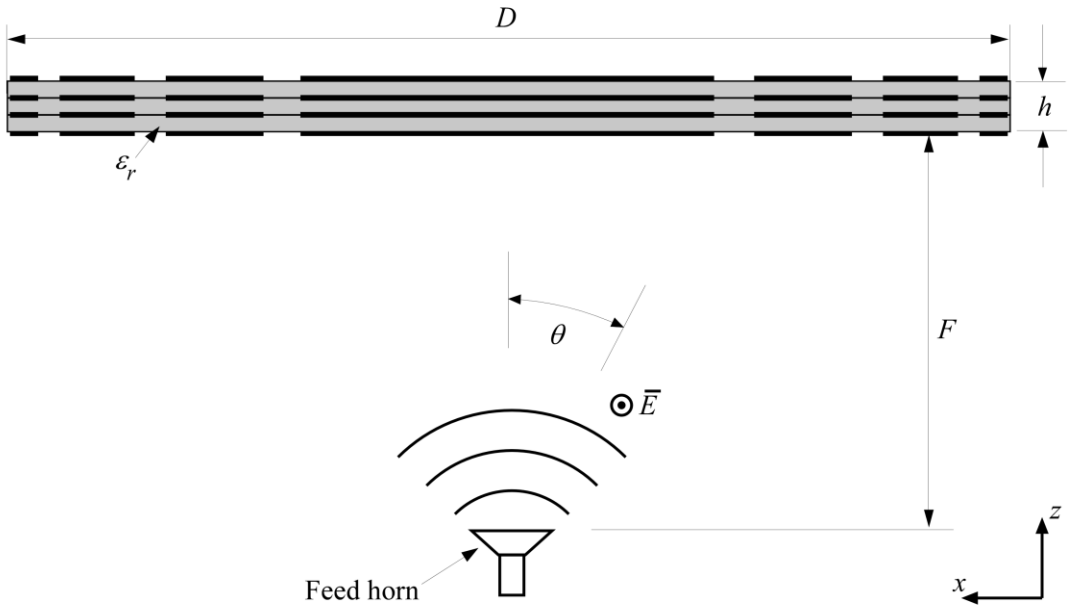

Fig.1.1-3 : Side view of the horn-fed transmittarray antenna, for the case of a four-conducting-layer printed surface (After [30])

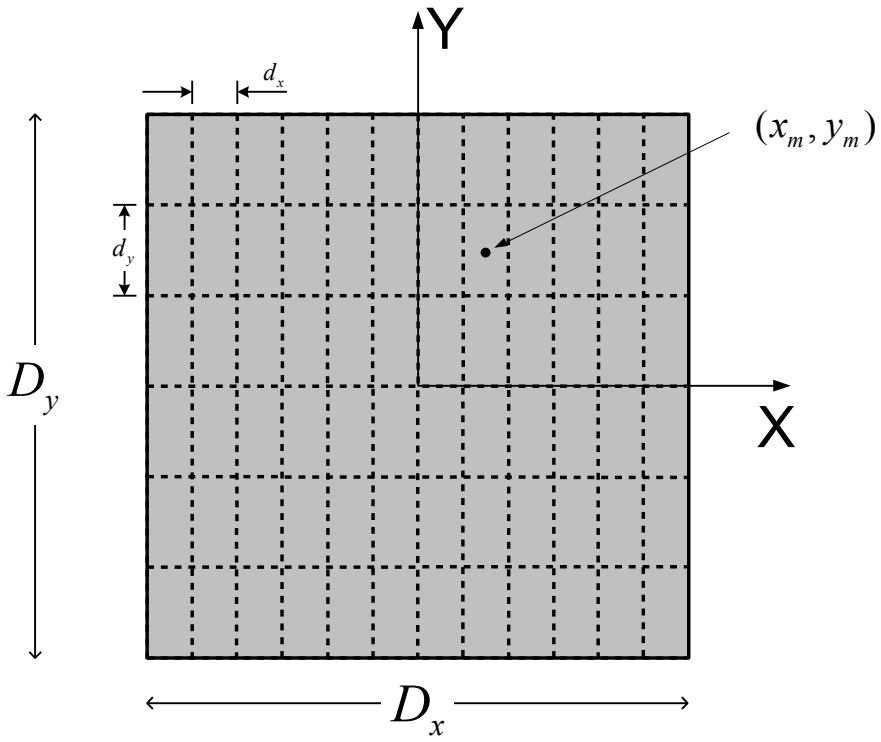

Fig.1.1-4 : Quantized output aperture of the transmitarray antenna.

We are now able to continue the discussion of the reasons, identified in [31], for the measured radiation pattern performance of the flat-topped beam lens in the latter reference not as being quite what was expected. When the database used in the design of the PASS transmitarray structure was set up the conducting element was considered to be resident in an infinite periodic array of identically-sized elements, and the amplitude and phase of the structure's plane wave transmission coefficient computed. This was repeated for different element dimensions and the database of transmission coefficients versus these dimensions is tabulated. The correct element size was then selected for each cell in the PASS structure to obtain the desired amplitude and phase at each point over the output aperture of the structure. In the final PASS lens the elements in adjacent cells are of course not identical; if this were not so it would defeat the whole purpose of their being used to control the aperture distribution. Thus the actual environment of each element is not precisely the same as that experienced by the element in the infinite periodic environment (of identical elements) used in establishing the above-mentioned database. In most cells, the database transmission coefficient values are sufficiently accurate since there are only small changes in the conductor shape on adjacent cells, ensured by selecting a sufficiently small cell size. The exception occurs in the vicinity of aperture phase transition boundaries, where there are large "discontinuities" in the shape of adjacent elements. The pattern degradation due to such discontinuities has been noted in [31] in the context of reflectarray antennas (which is concerned with reflection rather than transmission coefficients), and is suspected [31] to be the *first reason* for the pattern degradation observed in the case of the flat-topped PASS lens antenna as well. A *second reason* for the less-than-favourable radiation patterns of the flat-topped PASS antenna is the fact that, in setting up the database for [31], it was always assumed that the incident plane wave had normal incidence. Thus the differing incidence angles of the feed fields at different points on the input side of the actual printed lens were not taken into account. Although not specifically mentioned in [31] a *third reason* that, like the second, is inherent to the PASS structure, might be the fact that the structure requires the amplitude of the reflection coefficient to become large whenever the excitation amplitude (controlled using the transmission coefficient amplitude) at some cells on the output surface of the aperture is to be reduced. This implies backscattering from the particular cell(s) back to the feed, which is analogous to

spillover loss in reflector and reflectarray antennas, and so will lead to decreased gain[3]. This is less severe with PSS structures (which are used for pencil beams), in which maximum transmission amplitude is always desired and only the transmission phase is varied. Finally, a *fourth reason* might also be the fact that the database has a finite number of complex transmission coefficient (T_n) values to choose from. In [31] a synthesis process was used to find the continuous aperture distribution needed to give the flat-topped beam. This continuous distribution was then sampled to find the required T_n for each cell. These values are not all available in the database, and the "nearest" database value[4] is used instead.

1.3 THE CONSTRAINED ARRAY ELEMENT EXCITATION SYNTHESIS PROBLEM

The array antenna excitation synthesis problem consists of finding the complex excitations (that is, the excitation amplitudes and phases) of the elements of a given array to achieve a specific radiation pattern performance. A more detailed review of excitation synthesis methods is provided in Chapter 2. Suffice it to state here that whereas the problem of excitation synthesis has been a subject of study since the 1940s, classical methods based on the use of polynomials do not allow the imposition of restrictions on the values that the excitation amplitudes and phases of the elements may take, or the synthesis of excitation sets that provide radiation patterns of some desired arbitrary shape. These classical methods also adjust only the amplitudes of the excitations, the phases being assumed to be the same for all elements, and the excitation amplitudes[5] may take on any value in the range zero to unity. In other words there are no constraints on the excitation amplitudes. The more serious limitation as regards the goals of this thesis is the fact that such classical methods are generally used for pencil beams and difference beams. Nevertheless, such methods now serve as benchmarks against which to measure computationally based techniques.

More general numerical approaches, on the other hand, allow one to set more complex pattern shape specifications and permit one to place constraints on the excitations. These numerical

[3] It can also degrade the input reflection coefficient of the feed.
[4] More will be said about this in Chapter 3.
[5] We will always work with the normalized excitation amplitudes, for which the largest value is always 1.0, and the smallest value may be anything in the range 0.0 to 1.0.

optimisation based methods[6] (which exploit genetic algorithms, particle swarm optimisation, simulated annealing, gradient methods, or some other numerical optimisation algorithm) require users to select an objective function whose minimisation they believe will lead to the best solution of the problem they have in mind. Both pattern and excitation constraints have to be incorporated into a single objective function whose variables are the complex excitations of the array. The objective function must favour radiation patterns close to the desired ideal one, and penalize excitations that fall outside the allowed complex values. Good results can only be achieved with the proper experience. The process of selecting this objective function is thus unavoidably somewhat "subjective", and different solutions are obtained if the objective functions are altered. The reason is of course that, while a simulated annealing algorithm (for instance) might provide a global optimum of the objective function used, the said objective function may not fully represent the array synthesis goals and constraints. Thus a global optimum of the synthesis problem may not be reached even though a global optimum of the specified objective function may be reached. This aspect of numerical optimisation based excitation synthesis methods can be removed for certain classes of array excitation synthesis that can be formulated as so-called convex programming problems[7], which are more general than those that can be approached by classical methods, but not sufficiently general for the type of synthesis we wish to perform in this thesis.

An alternative numerical approach is that of the method of generalised projections[8]. This obviates the need to define such overall objective functions. The array synthesis problem is instead viewed as determining the intersection of two sets. The first is the set of all radiation patterns possible with the given array geometry when the excitations comply with the required excitation constraints. The second is the set of all radiation patterns possible with the given array that comply with the required radiation pattern constraints. The method can be described as synthesis in "radiation pattern space". The same projection method can also be used in the "excitation space". The synthesis problem in the latter case is one of finding the intersection of the set of all excitations that satisfy the specified excitation constraints, and the set of all excitations that produce radiation patterns that satisfy the specified pattern constraints. Array synthesis procedures that use some form of the method of projections are particularly attractive

[6] Discussed in Section 2.5.
[7] Mentioned in Section 2.6.
[8] Reviewed in Section 2.7.

because of the quite natural way that a wide variety of desirable constraints (eg. excitation constraints) can be implemented with a reliability not possible using other approaches. We will use the method of projections in the work of this thesis.

1.4 OVERVIEW OF THE THESIS

The goal of this thesis is the development of synthesis methods that could be used in the design of printed lenses to achieve shaped patterns, but subject to various constraints on the transmission coefficients of the lens elements. The hope is that by using aperture control it might be possible to overcome the problem issues identified in Section 1.1 and yet achieve reasonably good shaped beam pattern performance.

Chapter 2 provides a review of array pattern synthesis methods, with an emphasis on those methods relevant to the aims of this thesis. The method of projections is identified there as being that most applicable for present purposes. A tutorial-like elucidation of the method of projections in an applications-oriented format is provided. We give a systematic description of three classes of shaped beam, namely flat-topped beams, isoflux beams and cosecant beams, which are used in practice. Quantative means of specifying the shaped beams are given. We define what we mean by radiation pattern masks.

In Chapter 3 we develop both serial and parallel projection methods (for the synthesis of shaped beams) that operate in lens element transmission coefficient space[9]. Thus the transmission coefficients of the printed lens elements (or cells) are directly the variables in the synthesis process. This makes it possible to immediately perceive what influence constraints on the actual transmission coefficients have on the possible radiation pattern performance. In addition, we develop an approach that allows us to constrain the transmission coefficient to values that must be selected from a set of available transmission coefficients. We believe this approach, as straightforward as it appears with hindsight, offers a multitude of possibilities for printed lens antennas / transmitarrays. Transmission coefficient constraints of any kind can easily be imposed. In the last part of Chapter 3 we describe a useful approach for conveniently determining the starting points for a shaped beam synthesis via the projection method. Good starting values are crucial for the success of any numerically-based synthesis method.

[9] This terminology is made clear in Section 2.7.

Chapter 4 presents a demonstration of what is physically possible as regards the performance of a cylindrical lens antenna for three different types of widely-used shaped beams (sector beam, cosecant beam, and isoflux beam), when either the transmission coefficient amplitudes, or transmission phases, or both, are restricted in some way. It appears that this is the first time that shaped beam synthesis subject to the variety of transmission coefficient constraints has been reported, and certainly so for the phase-only synthesis of such shaped beams or synthesis that restricts the transmission coefficients to be members of a specified database (as an *integral part* of the synthesis procedure).

1.5 REFERENCES FOR CHAPTER 1

[1] C. A. Balanis (Edit.), *Modern Antenna Handbook* (Wiley, 2008).

[2] J. Volakis (Edit.), *Modern Antenna Handbook* (McGraw-Hill, 2007)

[3] G. Thiele and W. Stutzman, *Antenna Theory & Design* (Wiley, 1998) Chap.8

[4] L. J. Ricardi, "Satellite Antennas", Chapter 36 in : R.C. Johnson, *Antenna Engineering Handbook* (McGraw-Hill, 1993) 3rd Edition.

[5] D. G. Bateman, S. G. Hay, T. S. Bird & F. R. Cooray, "Simple Ka-band Earth-coverage antennas for LEO satellites", Proc. Australian Symposium on Antennas, Feb. 1999.

[6] S. G. Hay, D. G. Bateman, T. S. Bird and F. R. Cooray, "Simple Ka-band earth-coverage antennas for LEO satellites," in *IEEE Antennas and Propagation Soc. Symp.,* vol.1, pp. 708-711,1999.

[7] P. Brachat, "Sectoral patern synthesis with primary feeds", *IEEE Trans. Antennas Propagat.*, vol.42, no. 4, pp. 484-491, April 1994.

[8] P. Metzen, "Satellite communications antennas for Globalstar", Proc. Int. Antennas Symp. (JINA), Nice, France, pp.574-583, Nov.1996.

[9] F .J. Dietrich, P. Metzen & P. Monte, "The Globalstar cellular satellite system", *IEEE Trans. Antennas Propagat.*, vol.46, no. 6, pp. 935-942, June 1998.

[10] L. T. Hildebrand, D. A. McNamara & G. Arbery, "Low-cost physically-small TT&C antennas for LEO satellite applications", Proc. 11th CASI Conference on Astronautics (*ASTRO'2000*), Ottawa, Canada, 7-9 November 2000.

[11] A. Kumar, "Highly shaped beam telemetry antenna for the ERS-1 satellite", IEE Proc., Vol.134, Pt.H, No.1, pp.106-108, Feb.1987.

[12] J. E. Fernández Del Rio, A. Nubla, L. Bustamante & K. van't Klooster, "SOPERA: A new antenna concept for low earth orbit satellites," in *IEEE Antennas and Propagation Soc. Symp. Digest,* Vol. 1, pp. 688-691, June 1999.

[13] J. E. Fernández Del Rio, A. Nubla, L. Bustamante, F. Vila, K. van't Klooster and A.Frandsen, "Novel isoflux antenna alternative for LEO satellites downlink", Proc. 29th European Microwave Conference, pp.154-157, Munich, Germany, 1999.

[14] *RYMSA*, Ctra. Campo Real, Km 2, 100– 28500 Arganda del Rey, Madrid, Spain (www.rymsa.com).

[15] G. van Dooren & R.Cahill, "Design, analysis and optimisation of quadrifilar helix antennas on the European Metop spacecraft", *Proc. Int. Conf. Antennas & Propagation*, pp.1.536-1.542, Edinburgh, United Kingdom, 1997.

[16] M. I. Skolnik, *Introduction to Radar Systems* (McGraw-Hill, 1962).

[17] S. Drabowitch, A. Papiernik, H. D. Griffiths, J. Encinas & B. L. Smith, *Modern Antennas* (Springer, 2005) 2nd Edition.

[18] E. Holzman, "Pillbox antenna design for millimeterwave base-station applications", IEEE Antennas & Propagation Magazine, Vol.45, No.1, pp.27-37, Feb.2003.

[19] M. I. Skolnik (Edit.), *Radar Handbook* (McGraw-Hill, 1990) 2nd Edition.

[20] M. M. S. Taheri, A. R. Mallahzadeh & A. Foudazi, "Shaped beam synthesis for shaped reflector antenna using PSO algorithm", Proc. 6th European Conf. Antennas Propagat. (EuCAP), Prague, Czech Republic, March 2012.

[21] L. I. Vaskelainen & K. J. Markus, "Array-fed parabolic-cylindrical reflector antenna for multifunction surveillance radar", IEE Radar Conf., (Radar 97), pp.379-382, Oct. 1997.

[22] K. Y. Hui and K. M. Luk, "Design of wideband base station antenna arrays for CDMA 800 and GSM 900 systems", Microwave Optical Tech. Letters, Vol.39, No.5, pp.406-409, 2003.

[23] S. K. Rao and M. Q. Tang, "Stepped-reflector for dual-band multiple beam satellite communications payloads", IEEE Trans. Antennas Propagation, 54 (2006), 801-811.

[24] R. Sauleau and B. Bares, "A complete procedure for the design and optimization of arbitrarily-shaped integrated lens antennas", IEEE Trans. Antennas Propagation, 54 (2006), 1122-1133.

[25] N. T. Nguyen, R. Sauleau, L. Le Coq, "Lens antennas with flat-top radiation patterns: Benchmark of beam shaping techniques at the feed array level and lens shape level", Proc. 3rd European Conf. Antennas Propagat. (EuCAP), pp. 2834 – 2837, March 2009.

[26] C. A. Fernandes, "Shaped dielectric lenses for wireless millimeter-wave communications", IEEE Antennas Propagation Mag., 41 (1999), 141-150.

[27] S. H. Duffy, D. D. Santiago and J. S. Herd, "Design of overlapped subarrays using an RFIC beamformer", IEEE Int. Antennas Propagation Symp. Digest, USA, (2007) 1949-1952.

[28] N. Gagnon, A. Petosa & D. A. McNamara, "Comparison between Conventional Lenses and an Electrically Thin Lens Made Using a Phase Shifting Surface (PSS) at Ka Band", in *Loughborough Antennas & Propagation Conference (LAPC 2009)*, Loughborough, UK, pp. 117-120, November 2009.

[29] N. Gagnon, A. Petosa & D. A. McNamara, "Thin Microwave Phase-Shifting Surface (PSS) Lens Antenna Made of Square Elements", *Electronics Letters*, vol. 46, no. 5, pp. 327-329, March 2010.

[30] N. Gagnon, A. Petosa & D. A. McNamara, "Thin Microwave Quasi-Transparent Phase-Shifting Surface (PSS)", *IEEE Transactions on Antennas and Propagation*, vol. 58, no. 4, pp. 1193-1201, April 2010.

[31] N. Gagnon, A. Petosa & D. A. McNamara, "Electrically Thin Free-Standing Phase and Amplitude Shifting Surface for Beam Shaping Applications", *Microwave & Optical Technology Letters*, Vol.54, No.7, pp.1566-1571, July 2012.

[32] M. A. Milon, R. Gillard and H. Legay, "Rigorous analysis of the reflectarray radiating elements : Characterisation of the specular reflection effect and the mutual coupling effect", *29th ESA Antenna Workshop*, Netherlands, 2007.

CHAPTER 2

Review of Array Antenna Excitation Synthesis Techniques

2.1 INTRODUCTION

Searches of the technical literature on array excitation synthesis reveal an enormous number of papers on the topic, starting in the 1940's and continuing unabated up to the present time. A few of the early papers on polynomial-based synthesis methods continue to be of importance as benchmarks against which to rate numerical synthesis techniques used to obtain pencil beams. However, numerical techniques are able to synthesize radiation patterns of a more general nature. Such methods also allow one to build in excitation constraints, something that the polynomial-based approaches are not able to do. Many numerical synthesis methods have been developed, and a review of all work on the subject would be a tome in itself. Fortunately certain of these techniques have proved to be superior, or have been subsumed into more general versions of some method. In order to make this review both manageable and relevant to the present thesis, we make the following assumptions:

♦ We are interested **in linear and planar arrays**[10] only, with potentially unequal inter-element spacings along the x- and y-axes over the aperture in the planar array cases. Thus conformal arrays are not considered at all in the review.

♦ We are interested in arrays with **rectangular lattices only**. Thus arrays with circular grids are not included in the review.

♦ We are interested in **fully populated arrays**. Thinned arrays are kept out of the purview of the present research work.

♦ We are interested in techniques for the **direct synthesis of arrays of discrete elements**. Thus we will not make reference to methods that synthesize continuous aperture distributions and then sample these in some way in order to apply to the discrete case.

[10] We will in this thesis eventually concentrate on linear arrays only, as mentioned in Section 1.4. However, methods applicable to planar arrays with rectangular lattices are also applicable to linear arrays, and hence form part of this review, but only so far as their use in linear array work is concerned.

Section 2.2 will summarize the analysis used to find the radiation patterns of arrays with specified excitations, and specifically those expressions needed for the work in this thesis. This is needed before any synthesis can be done. Before proceeding to a review of array synthesis methods, we will in Section 2.3 elaborate on the connection between printed lens / transmitarray antennas and array synthesis. Classical synthesis methods are reviewed in Section 2.4. Then Section 2.5 reviews synthesis methods based directly on numerical optimization, but only those that have stood the test of time and have not been superseded. Such methods find widespread use in antenna engineering. Although convex programming is a numerical optimisation procedure, it is set apart from the rest in Section 2.6, for reasons that will be stated there.

Section 2.7 describes the principles behind another class of numerical synthesis techniques, namely the method of generalized projections. This will be the chosen synthesis method for the work of this thesis, for reasons that will become apparent in later sections. Quite a bit of background on it will therefore be given in order to lay the foundations for Chapter 3. Section 2.7.2 describes the various versions of the method in general terms[11]. Although, at least for engineers such as the present author, descriptions of the method in many papers might at first seem unconnected to reality, the subject quickly begins to make sense once concrete forms of the various operators and sets have been defined for a particular application. Since the actual implementation must always be done in terms of matrices, we will write operators and functions in terms of matrices and column-vectors, respectively, right from the start of Section 2.7.3 onwards.

2.2 ARRAY PATTERN ANALYSIS EXPRESSIONS

2.2.1 General Remarks

All analysis will be at a single frequency at a time, and so we will work with phasor quantities. We are interested in the far-zone fields only, and can thus write the electric field of the antenna in the form

$$\bar{E}(r,\theta,\phi) = \frac{e^{jkr}}{r}\bar{E}(\theta,\phi) \qquad (2.2\text{-}1)$$

[11] The method has been used for many types of problem in electrical engineering (eg. image restoration) and not only array synthesis.

where *r* is the distance from the coordinate origin located in the vicinity of the array antenna, (θ,ϕ) is the usual spherical coordinate angle pair, and $k = 2\pi/\lambda = \omega\sqrt{\mu_0\varepsilon_0}$ is the free-space wavenumber. In the previous expression λ is the free space wavelength, $\omega = 2\pi f$ the radial frequency, and *f* the frequency in Hz. As in most antenna work the distance dependent term can be suppressed and we can work with the direction dependent term $\bar{E}(\theta,\phi)$ only. Nevertheless, $\bar{E}(\theta,\phi)$ will still be referred to it as the 'electric field', as is customary in antenna work. It is convenient to define the following quantities:

- A single index *n* will be used to number the elements of the array. The total number of elements in the array is N_e, so that *n = 1,2,.....,* N_e.
- The location of the n-th element in the array is (x_n, y_n, z_n).
- The relative complex excitation of the n-th element is

$$a_n = |a_n| e^{j\phi_n} \tag{2.2-2}$$

- The far-zone radiation pattern of the n-th element in the array, with $a_n = 1$, *when located at the origin of the coordinate system*, is

$$\bar{E}^{(n)}(\theta,\phi) = E_\theta^{(n)}(\theta,\phi)\hat{\theta} + E_\phi^{(n)}(\theta,\phi)\hat{\phi} \tag{2.2-3}$$

It then follows that by superposition the electric field of the entire array is [1]

$$\bar{E}(\theta,\phi) = \sum_{n=1}^{N_e} a_n \bar{E}^{(n)}(\theta,\phi) e^{jkx_n \sin\theta\cos\phi} e^{jky_n \sin\theta\sin\phi} e^{jkz_n\cos\theta} \tag{2.2-4}$$

If, as in most arrays, the elements are identical, then it is almost exactly true[12] that the radiation patterns of the individual elements are also identical (except for a phase factor dependent on its location in the array). We then can write $\bar{E}^{(n)}(\theta,\phi) = \bar{E}^e(\theta,\phi)$ for all *n*, and (2.2-4) becomes

[12] Elements near the edges of the array will in practice have radiation patterns that are slightly different from the rest even though they may be structurally identical. However, if the array is not too small, the effect of this difference between the *in situ* patterns of the elements is small. Then the radiation patterns of all elements can be assumed to be identical, except for the location-dependent phase factor in (2.2-4). This is not true in conformal arrays for which the elements do not all point in the same direction; but as stated earlier conformal arrays are outside the scope of this thesis.

$$\bar{E}(\theta,\phi) = \bar{E}^e(\theta,\phi)\sum_{n=1}^{N_e} a_n e^{jk x_n \sin\theta\cos\phi} e^{jk y_n \sin\theta\sin\phi} e^{jk z_n \cos\theta} = \bar{E}^e(\theta,\phi)\, F(\theta,\phi) \tag{2.2-5}$$

with

$$F(\theta,\phi) = \sum_{n=1}^{N_e} a_n e^{jk x_n \sin\theta\cos\phi} e^{jk y_n \sin\theta\sin\phi} e^{jk z_n \cos\theta} \tag{2.2-6}$$

referred to as the array factor. Identical element patterns will indeed be assumed in this thesis.

2.2.2 Planar Arrays

If the array is planar then z_n is the same for all n. We write this as $z_n = z_{ref}$, and then (2.2-4) becomes

$$\bar{E}(\theta,\phi) = e^{jk z_{ref} \cos\theta}\, \bar{E}^{(e)}(\theta,\phi) \sum_{n=1}^{N_e} a_n\, e^{jk x_n \sin\theta\cos\phi}\, e^{jk y_n \sin\theta\sin\phi} = \bar{E}^{(e)}(\theta,\phi)\, F(\theta,\phi) \tag{2.2-7}$$

and the simplified form (2.2-7) has the array factor

$$F(\theta,\phi) = e^{jk z_{ref} \cos\theta} \sum_{n=1}^{N_e} a_n e^{jk x_n \sin\theta\cos\phi} e^{jk y_n \sin\theta\sin\phi} \tag{2.2-8}$$

with $z_n = z_{ref}$ usually set equal to zero.

2.2.3 Linear Arrays : General Case

In the case of a linear array the expressions for the far-zone fields are the same as those for the general array, except that $y_n = y_{ref}$ and $z_n = z_{ref}$ for all elements, yielding

$$\bar{E}(\theta,\phi) = e^{jk y_{ref} \sin\theta\sin\phi} e^{jk z_{ref} \cos\theta}\, \bar{E}^{(e)}(\theta,\phi) \sum_{n=1}^{N_e} a_n\, e^{jk x_n \sin\theta\cos\phi} = \bar{E}^{(e)}(\theta,\phi)\, F(\theta,\phi) \tag{2.2-9}$$

and

$$F(\theta,\phi) = e^{jk y_{ref} \sin\theta\sin\phi} e^{jk z_{ref} \cos\theta} \sum_{n=1}^{N_e} a_n e^{jk x_n \sin\theta\cos\phi} \tag{2.2-10}$$

Without loss of generality (as far as linear array analysis is concerned) we can set $y_{ref} = z_{ref} = 0$, implying that the elements of the linear array are located on the x-axis. The *array factor* is then

rotationally symmetric about the x-axis[13], as illustrated in Fig.2.2-1. We can therefore simply study its shape in any one plane parallel to the x-axis, which we will choose to be the xz-plane (for which $\phi = 0$). Thus we work with the array factor

$$F(\theta) = \sum_{n=1}^{N_e} a_n e^{jk x_n \sin\theta} \tag{2.2-11}$$

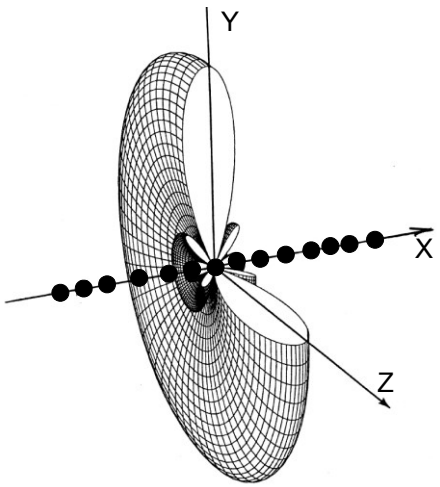

Fig.2.2-1 : Illustration of the rotational symmetry of the array factor $F(\theta,\phi)$ of a linear array (Adapted from [2]).

In the expressions up to this point we may number the array elements as we please. However, for later consistency we will be specific and number them as shown in Fig.2.2-2, and then the array factor expressions are

$$F(\theta) = \begin{cases} \sum_{n=1}^{2N} a_n e^{jk x_n \sin\theta} & 2N \text{ Elements} \\ \sum_{n=1}^{2N+1} a_n e^{jk x_n \sin\theta} & 2N+1 \text{ Elements} \end{cases} \tag{2.2-12}$$

If the elements are uniformly spaced (which will always be the case in this thesis), with inter-element spacing *d*, then the x-axis location of the n-th element is

[13] Although in practice the final array pattern will not be so, due to the pattern multiplication effect of the element pattern.

$$x_n = \begin{cases} \left(n - N - \frac{1}{2}\right)d & n = 1, 2, ..., 2N \quad 2N \text{ Elements} \\ (n - N - 1)d & n = 1, 2, ..., 2N+1 \quad 2N+1 \text{ Elements} \end{cases} \tag{2.2-13}$$

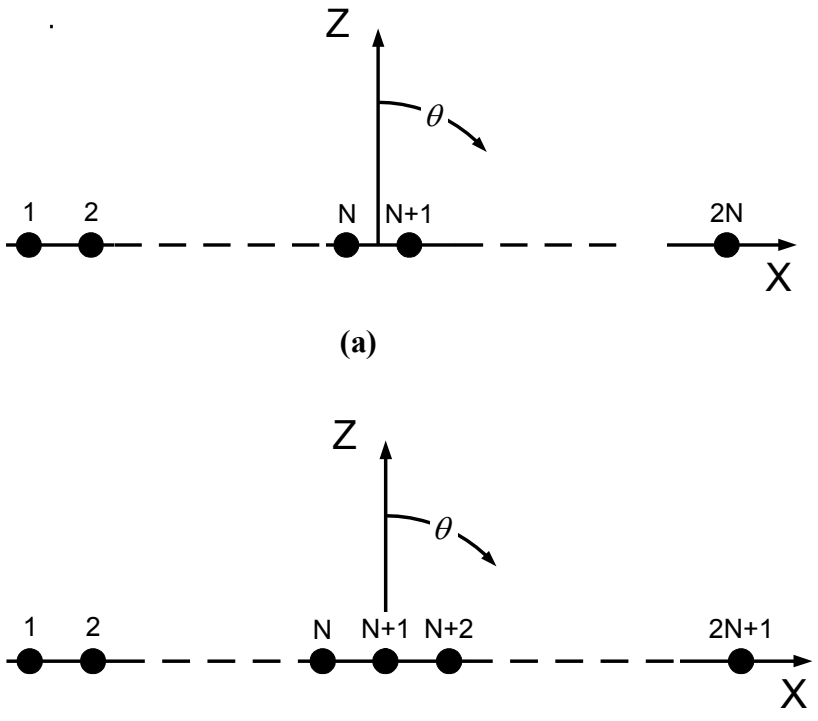

Fig.2.2-2 : Element numbering schemes for arrays with an even and odd number of elements.

2.2.4 Linear Arrays : Symmetrical Case

If the array of 2N elements is symmetrical (in terms of the excitations and locations of corresponding elements on the left and right hand sides of the array) then we need only explicitly consider the elements on one of the sides (which we take to be the right hand side). Then expression (2.2-12) becomes

$$F(\theta) = 2\sum_{n=1}^{N} a_n \cos(k\, x_n \sin\theta) \tag{2.2-14}$$

with the element numbering now as shown in Fig.2.2-3(a). A similar thing can be done for an array of 2N+1 elements that has symmetry. In this case

$$F(\theta) = \left\{ a_0 + 2\sum_{n=1}^{N} a_n \cos(k\, x_n \sin\theta) \right\} \qquad (2.2\text{-}15)$$

with the element numbering now as shown in Fig.2.2-3(b). The element locations in the two symmetrical cases are

$$x_n = \begin{cases} \left(n - \dfrac{1}{2}\right)d & n = 1, 2, ..., 2N \quad 2N \text{ Elements} \\ nd & n = 0, 1, 2, ..., 2N+1 \quad 2N+1 \text{ Elements} \end{cases} \qquad (2.2\text{-}16)$$

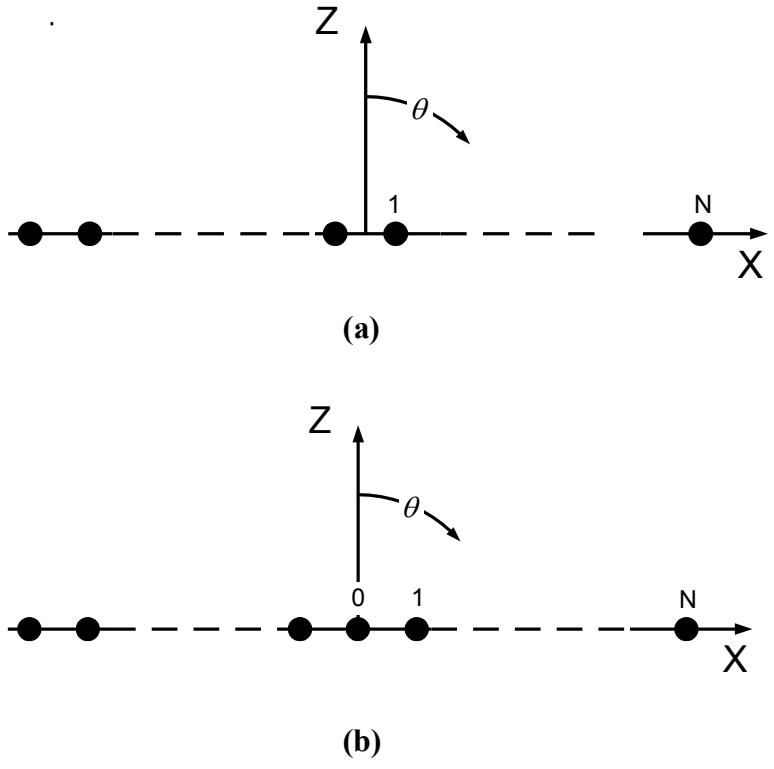

Fig.2.2-3 : Element numbering schemes for symmetrical arrays.

2.2.5 Remarks on Co- and Cross-Polarized Fields

The pattern (2.2-3) is often written in the alternative form

$$\bar{E}(\theta,\phi) = E_{co}(\theta,\phi)\hat{e}_{co} + E_{cr}(\theta,\phi)\hat{e}_{cr} \tag{2.2-17}$$

The unit vectors indicate the orientation of the co-polarised (CO) and cross-polarised (CR) fields. In the case of a general array we would have

$$\bar{E}(\theta,\phi) = \bar{E}^{e}(\theta,\phi)\,F(\theta,\phi) \tag{2.2-18}$$

where

$$E_{co}(\theta,\phi) = E^{e}_{co}(\theta,\phi)\,F(\theta,\phi) \tag{2.2-19}$$

$$E_{cr}(\theta,\phi) = E^{e}_{cr}(\theta,\phi)\,F(\theta,\phi) \tag{2.2-20}$$

and $F(\theta,\phi)$ is given by expression (2.2-6). The element pattern is

$$\bar{E}^{e}(\theta,\phi) = E^{e}_{co}(\theta,\phi)\hat{e}_{co} + E^{e}_{cr}(\theta,\phi)\hat{e}_{cr} \tag{2.2-21}$$

In this thesis we will directly synthesise only the co-polarized fields, and so expression (2.2-19) will be the one of interest.

2.3 PRINTED LENS / TRANSMITARRAY ANTENNA DESIGN AS AN ARRAY EXCITATION SYNTHESIS PROBLEM

2.3.1 Preliminary Remarks

We intimated in Section 1.1 that the determination of the printed lens can be considered to be a space-fed array. A more complete discussion will be given here.

2.3.2 Cylindrical Lens Antennas and Their Two-Dimensional (2D) Idealizations

The intent of this thesis is to explore means of synthesizing excitation distributions that might provide shaped beams for printed-lens/transmitarray antennas by relying principally on the excitation phases[14]. In order to achieve this we need to develop a synthesis approach that is able to incorporate a flexibly wide range of excitation constraints. The idea is that such excitation constraints can be used to ensure that the resulting printed-lens/transmitarray structure (namely distribution of elements) is such that some of the difficulties outlined in Section 1.2 are lessened. The flexibility referred to is necessary because we do not actually want to do a phase-only synthesis, since the inherent amplitude taper of the incident field from the feed and any inevitable slight transmission amplitude variations that might be dictated by the particular elements used to realize the lens, must be taken into account. We would also like the change in the excitation from one element to another to be sufficiently small so that adjacent element geometries are similar.

Fig.2.3-1 shows a sketch of a cylindrical lens antenna that uses three-layer strip elements, for example. We assume that the lens is illuminated by some type of line feed[15], with a y-directed electric field incident on the input surface of the lens. The properties of the elements are varied along the x-axis so that a shaped beam pattern is obtained in the xz-plane (H-plane). The pattern in the yz-plane (E-Plane) would be that of a conventional pencil beam and is largely dictated by the pattern of the feed in that plane. This allows us to model the cylindrical lens antenna excitation synthesis problem as a linear array synthesis one.

[14] The benefits of having "phase-only" distributions to realise have already been mentioned in Section 1.3.
[15] Analogous to what is used to feed cylindrical parabolic reflector, for example [3,4].

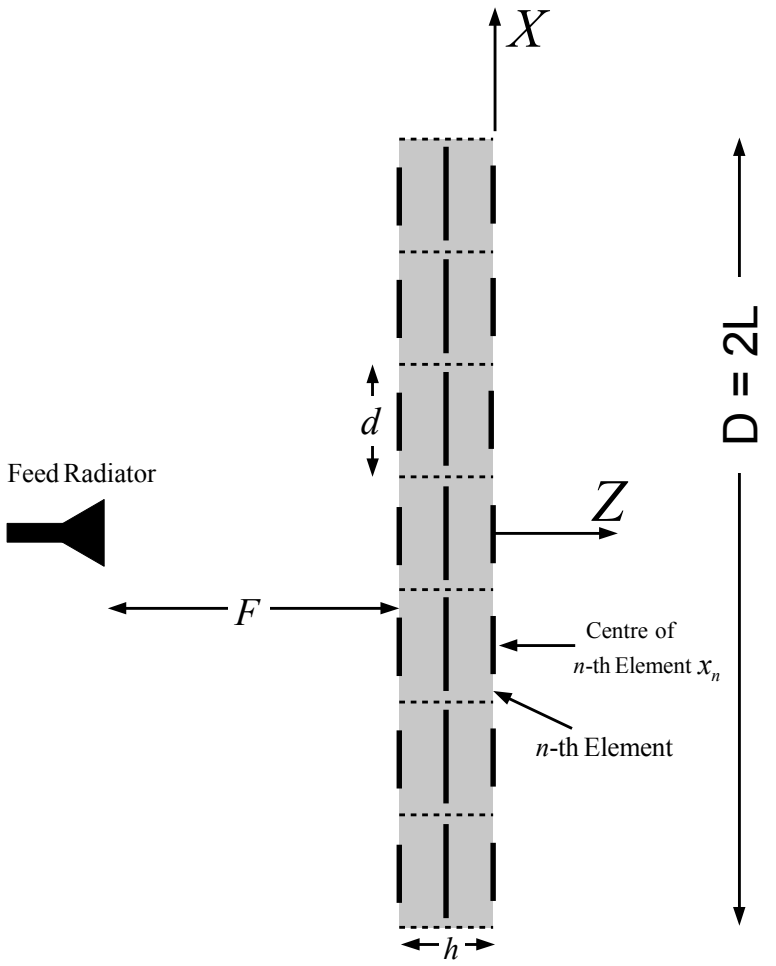

Fig.2.3-1 : Cross-section through cylindrical printed lens.
(The half-width symbol L is used in Section 3.9)

The feed field can be written as $E_y^{in}(x,z)$, and so at points on the lens input surface it would be $E_y^{in}(x,-h)$. The field on the output surface of the lens is then taken (similar to what was done in [5]) to be

$$E_y^{out}(x_n,0) = b_n\, E_y^{in}(x_n,-h) \qquad (2.3\text{-}1)$$

Quantity b_n is the transmission coefficient of the n-th element. It is assumed to be equal to the transmission coefficient of a plane wave that is normally incident on a structure composed of an infinite number of elements along the x-axis that are all identical to the n-th element (which reduces it to a periodic structure). This is of course an approximation, since the n-th element in

the actual lens will not be surrounded by elements identical to itself. However, the success of such an approach in reflectarray and printed lens design is overwhelmingly in favour of its adoption. The value of b_n will be a function of frequency, the properties of the substrate material, and the widths of the conductors at each layer of the n-th cell. Tabulated values of b_n are referred to as the design database for the printed lens antenna. The above-mentioned approximation is not the only one. In writing (2.3-1) we are implicitly assuming that ray-optic tracking of the field is valid; that the feed field travels along a ray from the focal point to the centre of the input surface of the n-th cell and then parallel to the z-axis through the said cell[16] to the output surface. This is not rigorously correct but has been used successfully in printed lens design by others [5].

Each cell is viewed as an element in a linear array located along the x-axis. The excitation of the n-th element is taken to be

$$a_n = E_y^{out}(x_n, 0) = b_n \, E_y^{in}(x_n, -h) \tag{2.3-2}$$

The far-zone array factor in the xz-plane is then

$$F(\theta) = \sum_{n=1}^{N_e} a_n e^{jk\, x_n \sin\theta} \tag{2.3-3}$$

The final far-zone pattern would include the element pattern for a single cell, which in this case could be approximated as

$$E_y^e(\theta) = \frac{\sin\left(\frac{kd}{2}\sin\theta\right)}{\frac{kd}{2}\sin\theta} \tag{2.3-4}$$

However, the cell width (equivalent to the inter-element spacing from the array viewpoint) *d* is very small, and so the element pattern (2.3-4) is broad.

The design procedure for the cylindrical printed lens is then as follows:

- Specify the operating frequency f_o. This allows us to compute the free space wavelength at this frequency $\lambda_o = c / f_o$ with speed of light c = 3 x 10^8 m/s.
- Specify the aperture width D = 2L of the cylindrical lens.

[16] As a normally incident plane wave would.

- Specify the F/D ratio to be used. This allows us to compute the focal length F of the lens.

- Specify the number of elements (2N in the case of even elements, and 2N+1 for an odd number of elements). This enables us to compute the cell width as

$$d = \begin{cases} \dfrac{D}{2N-1} & 2N \text{ Elements} \\ \dfrac{D}{2N} & 2N+1 \text{ Elements} \end{cases} \tag{2.3-5}$$

The number of elements is selected, and d computed, after which a synthesis subject to the imposed pattern and excitation constraints is attempted. If it is found that the pattern performance is not achieved, the number of elements is increased, a new value for d calculated, and a synthesis attempted once again. It is solely this synthesis process that is the subject of the present thesis.

If there are 2N elements then the centre of the n-th cell is at

$$x_n = \left(n - N - \frac{1}{2}\right)d \qquad n = 1, 2, ..., 2N \tag{2.3-6}$$

If there are 2N+1 elements then it is at

$$x_n = (n - N - 1)d \qquad n = 1, 2, ..., 2N+1 \tag{2.3-7}$$

- Once the synthesis procedure has provided the set of required excitations a_n, for $n = 1, 2, ..., N_e$, expression (2.3-2) is used to find the required transmission coefficient of the n-th element, namely

$$b_n = \frac{a_n}{E_y^{in}(x_n, -h)} \tag{2.3-8}$$

which we can write more compactly as

$$b_n = \frac{a_n}{E_y^{in}(x_n)} \tag{2.3-9}$$

The design database is consulted to determine the conductor dimensions of the n-th element. This allows the layout of the lens to be completed.

2.4 CLASSICAL EXCITATION SYNTHESIS TECHNIQUES & THEIR LIMITATIONS

2.4.1 Preliminaries

Almost all classical excitation synthesis methods are only applicable to pencil beams. Those that can be used for the synthesis of shaped beams either do not allow any sidelobe control at all, or allow sidelobe control but are not able to constrain the excitations in any way. All these methods are outlined in the sub-section below. Although we will not make use of them they allow the reader to appreciate the choice of synthesis method that will be used for the work in this thesis.

2.4.2 Directivity Maximisation Subject to a Uniform Excitation Phase Constraint

Consider a linear array with Q elements and a fixed spacing (d) between elements. We assume that the element excitations necessary for maximisation of the directivity in the broadside direction are desired, without any other pattern or excitation constraints. The directivity can be written as the ratio of two quadratic forms, both of whose operator matrices are Hermitian, with that in the denominator being in addition positive-definite. Such properties enable the desired excitations to be obtained directly as the solution of a set of linear simultaneous equations. Results of such computations have been considered by Ma [6], Cheng [7], Pritchard [8], Lo et.al. [9], and Hansen [10]. Hansen [10] has shown that for spacings above a half-wavelength, the maximum directivity is almost identically that obtained with the elements excited with uniform amplitude and phase, providing a pencil beam pattern. For smaller spacings the maximum directivity obtainable is greater than that of a uniform array; this phenomenon is called superdirectivity. However, in the latter situation there are large oscillatory variations in excitation amplitude and phase from one element to another [10]. This is always associated with an enormously large sensitivity to small changes in the excitations. Experimentally it is simply not easy to produce an array with a directivity much in excess of that produced by a uniformly excited array.

2.4.3 Determination of the Array Excitations from the Array Factor Zeros

In order to appreciate the classical analytical synthesis methods to be described in the remaining sub-sections of the present Section 2.4, it is essential to recognize that the element excitations can be determined from the array factor zeros (in general these can be complex), and vice versa. This is

best understood by actually describing exactly how to do it. We next do so for the case of symmetrical arrays[17] of real excitations (that is, all the excitations have the same phase). The angular variable $\psi = kd\sin\theta$ is used, and hence the array factors in (2.2-14) and (2.2-15) can be written as

$$F(\psi) = 2\sum_{n=1}^{N} a_n \cos\left\{(2n-1)\frac{\psi}{2}\right\} \tag{2.4-1}$$

and

$$F(\psi) = a_0 + 2\sum_{n=1}^{N} a_n \cos(n\psi/2) \tag{2.4-2}$$

respectively.

We first consider arrays of 2N elements. Because we are interested in the relative excitations only, we can assume $a_N = 1$, and then the (N-1) unknowns to be determined are $a_1, a_2, \ldots\ldots, a_{N-1}$, implicitly normalised with respect to a_N. Expression (2.4-1) can therefore be written as

$$F(\psi) = \cos\left[(2N-1)\psi/2\right] + \sum_{n=1}^{N-1} a_n \cos\left[(2n-1)\psi/2\right] \tag{2.4-3}$$

If we evaluate this at each of the (assumed known) zeros ψ_m where $F(\psi_m) = 0$, we can re-arrange (2.4-3) as

$$\sum_{n=1}^{N-1} a_n \cos\left[(2n-1)\psi_m/2\right] = -\cos\left[(2N-1)\psi/2\right] \qquad m = 1,2,...,N-1 \tag{2.4-4}$$

This is a set of (N-1) equations in the (N-1) unknowns $a_1, a_2, \ldots\ldots, a_{N-1}$. We can write this system of equations as the matrix equation [G][A] = [B] with matrix elements

$$G_{mn} = \cos\left[(2n-1)\psi_m/2\right] \qquad m,n = 1,2,.....,N-1 \tag{2.4-5}$$

$$B_m = -\cos\left[(2N-1)\psi_m/2\right] \qquad m = 1,2,.....,N-1 \tag{2.4-6}$$

[17] It can be done for non-symmetrical arrays also. We will not consider this case here because we will not be using analytical synthesis methods anyway. They are only being reviewed to place the synthesis methods we will be developing in context.

$$A_m = a_m \qquad m=1,2,.....,N-1 \tag{2.4-7}$$

Once we have found a_1, a_2,……,a_{N-1}, and recall that $a_N = 1$, we can normalise these all with respect to the maximum value rather than a_N. Similar considerations applied to the 2N+1 element array lead to a system of N equations in N unknowns with

$$G_{mn} = \cos(n\psi_m / 2) \qquad m,n=1,2,.....,N \tag{2.4-8}$$

$$B_m = -1/2 \qquad m=1,2,.....,N \tag{2.4-9}$$

$$A_m = a_m \qquad m=1,2,.....,N \tag{2.4-10}$$

where we have assumed the excitation of the centre element to be $a_0 = 1$ and the above equation is solved for the N unknown excitations a_1, a_2, …… , a_N, which are implicitly normalised to a_0.

2.4.4 Beamwidth Minimisation Under Sidelobe Constraints : Dolph-Chebyshev Pencil Beam Synthesis

It is not possible to develop closed-form analytical techniques to determine the array element excitations that provide maximum *directivity* subject to a constraint on the maximum sidelobe level. Instead, *beamwidth minimisation*[18] subject to a constraint on the sidelobe ratio is the classical array synthesis problem solved by C.L.Dolph in his monumental 1946 paper [11]. The underlying argument behind Dolph's approach has been put concisely by Hansen [12] : "A symmetrically tapered (amplitude) distribution over the array ..... is associated with a pattern having lower sidelobes than those of the uniform (amplitude) array. Lowering the sidelobes broadens the beamwidth ..... Some improvement in both beamwidth and efficiency is obtained by raising the farther out sidelobes. Intuitively one might expect equal level sidelobes to be optimum for a given sidelobe level". In order to synthesize such a pattern for broadside arrays

[18] Minimisation of beamwidth does not always imply maximisation of directivity, as will be mentioned in Section 2.4.4.

with interelement spacing greater than or equal to a half-wavelength, Dolph made use of the Chebyshev polynomials.

Consider the problem of best approximation (in the minimax sense) of the function f(x) = 0 over[19] the interval $-1 \le x \le 1$ by a polynomial $P_M(x)$ of specified order M. In other words, given the above f(x), determine whatever details are needed to completely define $P_M(x)$ so that we are able to evaluate it for any x in the above interval. Since $P_M(x)$ is a polynomial this same information will in fact allow us to evaluate it for any $-\infty \le x \le \infty$. A purely mathematical theorem [13,14] proves that the required polynomials are the so-called Chebyshev polynomials $T_M(x)$, defined by

$$T_M(x) = \begin{cases} (-1)^M \cosh\left(M \cosh^{-1}|x|\right) & x < -1 \\ \cos\left(M \cos^{-1} x\right) & -1 \le x \le 1 \\ \cosh\left(M \cosh^{-1} x\right) & x > 1 \end{cases} \qquad (2.4\text{-}11)$$

A sketch of the polynomial $T_8(x)$ is shown in Fig.2.4-1. It is possible to write $T_M(x)$ in conventional polynomial form, but the coefficients tend to be large and of alternating sign. Direct use of (2.4-11) is satisfactory for numerical computation for the range of x values needed for array synthesis problems.

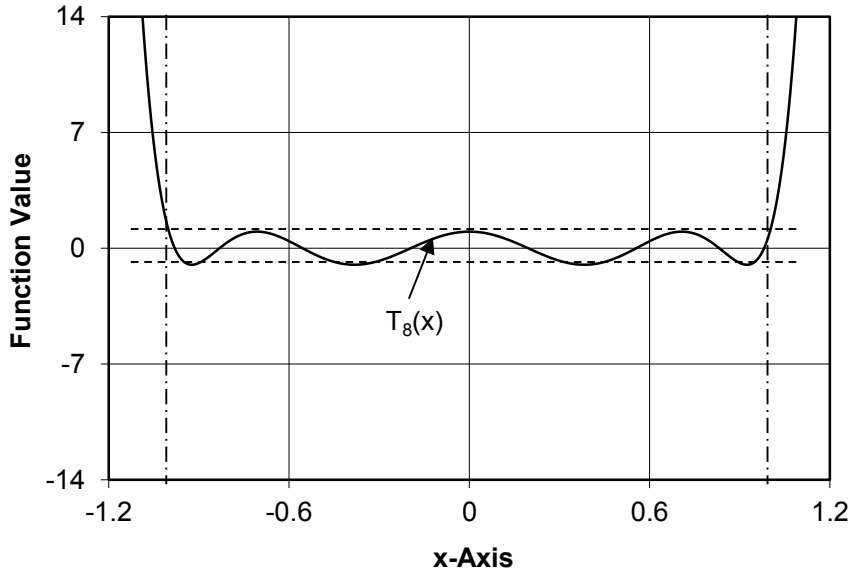

Fig.2.4-1 : Graph of Chebyshev polynomial $T_8(x)$. The two horizontal dashed lines (- - - - -) pass through ±1 on the vertical axis. The two vertical dot-dashed lines (· – · – · – ·) are located at x = ± 1.

[19] The variable x here is just a convenient variable. It should not be taken to be the same as the axis along which the array elements are assumed to be located.

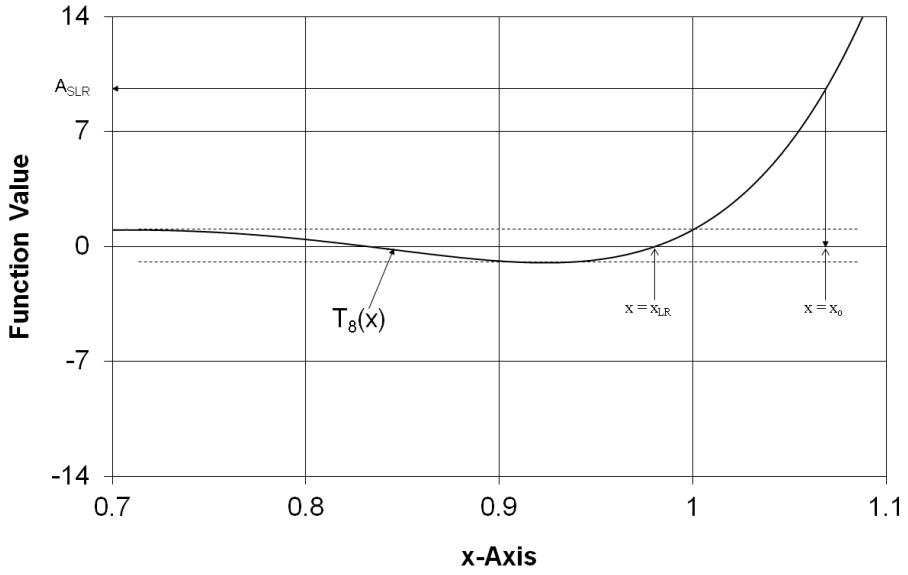

Fig.2.4-2 : Enlargement of a portion of the graph of polynomial $T_8(x)$ from Fig.2.4-1, and quantities related to Chebyshev array synthesis.

At this point all we have are some mathematical facts. The creative idea of relating array factors to Chebyshev polynomials, using this transformation to synthesise array excitations, and providing a proof of the optimality of the resulting arrays, was provided by Dolph [11]. Observe from (2.4-11) and Fig.2.4-1 that in the range $-1 \le x \le 1$ the function $T_M(x)$ ripples in amplitude between the limits ±1. We next refer to Fig.2.4-2, which shows an enlarged portion of the $T_8(x)$ of Fig.2.4-1. Of all polynomials $P_M(x)$ of degree M which pass through the given point (x_o, A_{SLR}) and which remain within the bounds ±1 in the interval $|x| \le 1$, the Chebyshev polynomial $T_M(x)$ minimises the length of the interval $(x_o - x_{LR})$, where x_{LR} is the largest zero of $P_M(x)$. Outside of this range of x-values $T_M(x)$ increases hyperbolically, with $|T_M(x)| > 1$. Dolph [11] recognised these properties as being what is required to synthesise a linear array that, for a given number of elements and specified sidelobe level, has the minimum beamwidth between first nulls. To achieve such a synthesis he used the transformation $x = x_o \cos(\psi/2)$ to establish a correspondence between $T_M(x)$ and an associated array factor, with the constraint $T_M(x_0) = A_{SLR}$ setting the required sidelobe ratio. Observe that as θ varies over the visible angular range from -π/2 to π/2 the variable x varies from $x = \alpha = x_o \cos(kd/2)$ at $\theta = -\pi/2$, to $x = x_o$ when $\theta = 0$, and finally to $x = \alpha$ at $\theta = \pi/2$. If $d = \lambda/2$ then $\alpha = 0$, while for $d > \lambda/2$ we have $\alpha < 0$. Thus for $d \ge \lambda/2$, as the observation angle varies over the visible range, the

range of the variable x includes all the polynomial zeros in the interval $(0, x_o)$ for either even or odd arrays.

The polynomial $T_{2N-1}(x)$ is used to synthesise arrays of size 2N, and $T_{2N}(x)$ for arrays of size 2N+1. The zeroes of the appropriate polynomial are easily determined, from which the array factor zeros ψ_m are calculated using the inverse of the transformation $x = x_o \cos(\psi/2)$. Once the latter are known it is a matter of algebra to obtain the excitations. Dolph was able to prove [11] that the array so synthesised is optimum in the sense that for the specified sidelobe ratio and element number, the beamwidth (between first nulls) is the narrowest possible. Alternatively, for a specified first-null beamwidth, the sidelobe level is the lowest obtainable from the given array geometry. This means that it is impossible to find another set of excitation coefficients yielding better performance, in both beamwidth and sidelobe ratio, for the given element number and uniform spacing d. It represents a closed form solution to the optimisation problem of beamwidth minimisation subject to sidelobe constraints.

Many expressions have been derived for the Cheyshev array excitations, the relative importance of which have changed over the years as computational capabilities have improved. The most straightforward approach is that which directly exploits the fact that $F(\psi_m) = 0$ for each of the array factor zeros ψ_m, and which therefore (taking each of the ψ_m in turn) represents a set of simultaneous linear equations with the excitations as the unknowns. This was described in Section 2.4.3, and enables us to apply one of the many computationally efficient simultaneous linear equation solver algorithms that are now so readily available as coded routines. Once the process has been coded it is as good as, and possibly better than, "closed-form" expressions as far as numerical computation is concerned.

The original formulation by Dolph [11] for synthesising linear Chebyshev arrays is applicable to the case of an even (2N) or odd (2N+1) number of array elements when the inter-element spacing $d \geq \lambda/2$, where λ is the wavelength. The restriction on d, initially noted by Riblet [15], is needed to ensure that the transformation responsible for the polynomial $\Leftrightarrow$ array factor correspondence provides a radiation pattern that is optimal in the sense of yielding the minimum first-null-beamwidth for the given number of elements and specified sidelobe ratio (SLR). As cautioned in [1,6,10,16,17,18] this transformation does not guarantee optimality if $d < \lambda/2$. Subsequent formulations [15,19,20] showed how the transformation must be altered to reclaim

optimality when $d < \lambda/2$, but only for arrays of 2N+1 elements. A means of synthesizing such optimal arrays when there are 2N elements and $d < \lambda/2$ was more recently given in [21].

2.4.5 Villeneuve $\bar{n}$-Distributions : Pencil Beam Synthesis

Optimum beamwidth arrays do not necessarily provide optimum directivity, especially if the array is large [17]. To see this, one can consider a Dolph-Chebyshev array with a fixed sidelobe ratio. Let the array size increase (increase the element number with the spacing held fixed), at each stage keeping the sidelobe ratio constant and normalising the radiation pattern. This is permissible because the directivity to be found at each stage is only dependent on the angular distribution of the radiation and not on any absolute levels. It is then observed that the denominator of the directivity expression is dominated by the power in the sidelobes after a certain array size is reached, and remains roughly constant thereafter. Thus it is found that the Dolph-Chebyshev distribution has a directivity limit [22] because of its constant sidelobe level property, and for a given array size and maximum sidelobe level, may not be optimum from a directivity point of view.

The above “directivity compression” is usually accompanied by an undesirable upswing in the amplitude of the excitations near the array edges ("edge brightening"). For a given number of elements there will be a certain sidelobe ratio for which the distribution of excitations is "just" monotonic. If the number of elements is increased but this same sidelobe ratio is desired, the required distribution will be non-monotonic. Increasing the sidelobe ratio (lower sidelobes) will allow a monotonic distribution once more. Peaks in the distribution at the array ends are not only disadvantageous in that they are difficult to implement and make an array which is realised more susceptible to edge effects, but they are also indicative of an increase in the tolerance sensitivity [23]. To remove these practical drawbacks a taper must be incorporated into the far-out sidelobes. This is achieved by the Villeneuve distribution [24].

The Villeneuve distribution utilises the principle of synthesising excitation distributions by correct positioning of the array factor zeros. The application of the approach consists of the following steps once the number of array elements, inter-element spacing and maximum sidelobe level have been specified :

Step#1 – Determine the array factor zeros for a Dolph-Chebyshev distribution on an array of the same number of elements with the same sidelobe level, as described in Section 2.4.4. (Such an array will have a uniform sidelobe envelope).

Step#2 – Determine the array factor zeros of a uniformly excited array of the same number of elements. (Such an array will have a tapered sidelobe envelope).

Step#3 – Alter the zeros of the Dolph-Chebyshev array so that all except the first $\bar{n}$-1 zeros now coincide with those of the uniformly excited array. In addition multiply each of the first $\bar{n}$-1 Chebyshev zeros by a dilation factor σ. The quantity $\bar{n}$ is referred to as the transition index. The dilation factor is given by [24]

$$\sigma = \frac{\bar{n}\pi}{(2N+1)\cos^{-1}\left\{\frac{1}{u_0}\cos\left[(2\bar{n}\text{-}1)\frac{\pi}{4N}\right]\right\}} \tag{2.4-12}$$

where

$$u_0 = \cosh\left\{\frac{1}{2N}\ln\left[\xi + \sqrt{\xi^2+1}\right]\right\} \tag{2.4-13}$$

and

$$\xi = 10^{-SLR/20} \tag{2.4-14}$$

for an array of 2N+1 elements. Similar expressions are provided in [24] for an array of 2N elements. The sidelobe ratio (in dB) is denoted by SLR.

Step#4 – Use these final zeros of the perturbed Chebyshev array to determine the final element excitations[20].

The result will be an array factor whose near-in sidelobes are close to the maximum sidelobe level specified, with the further out ones decreasing in level at a rate close to that of the uniformly excited array. This behaviour has been shown to provide arrays with the desired maximum sidelobe level but higher aperture efficiency than one would get if some arbitrary tapered excitation distribution were to be used.

The Villeneuve distribution was generalized in [25]. Although the quantities σ and $\bar{n}$ are retained, an additional parameter v, called the taper parameter is introduced. This allows the taper rate of the sidelobe envelope to be controlled. In other words, like the Villeneuve distribution, the Dolph-Chebyshev distribution serves as a "parent" space factor. The correct perturbation of the zeros of this parent space factor serves to incorporate the sidelobe behaviour desired, while at the

[20] In his original paper Villeneuve [24] derived closed-form series expressions for the excitations, but they are found just as easily using the technique described in Section 2.4.3.

same time keeping the excitation efficiency and beamwidths as close to their optimum values as is possible under the required sidelobe ratio and envelope taper conditions. The level of the first sidelobe is set by the parent Dolph-Chebyshev distribution, the envelope taper rate controlled by the taper parameter ν, and the point at which the required taper proper begins determined by the transition index $\bar{n}$. The proper choice of the values of $\bar{n}$ and ν for a particular application will depend on the relative importance of the peak sidelobe level compared to that of the farther-out sidelobes, and their effect on the excitation efficiency.

2.4.6 Analytical Shaped Beam Synthesis Methods

The array factors have the form of a Fourier series, but with the number of terms of the same order as the number of elements in the array. An early Fourier series synthesis method does the following : The idealized shaped pattern[21] over the shaped region is expanded in a Fourier series. The element excitations are equated to the coefficients of this Fourier series expansion. Due to the limited number of terms in the Fourier series of the shaped pattern the resulting pattern exhibits large ripples around the idealized shaped pattern, and high sidelobes outside the shaped region.

An improvement on the above technique is the Woodward-Lawson [26,27] method. This technique relies on the fact that any pattern realizable using an N_e element array can be expressed as the weighted summation of a set of N_e orthogonal beams, each having a "$\sin(N_e x)/\sin(x)$" shape. The maximum value of each of these beams coincides with the zero in all other beams. The synthesis technique samples the idealized shaped pattern at increments of $N_e/2\pi$. The synthesized array is thus the superposition of array factors from N_e uniform amplitude, linear progressive phase excitations with the phase increment of each excitation such that the array factor peak is placed at a sampling point on the idealized shaped beam. Although the resultant array factor is equal to the idealized shaped pattern at the sample points, it also exhibits large ripples in the shaped beam region and high uncontrollable sidelobes in the sidelobe region.

A criticism of the Woodward-Lawson method is that it only uses data from N_e idealized pattern sampling points, whereas there are $2N_e$-2 degrees of freedom (namely N_e-1 relative

[21] Please see Section 2.9 for a discussion of the idealized forms of the flat-topped, isoflux and cosecant shaped patterns.

amplitudes and N_e-1 relative phases. Milne described a method [28] that effectively takes $2N_e$-1 sample points, spaced at intervals $2\pi/(2N_e-1)$. In essence it starts with some pencil beam pattern, copies of which are "scanned" to have their maxima at points in the shaped region and sidelobe region. This allows some limited control of the shaped beam region ripple and sidelobe levels.

2.4.7 Numerical Variation of the Complex Polynomial Roots

The best approach not based on numerical optimization of some objective function, or the method of projections, is that by Orchard et al. [29]. This is an iterative method in which the zeroes of the array factor are made complex, and their real and imaginary parts are simultaneously adjusted in an iterative fashion so that the amplitude of each ripple in the shaped beam region and the height of each sidelobe outside of this region are individually controlled. A recipe for such adjustments is provided in [29], but its use of far from routine.

2.4.8 Limitation of Classical Synthesis Methods

The reader will have noticed that the methods in Sections 2.4.2 through 2.4.5 can be used for pencil beam synthesis only. Although that in Sections 2.4.6 and 2.4.7 can be used for shaped beam synthesis, they cannot entertain any excitation constraints. Indeed, this is not possible with any classical analytical synthesis methods. This means that, for example, phase-only excitation synthesis is not possible either. In classical excitation synthesis methods we have to let the excitation amplitudes and phases "do what they please". These methods are thus not suited to the goals of this thesis.

2.5 SYNTHESIS METHODS DIRECTLY BASED ON CONVENTIONAL NUMERICAL OPTIMISATION ALGORITHMS

2.5.1 Introduction

Excitation synthesis techniques that rely explicitly on the use of numerical optimization algorithms all require that the synthesis requirements (both pattern and excitation constraints) be encapsulated in a single objective function

$$F_{obj}\left\{a_1, a_2, ..., a_{N_e}\right\} \tag{2.5-1}$$

that is, as indicated, a function of the array excitations. There are numerous numerical optimization algorithms that can be used to efficiently locate the minimum of a given objective function F_{obj}. In array synthesis work these are only useful if we are able to so define F_{obj} that, when its minimum is attained, we have an array antenna whose performance is indeed what we seek. In other words, what we are able to achieve depends on how well we have translated our desired antenna specifications into a mathematical expression which, when optimized, provides a performance that meets our requirements. These requirements will be both pattern constraints and excitation constraints.

The objective functions are non-linear, and usually have many local minima that can trap the algorithm. Evolutionary algorithms (eg. genetic algorithm) have been successfully used to avoid the problem of getting stuck in local minima. These global optimization approaches are very heavy on computation, but this is less of an issue these days. One disadvantage (compared to the projection synthesis methods to be described in Section 2.7, and which will be the chosen method for this thesis) is that the pattern and excitation constraints are intertwined in some objective function. It would be preferable if the excitation constraints could be made more explicit, making it possible to more easily recognize trade-offs and to judge the plausibility of some excitation constraint. Nevertheless such synthesis techniques, especially using the genetic algorithm (in its many forms) as the numerical optimization algorithm of choice, could be used for the problem of interest in this thesis. However, we have selected the projection method described in Section 2.7, for reasons that will become clear in that section.

2.5.2 Least Squares Based Methods

In order to describe the least squares approach we will use the radiation pattern analysis model in expression (2.2-19) namely[22]

$$E_{CO}(\theta) = \sum_{n=1}^{N_e} a_n F_n(\theta) \tag{2.5-2}$$

where

$$F_n(\theta, \phi) = e^{jkx_n \sin\theta} \tag{2.5-3}$$

We will next define certain matrices that will be used in the writing of the projection synthesis formulations in concrete terms in Section 2.7; they are provided here already because they turn out to be equally useful for an explanation of the least-squares methods with which we are immediately concerned in the present section. Expression (2.5-2) can be written as

$$E_{CO}(\theta) = \left[F_1(\theta) \,.....\, F_n(\theta) \,.....\, F_{N_e}(\theta) \right] \begin{bmatrix} a_1 \\ . \\ . \\ . \\ a_n \\ . \\ . \\ . \\ a_{N_e} \end{bmatrix} \tag{2.5-4}$$

This is a continuous function over the independent variables $0 \le \theta \le \pi$ and $0 \le \phi \le 2\pi$. If we are to actually implement any numerically based method, at some point in the procedure we of course need to obtain a finite-dimensional and discrete representation of the pattern vector in order to perform numerical computations. A finite-dimensional discrete pattern vector $[E_{CO}]$ can

[22] We discuss it for the linear array case (which is of interest in this thesis), although everything can be done for the planar array case too. In the linear array case we can write the array factor in terms of angle θ only, as shown. We will also ignore the broad element pattern. Hence the form of expression (2.5-2).

be obtained by selecting pattern points $\{\theta_1, \theta_2, ..., \theta_m, ...\theta_M\}$ at which $E_{CO}(\theta)$ is sampled. We can therefore write

$$[E_{CO}] = \begin{bmatrix} E_{CO}(\theta_1) \\ E_{CO}(\theta_2) \\ \text{g} \\ \text{g} \\ \text{g} \\ \text{g} \\ \text{g} \\ \text{g} \\ \text{g} \\ \text{g} \\ E_{CO}(\theta_M) \end{bmatrix} = [T_{EA}][A] = \underbrace{\begin{bmatrix} F_1(\theta_1) & F_2(\theta_1) & \bullet & \bullet & F_{N_e}(\theta_1) \\ F_1(\theta_2) & F_2(\theta_2) & & & F_{N_e}(\theta_2) \\ \bullet & \bullet & \bullet & & \bullet \\ \bullet & \bullet & & \bullet & \bullet \\ \bullet & \bullet & & & \bullet \\ F_1(\theta_M) & F_2(\theta_M) & \bullet & \bullet & F_{N_e}(\theta_M) \end{bmatrix}}_{[T_{EA}]} \underbrace{\begin{bmatrix} a_1 \\ a_2 \\ \bullet \\ \bullet \\ a_{N_e} \end{bmatrix}}_{[A]} \tag{2.5-5}$$

which also defines the matrix $[T_{EA}]$. It is understood that the definition of $[T_{EA}]$ implicitly includes normalisation of the resultant pattern vector $[E_{CO}]$.

If $[E_{CO}]$ is known, then the required excitations $[A]$ can be found by minimizing the objective function

$$F_{obj}\left\{a_1, a_2, ..., a_{N_e}\right\} = \left\| [T_{EA}][A] - [E_{CO}] \right\|^2 \tag{2.5-6}$$

This has a well-known solution, namely the so-called least-squares (also called the maximum likelihood solution)

$$[A] = \left([T_{EA}]^H [T_{EA}] \right)^{-1} [T_{EA}]^H [E_{CO}] \tag{2.5-7}$$

This was known in the mathematical literature long before the array synthesis problem had ever been important where it is recognised as the least-squares solution to an over-determined set of linear equations. An alternative solution also available in the mathematical literature is

$$[A] = \left([T_{EA}]^H [W][T_{EA}] \right)^{-1} [T_{EA}]^H [W][E_{CO}] \tag{2.5-8}$$

where $[W]$ is a diagonal weighting vector, and superscript "H" indicates the conjugate transpose operation. If $[W]$is selected to be the identity matrix the process reduces to conventional least squares (also referred to as the maximum likelihood method). Relative weights must be assigned to the weighting vector $[W]$. In array synthesis the main lobe region and each sidelobe region can be assigned a regional weight according to their relative importance in a particular application. In other words, the relative weights can be decreased at sampling angles that are less important as far as precise satisfaction of the pattern constraints is concerned.

If we had $[E_{CO}]$, by which we mean its complex values, which would mean that both the pattern amplitude and phase of the desired pattern is known at each sample angle θ_m, then we could simply use (2.5-7) or (2.5-8) to find $[A]$. The problem is that when we synthesize shaped beam patterns – as will be detailed in Section 2.9 – we do not know the precise shape of the complex pattern $[E_{CO}]$. We know only the masks within which the magnitudes of the pattern samples $\left|E_{CO}(\theta_m)\right|$ must lie; the phases of the complex field values $E_{CO}(\theta_m)$ are not specified. One might be tempted to declare that the pattern phase be constant with respect to θ. But there is a weakness in this argument. The masks[23] include not only the shaped beam region but also the sidelobe regions. Why would the pattern phase over this entire set of pattern angles necessarily be the same? Even within the shaped beam region the pattern phase need not be constant as a function of θ. So we do not wish to impose an artificial phase on the radiation pattern (in so doing perhaps missing some improved synthesis solution), and instead want it to develop in a natural way according to what the physics demands. In shaped beam methods that use a least-squares approach this is achieved by an iteration process. An initial guess (or "warm start" if we prefer the more technical terminology) is made, and then an iterative process such as that detailed in [30,31,32] is used to arrive at the required excitation vector $[A]$. However, the imposition of excitation constraints is not possible using the least-squares method just described. A least-squares method that allows phase-only synthesis (with all excitation amplitudes kept the same) has been described [33], but it can handle only small perturbations to the phase and so is not applicable to all beam shapes.

[23] To be discussed in some detail in Section 2.9.

2.5.3 Use of Gradient-Based or Evolutionary Numerical Optimisation Algorithms

Once an objective function F_{obj} has been defined any numerical optimization algorithm can be used for synthesis purposes. Gradient-based algorithms (eg. [54]) used to be utilized, but evolutionary algorithms are now preferred. There is an enormous literature on the subject, both in textbooks and journal papers, and the reader is referred to references [35] through [46], where array synthesis applications are described using mainly the genetic algorithm, but also the particle-swarm and simulated-annealing algorithms. The user has to be aware of the fact that objective functions that not only include pattern constraints but also excitation constraints are not as widely used in the references mentioned. Those that do include excitation constraints require quite a bit of "tuning" before they are satisfactorily represent the synthesis goals[24]. After all, we wish to converge to an optimum of the synthesis problem. If F_{obj} is not chosen properly we might achieve its optimum value but this might not provide us with a solution that represents the synthesis goals. As with all numerical optimization algorithms a warm start is needed for the excitation amplitudes and phases.

2.6 SYNTHESIS METHODS BASED ON CONVEX PROGRAMMING ALGORITHMS

Even though excitation synthesis methods based on convex programming can be classified under the same set of methods as that in Section 2.5 – after all it is based on the minimization of an objective function - it is often considered separately. The reason is that if it is possible to derive an objective function that is in fact a quadratic form then the numerical optimization algorithm known as convex programming can be used. The latter algorithm has the advantage that it will always converge to a global optimum of the objective function. This method was used several years ago to perform an excitation synthesis that maximizes directivity subject to sidelobe constraints [49,50]. However, it has recently been refined in the sense that objective functions applicable to a wider range of array synthesis problems have been derived [52 - 58].

[24] This is not always apparent from the literature.

Nevertheless, it is still not possible to use convex programming directly if we wish to apply excitation constraints[25]. Thus the method is not germane to the problem of interest in this thesis.

2.7 EXCITATION SYNTHESIS USING THE METHOD OF GENERALIZED PROJECTIONS

2.7.1 Introduction

In contrast to the excitation synthesis methods described in the previous three sections, the array synthesis problem can also be viewed as determining the intersection of two sets. The first is the set of all radiation patterns possible with the given array geometry (in other words patterns computed using the appropriate forward operator[26] for the particular geometry in question) when the excitations comply with the required excitation constraints. The second is the set of all radiation patterns possible with the given array that comply with the required radiation pattern constraints. The method can be described as synthesis in "radiation pattern space". This approach was used in [59], with major advances to the detail and breadth of applications being made in [60,61,62] and its use being extended to conformal arrays in [63,64,65]. These all used the so-called *generalized sequential* projection method.

In [66] the same sequential projection method was used, but in the "excitation space", the advantage being that certain relaxation methods can be applied to speed up convergence. The synthesis problem in the latter case is one of finding the intersection of the set of all excitations that satisfy the specified excitation constraints, and the set of all excitations that produce radiation patterns that satisfy the specified pattern constraints.

The *generalised parallel* projection method [67,68,69] was more recently introduced, albeit not in the context of array synthesis, based on ideas originally published by Pierra [70]. This parallel version of the method was applied in [71] to a "switched-element" pencil beam array synthesis problem in excitation space, but has not been applied to shaped beam synthesis.

[25] An exception is its use for phase-only synthesis [51], but it can handle only small perturbations to the phase, and so is not necessarily applicable to shaped beam synthesis.
[26] The forward operator will be defined in Section 2.7.4.

2.7.2 Mathematical Review of the Fundamentals of the Generalised Projection Method[27]

The essential idea is that an unknown f (eg. a set of array excitations) is known to lie in Q given sets C_q (q=1,2,…,Q), where each set[28] represents a constraint on f. The solution is then given by the intersection point of the Q constraint sets; the solution is the particular f that lies in all Q sets. Associated with each set is a projection operator P_q (q=1,2,…,Q), which is in general non-linear. By definition, for all sets (not only convex ones), we call $g = P_q f$ the projection of f onto C_q if :

- $g \in C_q$ (2.7-1)
- $\|g - f\| = \underset{All\ h \in C_q}{Min} \|h - f\|$ (2.7-2)

where $\|g\|$ denotes the norm of g. As a consequence of this definition a projection operator possesses the so-called *idempotent* property that Pq Pq $f = g$. The algorithm for determining the f that lies in the intersection of the above sets C_q is [60,67]

$$f_{k+1} = L_1 L_2 \ldots L_Q f_k \tag{2.7-3}$$

where f_o is the initial point chosen for f, about which we will have something to say in Section 2.7 and Section 3.6, and operator

$$L_q = I + r_q (P_q - I) \tag{2.7-4}$$

with q=1,2,…,Q and r_q a real number known as a *relaxation parameter*. The "I" is of course the identity operator appropriate to a particular application (eg. an identity matrix if projection operator P_q is expressed in matrix form). Index k denotes the number of the iterations[29].

A. Convex Projections

A projection P_q as defined above is a unique point if C_q is a convex set [60]. Furthermore, if all Q of the sets C_q are convex, then the iterative algorithm (2.7-3) is guaranteed [60] to converge to a point in $C_o = C_1 \cap C_2 \cap \ldots \cap C_Q$ provided C_o is not empty and $0 \le r_q \le 2.0$. If these conditions apply the method is sometimes referred to as the *method of convex projections* or more explicitly as the *method of alternating projections onto convex sets* [72].

---

[27] Sometimes also called the method of vector space projections.
[28] Examples of such sets for the excitation synthesis problem will shortly be given.
[29] Not the number of iterations.

B. Sequential (or Serial, or Successive) Generalised Projection Method

Although projection P_q as defined above is a unique point if C_q is a convex set, when this is not the case there may be a number of points, rather than a single point, that satisfy the definition of the projection. In actual applications we can usually find a procedure for uniquely selecting one of these points. More seriously though, if one or more of the sets C_q is not convex then convergence of the algorithm (2.7-3) is not guaranteed. In such circumstances the algorithm[30] is used with Q=2, namely

$$f_{k+1} = \mathcal{L}_1 \mathcal{L}_2 f_k \tag{2.7-5}$$

since this case has a useful *set distance reduction property* even when C_1 and/or C_2 are not convex. In order to state this property we note that in the absence of guaranteed convergence we need a measure to assess the performance of the algorithm at each iteration so that we can formulate a "stopping criterion". A measure that has been widely used is given by [60,67]

$$SDE\{g\} = \left\| \mathcal{L}_1 g - g \right\| + \left\| \mathcal{L}_2 g - g \right\| \tag{2.7-6}$$

It is usually called the *summed distance error* (SDE) since it is simply the sum of the distances from g to the two sets C_1 and C_2. It has the property [2] that $SDE\{g\} \geq 0$, with $SDE\{g\}=0$ only if $g \in C_1 \cap C_2$. The recursion algorithm (5) can then be shown to possess the property

$$SDE\{f_{k+1}\} \leq SDE\{\mathcal{L}_2 f_k\} \leq SDE\{f_k\} \tag{2.7-7}$$

for appropriately selected values of relaxation parameters r_1 and r_2. The property (2.7-7) does not extend to those cases where Q>2. However, in array synthesis problems at any rate, this is not restrictive. When the algorithm (2.7-5) is applied and its progress measured as indicated it is usually referred to as the *method of (sequential) generalised projections*. The adjective sequential is used because the projections are applied successively (that is, serially). The nemesis of the method is the occurrence of so-called stagnation points, which may be *traps* or *tunnels*. Traps (which occur only when non-convex sets are involved) occur at those points g at which $\mathcal{L}_1 \mathcal{L}_2 g = g$ (the so-called fixed points of the operator $\mathcal{L}_1 \mathcal{L}_2$) and are not valid solutions. Tunnels are those situations in which the solution is approached so slowly that for all practical purposes the algorithm has ceased functioning. A more complete and well-illustrated discussion of these aspects can be found in [67].

In any application of the method (and these are what distinguish one application from another) it is necessary to define the sets C_q, define norms in these sets, derive the associated

[30] Which iteratively projects between the latter sets to find the intersection.

projection operators P_q, and select the starting point f_o. Repeating slightly what we stated in Section 2.7.1, the array synthesis problem (in "radiation space") can be viewed as determining the intersection of two sets, the one being the set of all radiation patterns possible with the given array geometry (including constraints other than those on the radiation patterns), and the other being that consisting of all radiation patterns that comply with the required radiation pattern constraints. If the method is applied in "excitation space", the synthesis problem is one of finding the intersection of the set of all excitations that satisfy the specified excitation constraints and the set of all excitations that produce radiation patterns which satisfy the specified pattern constraints.

C. Parallel Generalised Projection Method

An alternative to the serial version is the *generalized parallel* projection algorithm [67,68], which can be written succinctly as

$$f_{k+1} = f_k + r_k \left\{ \sum_{q=1}^{Q} \alpha_q P_q f_k \; - \; f_k \right\} = (1 - r_k) f_k + r_k \sum_{q=1}^{Q} \alpha_q P_q f_k \tag{2.7-8}$$

$$\sum_{q=1}^{Q} \alpha_q = 1 \tag{2.7-9}$$

$$SDE\{g\} = \left[\sum_{q=1}^{Q} \alpha_q \left\| P_q g - g \right\|^2 \right]^{1/2} \tag{2.7-10}$$

$$SDE\{f_{k+1}\} \le SDE\{f_k\} \tag{2.7-11}$$

where the α_q are real weighting factors and now Q can be larger than two. Although it is possible [67] to estimate the best relaxation parameter at each iteration (hence the subscript notation in the symbol r_k) it has been found that it is in practice sufficient to execute the synthesis process for several different relaxation parameter values that are the same at each iteration and then simply select the one which leads to the most rapid solution for the particular problem at hand. The above parallel version of the algorithm has similar convergence properties to the serial version when the sets intersect. However, it has some advantages over the serial version. Firstly, it possesses the SDE reduction property even when more than just two sets (one or more of which may be non-convex) are involved. Secondly, the weights α_q can be used to give greater (or lesser) weight to a particular set of constraints. Finally, for inconsistent constraint problems

(that is, where the constraints sets C_q do not all intersect) the parallel algorithm converges to a weighted least-square solution [73] that is preferable to the cycling ("trapped") behaviour of the serial algorithm. In the sections to follow we discuss the sets and operators for the formulations of the method for use in array synthesis[31].

2.7.3 The Excitation Vector & Excitation Space

The excitation vector $[A]$ is the column vector $[a_1,a_2,\ldots..,a_N]^T$, where the superscript denotes the transpose operation (without complex conjugation), and $a_n = |a_n| e^{j\psi_n}$ is the complex excitation of the n-th radiator in the array. Quantity ψ_n is the excitation phase, with $0^o \le \psi_n \le 360^o$ in general. Quantity $|a_n|$ is the excitation amplitude, with $0 \le |a_n| \le 1$. In other words, we will **always** write the excitations in normalized form. We will define the *excitation space* S_A (see Fig.2.7-1) as the set of all possible excitation vectors $[A]$ of the given N-element array geometry, and note that we can consider S_A to be a discrete N-dimensional Euclidean space.

2.7.4 The Forward Operator, Radiation Pattern Vector & Radiation Pattern Space

The radiation pattern of the array antenna can be found via a *forward operator* T_{EA} as

$$\overline{E}(\theta,\phi) = \mathsf{T}_{EA}\{[A]\} \tag{2.7-12}$$

where the pattern vector

$$\overline{E}(\theta,\phi) = E_{co}(\theta,\phi)\hat{e}_{co} + E_{cr}(\theta,\phi)\hat{e}_{cr} \tag{2.7-13}$$

is considered to be a member of the *pattern space* that is the set of all possible pattern vectors $\overline{E}(\theta,\phi)$ obtainable from the given array geometry. Details of the operator T_{EA} will depend on the geometry of the array environment of interest[32]. Repeating the comments made in Section 2.5.2, but in the terminology of the projection method, the above pattern space is a continuum space (over the independent variables $0 \le \theta \le \pi$ and $0 \le \phi \le 2\pi$), and is in general infinite-dimensional. If we are to actually implement the projection method we need to work with a finite-dimensional discrete

[31] The parallel projection method has not yet been used for shaped beam synthesis.
[32] For instance, in the case of planar arrays it might be an FFT, while in other cases such as conformal arrays it might consist of a detailed analysis of the effects of the host surface using more detailed electromagnetic modelling.

representation of the pattern vector. So we sample the pattern at specific angles $\{\theta_1, \theta_2, ..., \theta_m, ...\theta_M\}$ and define a forward operator T_{EA} which maps S_A directly onto a finite-dimensional discrete *pattern space* $S_{F.}$, namely

$$T_{EA}\{[A]\} = [E_D] = [E_{CO}(\theta_1), E_{CO}(\theta_2), .., E_{CO}(\theta_M), E_{CR}(\theta_1), E_{CR}(\theta_2), .. , E_{CR}(\theta_M)]^T \qquad (2.7\text{-}14)$$

We will thus write the forward operator as a matrix $[T_{EA}]$, so that $[E_D] = [T_{EA}][A]$. Note that $[T_{EA}]$ will not be square because there are more pattern sampling points than array elements. $[E_D]$ lies in the pattern space S_F. If both co- and cross-polarised patterns are being considered, then $[E_D]$ is a 2M-dimensional column vector as shown; if only co-polarised patterns enter into the synthesis procedure then it is M-dimensional. In the former case forward operator $[T_{EA}] : S_A \rightarrow S_F$ will be an N x 2M matrix, and in the latter case an N x M matrix. The forward operator $[T_{EA}]$ is needed in the definition of certain projection operators in later sections.

In this thesis we will directly synthesise only the co-polarised pattern, so that we will denote $[E_D]$ by $[E_{CO}]$, as already done in Section 2.5.2. The forward operator $[T_{EA}]$ is then that already defined by (2.5-5)

2.7.5 The Backward (or Reverse, or Inverse) Operator

In addition to the forward operator which maps an element from the excitation space S_A to an element in the discrete radiation space S_F we will, in the definition of certain projection operators to be described below, require a *backward* (or *reverse) operator* $T_{AE} : S_F \rightarrow S_A$ which maps an element of the discrete radiation space to an element in the excitation space S_A. In the discrete finite-dimensional spaces (that is, the matrix world) with which we are working this formally means that we require $[T_{AE}] = [T_{EA}]^{-1}$. Since $[T_{EA}]$ is not a square matrix some form of generalised inverse must be used.

One possibility is to use weighted least squares to determine the generalised inverse (and hence the backward operator), namely

$$[T_{AE}] = \left([T_{EA}]^H [W][T_{EA}]\right)^{-1} [T_{EA}]^H [W] \qquad (2.7\text{-}15)$$

where $[W]$ is a diagonal weighting vector, and superscript "H" indicates the conjugate transpose operation. If $[W]$ is selected to be the identity matrix the process reduces to conventional least squares (also referred to as the maximum likelihood method). In executing the backward operator the relative weights must be assigned to the weighting vector $[W]$. The main lobe region and each sidelobe region can be assigned a regional weight according to their relative importance in a particular application. In other words, the relative weights can be decreased at sampling angles that are less important as far as precise satisfaction of the pattern constraints is concerned. This will be demonstrated in Chapters 3 and 4.

Another possibility is to use the Moore-Penrose generalised inverse. This has the advantage that highly efficient routines for its execution are readily available [74,75].

We have not yet defined the projection operators needed for the application of the synthesis method under discussion. We are still in the process of defining various operators that will be used in the eventual definition of such projection operators in Section 2.7.6 and Section 2.7.7, and more completely in Chapter 3.

2.7.6 Operator Used to Implement Pattern Constraints

It is assumed that the pattern vector $[E_{CO}]$ has been normalized. Then the operator[33] that enforces pattern constraints will be defined as

$$P_E\left\{\,[E_{CO}]\right\}=[E'_{CO}]=\left[E'_{CO}(\theta_1)\quad E'_{CO}(\theta_2)\quad \bullet\quad \bullet\quad \bullet\quad E'_{CO}(\theta_M)\right]^T \tag{2.7-16}$$

where

[33] Note that this is also a projection operator. However, it is not one of the projection operators used directly in the projection algorithm. But it will be used, along with the forward and reverse operators defined earlier, to construct projection operators that are used directly in the algorithm.

$$\mathrm{E}'_{CO}(\theta_{\mathrm{m}}) = \begin{cases} \dfrac{E_{CO}(\theta_{\mathrm{m}})}{|E_{CO}(\theta_{\mathrm{m}})|} S_U(\theta_m) & \text{if } |E_{CO}(\theta_{\mathrm{m}})| > S_U(\theta_m) \\ E_{CO}(\theta_{\mathrm{m}}) & \text{if } S_L(\theta_m) \le |E_{CO}(\theta_{\mathrm{m}})| \le S_U(\theta_m) \\ \dfrac{E_{CO}(\theta_{\mathrm{m}})}{|E_{CO}(\theta_{\mathrm{m}})|} S_L(\theta_m) & \text{if } |E_{CO}(\theta_{\mathrm{m}})| < S_L(\theta_m) \end{cases} \tag{2.7-17}$$

and the functions $S_U(\theta)$ and $S_L(\theta)$ specify the upper and lower bounds of the pattern (that is, the mask). The operation described above is a quite straightforward one : (a). If at any point θ_m the computed pattern level is outside the pattern mask then the pattern magnitude at that point is changed while the phase at that point is retained. If it lies above (below) the mask it is simply made equal to the upper (lower) mask value at that sampling angle. (b). If at any point (θ_m) the computed pattern level is inside the pattern mask then the pattern at that point is left unchanged. It is understood that, as an integral part of the application of P_E, the resultant pattern vector is always normalised with respect to its member that has the largest magnitude.

One needs only this pattern constraint operator, as different pattern shapes are defined by simply changing functions $S_U(\theta)$ and $S_L(\theta)$. Examples of these radiation pattern masks were shown in Fig.1.1-1.

2.7.7 Operator Used to Implement Excitation Constraints

The development of such operators[34] is taken up in detail in Chapter 3, and forms part of the contribution of this thesis. However, in order to be able to describe the projection synthesis method we need to at least quote one example of such an operator, taken from the existing literature, that enforces simple[35] amplitude range constraints ($A_{\min} \le |a_n| \le 1$) on the excitation vector $[A]$. We write it as[36]

$$P_{A1}\{[A]\} = [a'_1, a'_2, ..., a'_n, ..., a'_N]^T \tag{2.7-18}$$

[34] Unlike the pattern constraint operator in Section 2.7.7, for which only one form is needed, different excitation constraint operators are needed for different types of excitation constraint.
[35] We refer to it as "simple" since the excitation constraint classes to be developed in the present chapter will be increasingly complex.
[36] It is assumed that [A] is magnitude-normalized before applying the constraint projector given immediately below.

where

$$a'_n = \begin{cases} a_n & \text{if } A_{\min} \le |a_n| \le 1 \\ \dfrac{a_n}{|a_n|} A_{\min} & \text{if } |a_n| < A_{\min} \end{cases} \qquad (2.7\text{-}19)$$

The subscript "A" in P_{A1} denotes[37] that it is an operator that constrains the vector [A], as opposed to the subscript "E" of P_E in (2.7-16) that constrains the vector $[E_{CO}]$. Expression (2.7-18) is just one of several operators that will be devised in Chapter 3 to apply various excitation constraints. Note that the class of excitation constraint (2.7-18) does not place any constraint on the excitation phases. All excitation amplitudes are constrained in a homogeneous manner over the array aperture; the dynamic range allowed for an element at the centre of the array is the same for one at the edge, and so on.

[37] The "1" in the subscript identifies that it is only one of several excitation constraint projection operators that will be used in this thesis, which will be uniquely identified as P_{A2}, P_{A3}, and so on. Only one pattern constraint projector P_E is needed though; but the masks that it enforces will change for different patterns shapes.

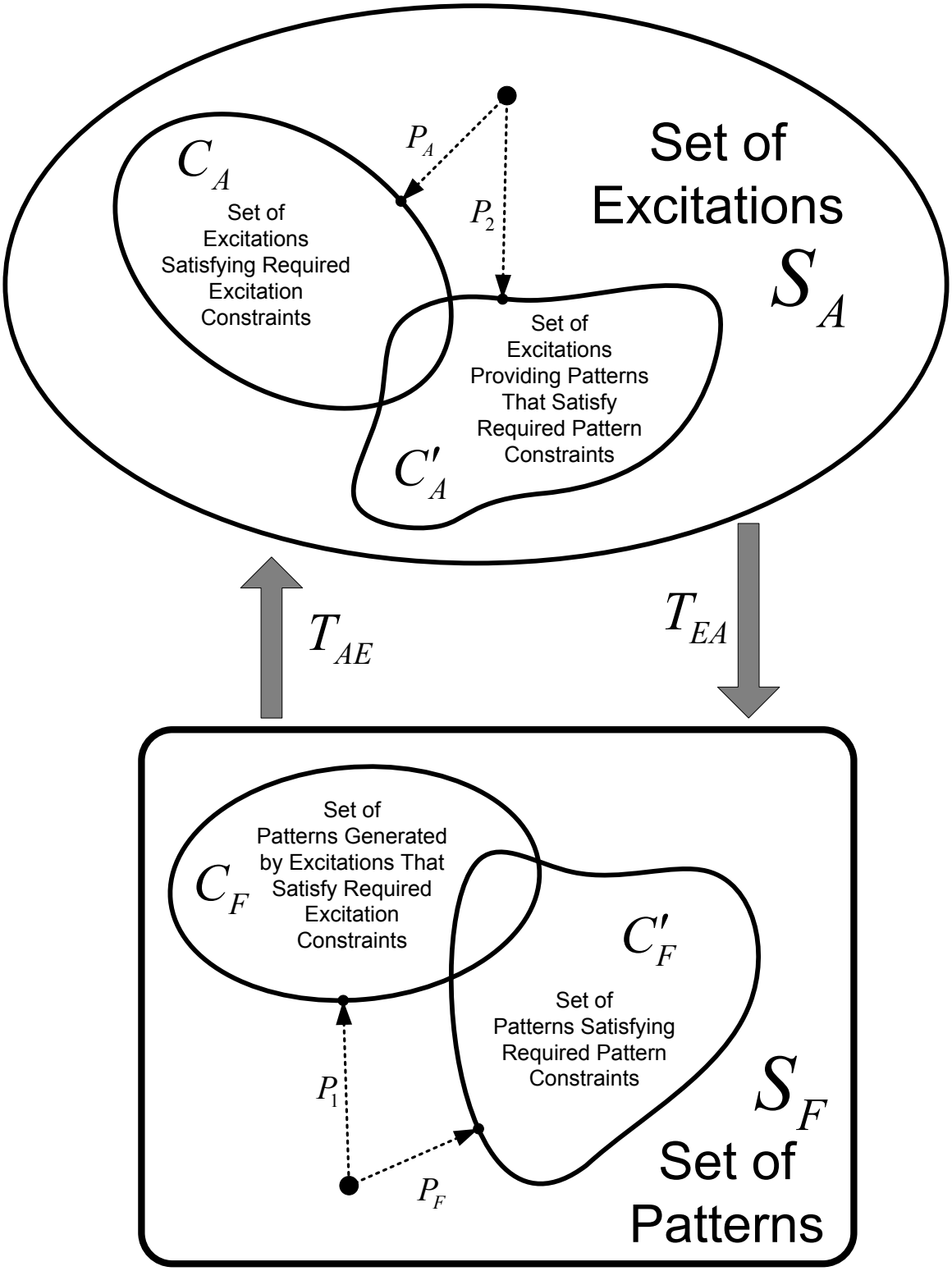

Fig. 2.7-1 : Excitation and pattern spaces in terms of which the method of generalized projections is defined (*Courtesy of D.A.McNamara*)

2.7.8 Serial Projection Method in Pattern Space

Recursion Algorithm :

$$\left[E_{CO}\right]_{k+1} = L_1 L_2 \left[E_{CO}\right]_k \tag{2.7-20}$$

$$L_1 \equiv P_1 \tag{2.7-21}$$

$$L_2 \equiv P_2 \tag{2.7-22}$$

Projection Operators :

$$P_1\left\{\left[E_{CO}\right]\right\} = [T_{EA}]P_A\left\{[T_{AE}][E_{CO}]\right\} \tag{2.7-23}$$

$$P_2\left\{[E_{CO}]\right\} = P_E\left\{[E_{CO}]\right\} \tag{2.7-24}$$

where P_A may be any one[38] of the excitation constraint operators P_{Am} (m=1,2,3,…) to be defined in Chapter 3.

Error Measure : A measure of the error at the k-th iteration is

$$\Lambda_k = \frac{1}{M}\sum_{m=1}^{M}\left\{ a_w(\theta_m,\phi_m)\left| 10\log\left|E'_{CO}(\theta_m,\phi_m)\right|^2 - 10\log\left|E_{CO}(\theta_m,\phi_m)\right|^2\right|\right\} \tag{2.7-25}$$

This measures the difference between the radiation pattern at the end of the k-th iteration and the radiation pattern that we obtain after applying the pattern constraints to it. In the computation of this error measure we may use many more pattern points (i.e. a larger value of M) than is used in forming the forward and reverse operator matrices in Sections 2.7.4 and 2.7.5. Quantity $a_w(\theta_m,\phi_m)$ is an optional weight that can be used to favour the contribution of certain pattern angles in the calculation of the SDE. Strictly speaking, the SDE of the form (2.7-7) should contain (in this excitation space synthesis case) terms which measure the error according to the difference between the excitation vector $[A]_k$ and its projected forms at each iteration. However, we have found the expression (2.7-25) to be an equivalent and more sensitive measure of what we actually want to achieve, and it is the one that has been used. This will be substantially demonstrated in Chapters 3 and 4.

[38] And only one, in this serial algorithm.

2.7.9 Serial Projection Method in Excitation Space

Recursion Algorithm :

$$[A]_{k+1} = L_1 L_2 [A]_k \tag{2.7-26}$$

$$L_1 \equiv P_1 \tag{2.7-27}$$

$$L_2 \equiv I + r_2(P_2 - I) \tag{2.7-28}$$

Projection Operators :

$$P_1\{[A]\} = P_A\{[A]\} \tag{2.7-29}$$

$$P_2\{[A]\} = [T_{AE}] P_E\{[T_{EA}][A]\} \tag{2.7-30}$$

where P_A may be any one[39] of the excitation constraint operators P_{Am} (m=1,2,3,…) to be defined in Chapter 3.

2.7.10 Parallel Projection Method in Excitation Space

Recursion Algorithm :

$$[A]_{k+1} = [A]_k + r_k \left(\alpha_1 P_1\{[A]_k\} + \alpha_2 P_2\{[A]_k\} + \alpha_3 P_3\{[A]_k\} - [A]_k \right) \tag{2.7-31}$$

with $\alpha_1 + \alpha_2 + \alpha_3 = 1$.

Projection Operators :

$$P_1\{[A]\} = [T_{AE}] P_E\{[T_{EA}][A]\} \tag{2.7-32}$$

$$P_2\{[A]\} = P_{A1}\{[A]\} \tag{2.7-33}$$

$$P_3\{[A]\} = P_{A2}\{[A]\} \tag{2.7-34}$$

It is possible to use more than three constraint projectors (that is, one pattern constraint and more than two excitation constraints.

[39] And only one, in this serial algorithm.

As mentioned in Section 2.7.2 the parallel approach can deal with more than two sets even if these are non-convex. We have written it in the form (2.7-31) to emphasise this. Note that we have assumed that two different types of excitation constraints, denoted by operators P_{A1} and P_{A2}, are being used.

2.7.11 Parallel Projection Method in Pattern Space

We are not aware of the application of the parallel projection method in pattern space. Although we will below write down what the algorithm would be in this case (for two constraint operators, although more could be used), in this thesis we implement the projection method in excitation space and thus will not pursue it further.

Recursion Algorithm :

$$\left[E_{CO}\right]_{k+1} = \left[E_{CO}\right]_k + r_k \left(\alpha_1 P_1 \left\{\left[E_{CO}\right]_k\right\} + \alpha_2 P_2 \left\{\left[E_{CO}\right]_k\right\} - \left[E_{CO}\right]_k\right) \tag{2.7-35}$$

with $\alpha_1 + \alpha_2 = 1$.

Projection Operators :

$$P_1\left\{\left[E_{CO}\right]\right\} = \left[T_{EA}\right] P_A \left\{\left[T_{AE}\right]\left[E_{CO}\right]\right\} \tag{2.7-36}$$

$$P_2\left\{\left[E_{CO}\right]\right\} = P_E\left\{\left[E_{CO}\right]\right\} \tag{2.7-37}$$

2.7.12 Usefulness of the Projection Method for Synthesis with Excitation Constraints

The method of projection is ideally suited to synthesis that requires excitation constraints in addition to pattern constraints. Thus it is suited to situations where phase-only synthesis is required. One advantage is that the process of incorporating constraints through the use of projection operators allows one to explicitly see what is being done in this regard. It is also possible to immediately see what price one has to pay (as far as the pattern performance is concerned) for wanting to impose excitation constraints. It is the synthesis method that will be used in this thesis.

2.8 SELECTION OF STARTING POINTS FOR NUMERICAL SYNTHESIS METHODS

A reasonable estimation of the starting values of the excitations (especially the excitataion phases) is crucial when using the projection method for the excitation synthesis of shaped beams[40]. These values do not need to be precise (otherwise the synthesis would already have been done!). But they must be such as to prevent the projection method from finding itself in a trap[41].

One method that is widely used in all numerical optimization based synthesis methods takes the average of the upper and lower pattern constraint masks[42] at each pattern sampling point and then finds the initial excitations by applying the backward operator. In other words, at each pattern sampling angle (θ_m) we can determine a pattern value given by the average value of the upper and lower mask[43] at that point as

$$E_{CO}(\theta_m) = \frac{1}{2}\left\{S_U(\theta_m) + S_L(\theta_m)\right\} \tag{2.8-1}$$

and then form a pattern vector $[E_{CO}]$ using these sampled values. It would represent a pattern with the same phase at all pattern sampling angles. When this is operated on by the backward operator we will obtain a set of excitations

$$[A] = [T_{AE}][E_{CO}] \tag{2.8-2}$$

that can be used as starting values. This could be used for projection pattern synthesis methods too. The disadvantage of this approach is that we force a particular phase distribution on the radiation pattern from the onset of the iterations, and this can hinder convergence of the synthesis process. One "trick" that sometimes overcomes this is to assign a random phase function or some other phase function based on additional information about the problem. Another possibility is to use the Woodward shaped beam synthesis method mentioned in Section 2.7.6 to find the starting

[40] This is actually true for all numerical optimisation based synthesis techniques mentioned in Sections 2.5 and 2.6 as well. This fact is often not clearly stated in the literature, but one realises it all too soon when attempting to implement such techniques.
[41] Equivalent to a numerical optimization algorithm finding itself stalled at a local optimum.
[42] Shaped beam pattern masks will be discussed in detail in Section 2.9.
[43] The upper and lower pattern masks $S_U(\theta)$ and $S_L(\theta)$ are real quantities.

excitations[44]. But this also suffers from the fact that the starting excitations are determined in a manner that imposes a uniform array pattern phase. Some authors have used variants of Woodward's method, but these significantly complicate the problem. In Section 3.7 we will show how an early continuous aperture distribution synthesis formulation, that is far too crude to be useful in current engineering practice in its own right, can be manipulated to provide excellent starting values for the projection synthesis method that, as stated in Section 2.7.12, is the technique of choice in this thesis.

2.9 SHAPED BEAM PATTERN MASKS

2.9.1 Introductory Remarks

Brief discussions of shaped beam pattern requirements are scattered throughout the literature, and when these are described this is done in a somewhat ad hoc fashion. We therefore thought it worthwhile to come up with a structured way of talking about such patterns, in particular for the three "canonical" shaped beams considered in this thesis - the flat-topped pattern, isoflux pattern and cosecant pattern[45]. We will systematize the process as one of first deciding on the idealised pattern shape (which is non-realisable) and then proceeding to developing from this a pattern mask (which will allow synthesis of a realizable array). Directly implementable forms of such pattern masks do not appear to be written down in the literature reviewed, and so we provide this in the present section. In order to connect this shaped beam material to what most of us are used to, we briefly first state this process for the case of a pencil beam pattern.

2.9.2 Pencil Beam Pattern Mask

In many applications (eg. point-to-point line of sight communications) we wish an antenna to radiate in a single direction and in no other. Such an idealized pencil beam antenna (for which the direction of desired radiation is assumed to be $\theta = 0°$) would have the radiation pattern shown in Fig.2.9-1. It is obviously not possible to obtain an antenna of finite size provide such a

[44] We are of course not suggesting the use of Woodward's method for the overall synthesis problem, since it is not able to enforce sidelobe or excitation constraints.

[45] The techniques we develop to synthesize these cases are applicable to other radiation pattern shapes as well. We have selected the above-mentioned three because we need to validate the methods on specific actual examples, and these three are ones that are used in practice.

pattern. Finite sized pencil beam antennas will have radiation patterns such as that depicted by the solid line in Fig.2.9-2, with the finite width main lobe and sidelobes that we are used to. In order to use synthesis techniques to arrive at array excitations that can provide realistic pencil beam patterns we have to define an upper mask $S_U(\theta)$, such that any radiation pattern point falling below this upper mask will satisfy the required specifications[46]. In the case of a pencil beam pattern this upper mask is the dashed line in Fig.2.9-2.

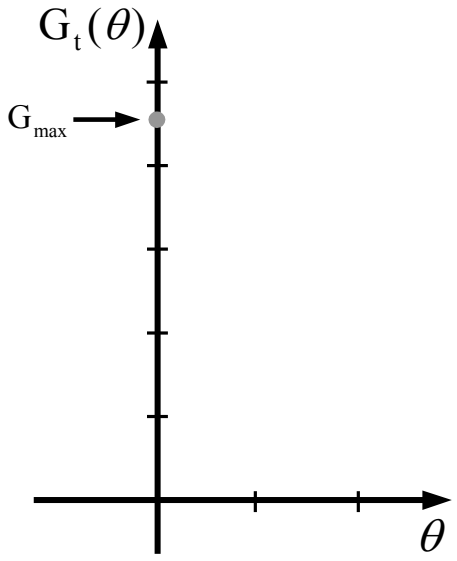

Fig. 2.9-1 : Idealized pencil beam gain pattern.

[46] In the case of the shaped beam patterns a lower mask $S_L(\theta)$ will be required as well, but this is not necessary for the case of a pencil beam.

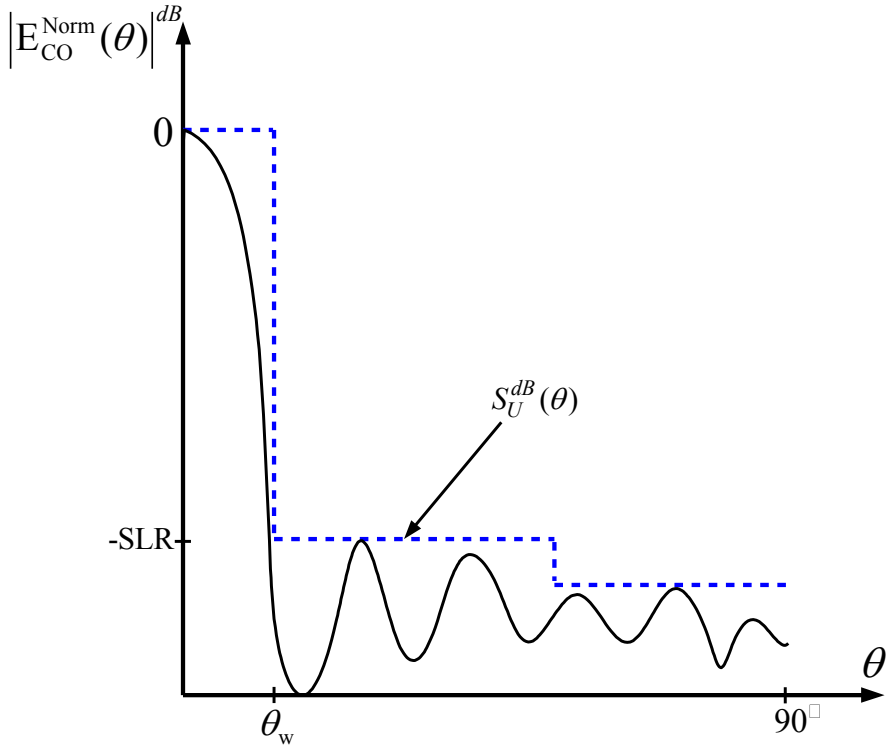

Fig. 2.9-2 : Pattern specification mask for use in the synthesis of pencil beam patterns.

2.9.3 Flat-Topped Beam (Sector Beam) Pattern Masks

The idealized flat-topped beam pattern is illustrated in Fig.2.9-3. We can write this idealized pattern in normalized field form as

$$S_{Ideal}(\theta) = \begin{cases} 0 & -90^o \le \theta \le -\theta_w \\ \sqrt{G(\theta)/G_{max}} = 1 & -\theta_w < \theta \le \theta_w \\ 0 & \theta_w < \theta \le 90^o \end{cases} \qquad (2.9\text{-}1)$$

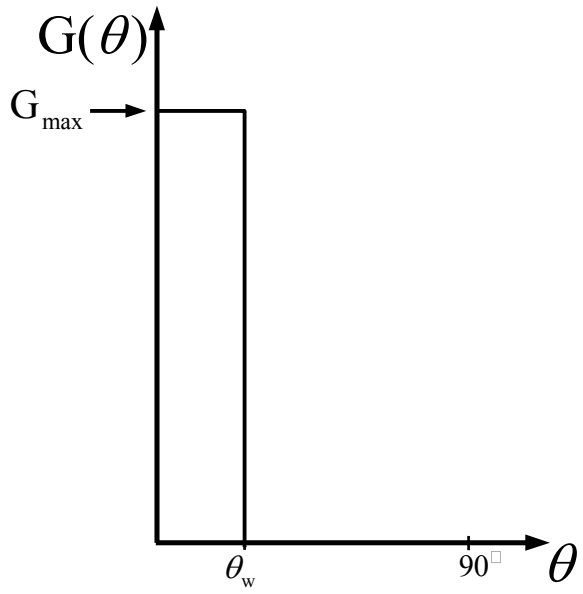

Fig. 2.9-3 : Idealized flat-topped (sector) beam gain pattern.

We know that this idealized pattern is unrealizable. It is necessary to specify pattern masks in order to be able to synthesize a realizable array that will provide a pattern that approximates the flat-top over the main beam region and yet recognizes the presence of sidelobes. Such masks are shown in Fig.2.9-4, expressed in deciBels. They can be written as[47]

$$\mathrm{S}_{\mathrm{U}}^{\mathrm{dB}}(\theta)=\begin{cases}-S_{\mathrm{slr}}^{\mathrm{dB}} & -90^{\mathrm{o}}\le\theta\le-\theta_{w2}\\ 0 & -\theta_{w2}<\theta\le\theta_{w2}\\ -S_{\mathrm{slr}}^{\mathrm{dB}} & \theta_{w2}<\theta\le 90^{\mathrm{o}}\end{cases} \tag{2.9-2}$$

and

$$\mathrm{S}_{\mathrm{L}}^{\mathrm{dB}}(\theta)=\begin{cases}-\infty\,dB & -90^{\mathrm{o}}\le\theta\le-\theta_{w1}\\ -S_{\mathrm{rip}}^{\mathrm{dB}} & -\theta_{w1}<\theta\le\theta_{w1}\\ -\infty\,dB & \theta_{w1}<\theta\le 90^{\mathrm{o}}\end{cases} \tag{2.9-3}$$

where a "- ∞ dB" over some angular region indicates that there is in fact no lower bound over that specific angular region. Quantity $S_{\mathrm{rip}}^{\mathrm{dB}}$ specifies the allowable pattern ripple amplitude over the main beam region, whereas $S_{\mathrm{slr}}^{\mathrm{dB}}$ sets the maximum allowable sidelobe level relative to the main beam

[47] Since the masks are normalized field quantities (as used in this thesis), one can convert to non-dB values using the usual relation $10^{(\text{Value in dB})/20}$.

maximum. More complicated sidelobe level envelopes that might be permitted in some applications are easily incorporated by adjusting the definition for $S_U(\theta)$ for $\theta > \theta_{w2}$.

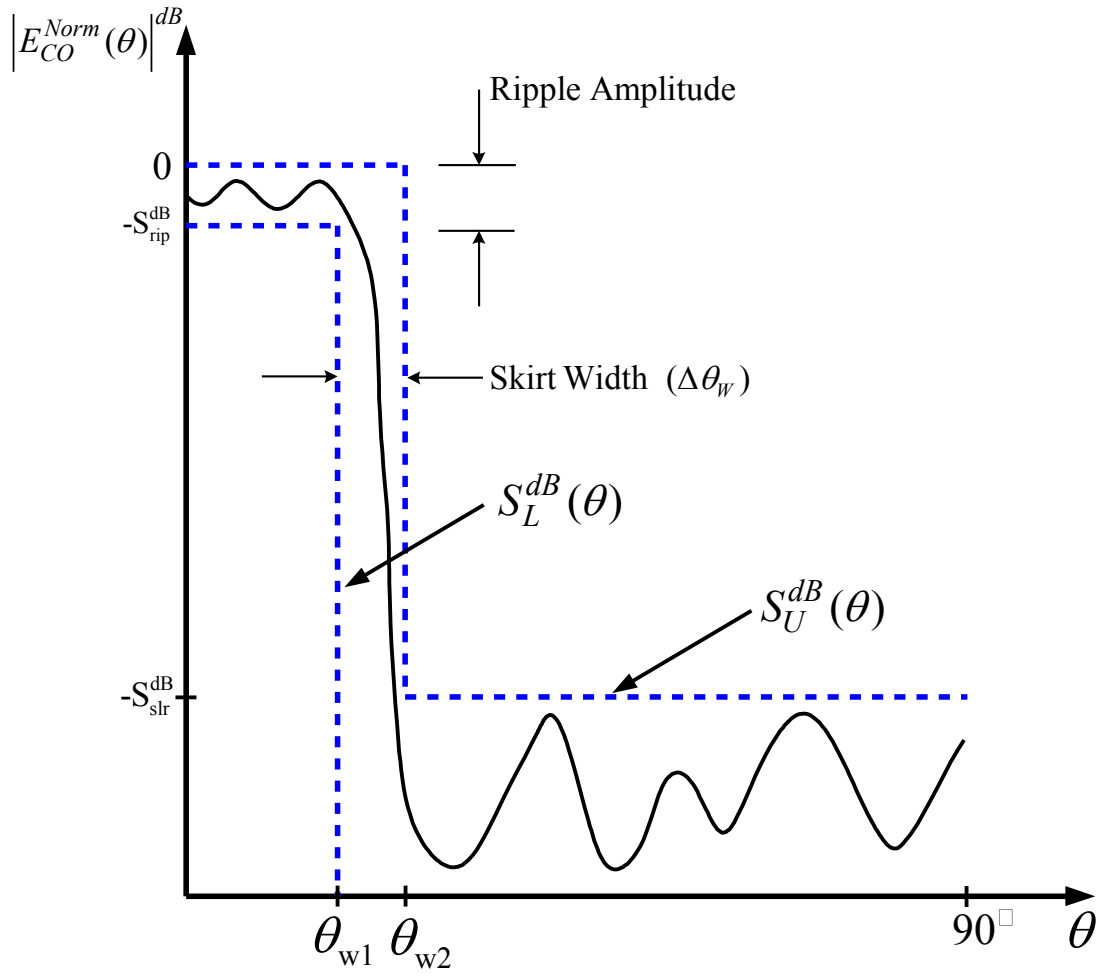

Fig. 2.9-4 : Idealized flat-topped (sector) beam pattern.

2.9.4 Earth-Coverage (Isoflux) Beam Pattern Masks

Earth-coverage or isoflux antennas (which form part of the satellite payload) are those that have a broad pattern which is shaped to give equal field strength at all points on the Earth within some defined field of view (FOV) of the satellite [77]. We refer to Fig.2.9-5, which shows a sketch of a satellite relative to the Earth, albeit not to scale of course. Each point on the Earth will have a different distance to the satellite and so we will denote this distance by $R(\theta)$ to indicate that it is in fact dependent on the angle θ, also shown in Fig.2.9-5.

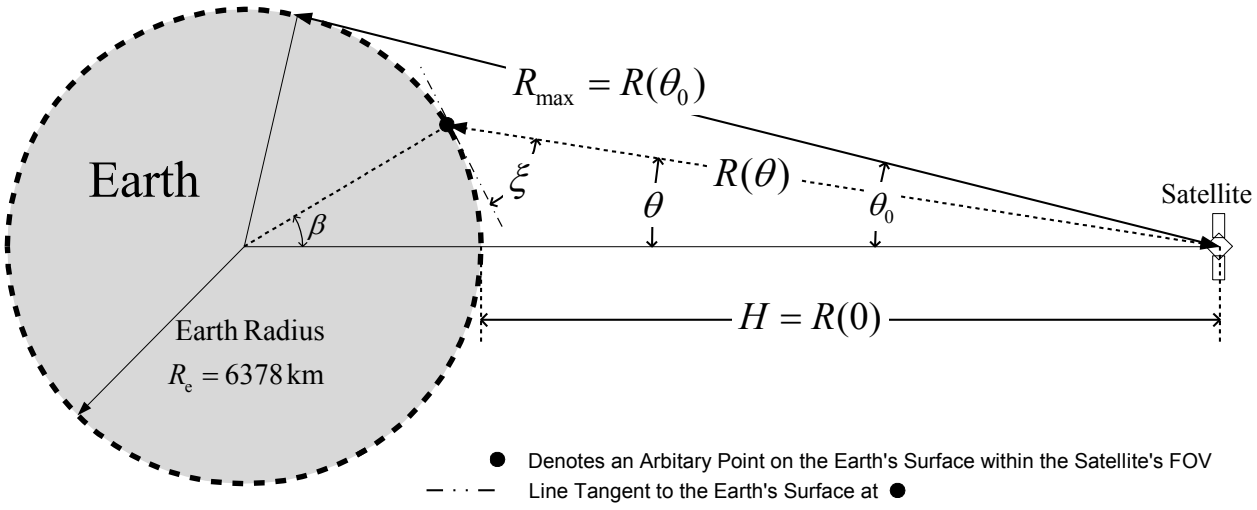

Fig. 2.9-5 : Sketch Illustrating Satellite-Earth Geometry for Derivation of the Shaped Pattern Characteristics Required for an Isoflux Antenna *(Courtesy of D.A.McNamara)*

The power density at a point on the Earth depends on the path length R between that point and the satellite, and on the atmospheric attenuation A along that path. The path length $R(\theta)$ can be determined using the cosine rule to be

$$R = \sqrt{R_e^2 + (R_e + H)^2 - 2R_e(R_e + H)\cos\beta} \tag{2.9-4}$$

which reduces to

$$R = H\sqrt{1 + 4[(R_e / H)^2 + R_e / H]\sin^2(\beta/2)]} \tag{2.9-5}$$

where

$$\beta = 90 - \theta - \xi \tag{2.9-6}$$

and

$$\xi = \cos^{-1}[(1 + H / R_e)\sin\theta] \tag{2.9-7}$$

Angle ξ is the elevation angle of the satellite at the specific point on the Earth within the FOV. It usually has a minimum value ξ_{min}, with atmospheric attenuation precluding use of the

communication link between points on the Earth and the satellite for which $\xi < \xi_{\min}$. This defines the maximum value of θ, namely

$$\theta_{\text{FOV}} = \sin^{-1}[R_e \cos \xi_{\min} /(R_e + H)] \tag{2.9-8}$$

for a point on the Earth at the edge of coverage (EOC), and the Earth-satellite distance is then at its maximum value of $R_{\max} = R(\theta_{\text{FOV}})$. Note that $\theta_{\text{FOV}} \le \theta_0$, with $\theta_0 = \sin^{-1}[R_e /(R_e + H)]$. If the point on the Earth is directly "below" the satellite (the sub-satellite point or nadir direction), so that $\theta = 0^{\text{o}}$, then the Earth-satellite distance is at its minimum value of $H = R(0^{\text{o}})$ that is the orbital height of the satellite. In the case of geostationary (GEO) satellites $H = 35786\,\text{km}$ and hence θ_{FOV} is less than 10°. In the case of low-Earth-orbit (LEO) satellites the EOC angle θ_{FOV} can be more than 60^{o}.

If $U(\theta)$ is the radiation intensity function (that is, the radiation pattern) of the antenna, then the power density at distance $R(\theta)$ from the antenna is $S(\theta) = R^2(\theta)U(\theta)$. In order to have the same power density at all points on the Earth we must have $S(\theta) = S(\theta)\big|_{\theta=0^{\text{o}}}$ for all values of $\theta < \theta_{\text{FOV}}$. If atmospheric attenuation is neglected[48], this implies that

$$\frac{U(\theta)}{R^2(\theta)} = \frac{U(0^{\text{o}})}{R^2(0^{\text{o}})} \tag{2.9-9}$$

which becomes

$$U(\theta) = R^2(\theta)\frac{U(0^{\text{o}})}{H^2} \tag{2.9-10}$$

The directivity function of this antenna is then

$$D(\theta) = \frac{4\pi U(\theta)}{\int_0^{2\pi}\int_0^{\theta_{\text{FOV}}} U(\theta)\sin\theta\, d\theta\, d\phi} = \frac{4\pi U(\theta)}{2\pi \int_0^{\theta_{\text{FOV}}} U(\theta)\sin\theta\, d\theta} = \frac{2R^2(\theta)}{\int_0^{\theta_{\text{FOV}}} R^2(\theta)\sin\theta\, d\theta} \tag{2.9-11}$$

Once the orbital height H and the minimum elevation angle $\xi_{\min}$ have been specified, expression (2.9-13) can be evaluated using numerical integration to give the ideal isoflux directivity pattern.

[48] Inclusion of atmospheric attenuation would be application specific (eg. it would depend on the operating frequency), and could be incorporated in what follows. In Chapter 3 we wish to establish how isoflux-type patterns could be synthesized under excitation constraints. Use of the zero atmospheric attenuation shape derived here will be able to tell how well such methods work with isoflux-type patterns generally.

Although we are considering linear arrays, we earlier explained the applicability of linear array synthesis to practical cylindrical lens antennas, and so use of the physical three-dimensional directivity definition is relevant.

As an implementational detail, we note that the expression (2.9-11) has been evaluated using the Matlab numerical integration routine *QUADL*[49]. Examples of its application are shown in Fig.2.9-6 for two different orbital heights.

[49] The Matlab manual reports that routine QUADL approximates the integral of the integrand function to within an error of 10^{-6} using high-order recursive Labatto adaptive quadrature.

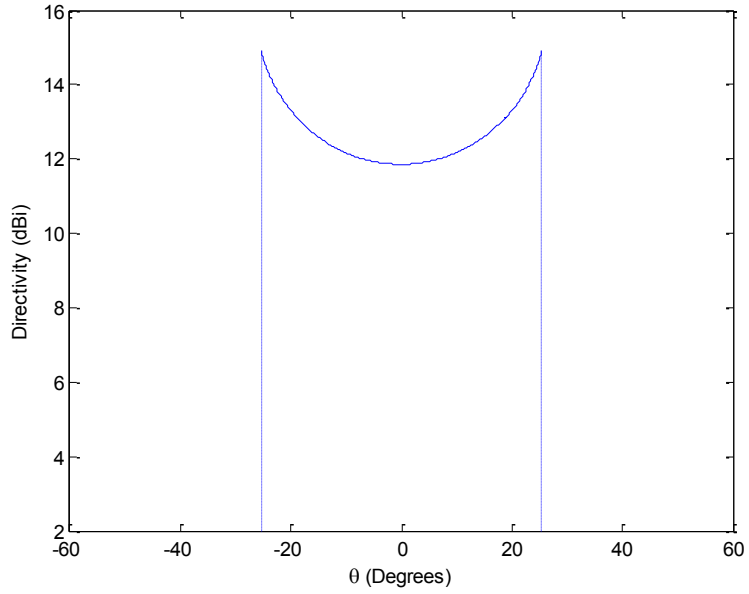

(a)

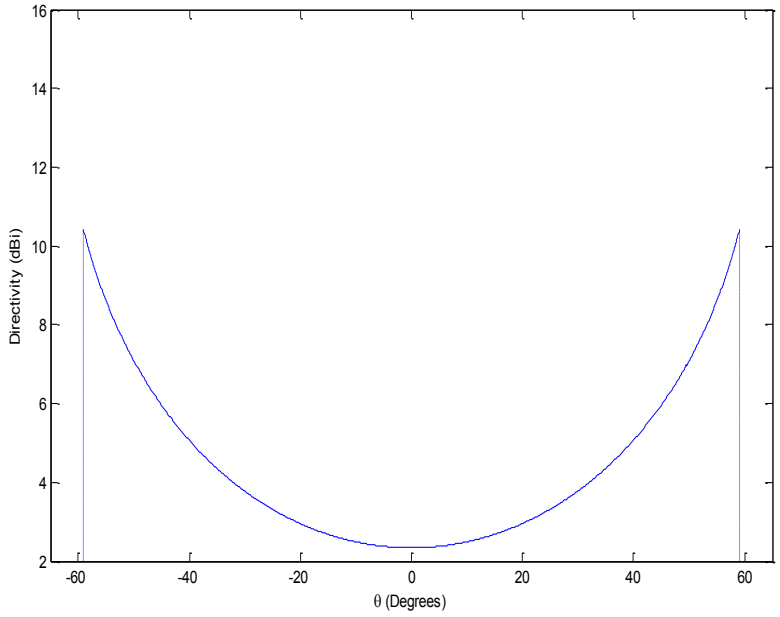

(b)

Fig.2.9-6: (a). Idealised directivity patterns for satellite orbital height 8000km and (b). 800km. The coverage regions are those for which $\xi_{\min} = 15^{o}$, giving $\theta_{\text{FOV}} = 25.4^{o}$ and $\theta_{\text{FOV}} = 59.1^{o}$ in cases (a) and (b), respectively.

The next step is to obtain the normalized field pattern over the field of view as

$$S_{Ideal}(\theta) = \begin{cases} 0 & -90^{o} \le \theta \le -\theta_{FOV} \\ \sqrt{D(\theta)/D(\theta_{FOV})} & -\theta_{FOV} < \theta \le \theta_{FOV} \\ 0 & \theta_{FOV} < \theta \le 90^{o} \end{cases} \qquad (2.9\text{-}12)$$

and of course

$$S^{dB}_{Ideal}(\theta) = 20\log_{10}\left[S_{Ideal}(\theta)\right] \qquad (2.9\text{-}13)$$

In order to perform an excitation synthesis we must use this idealized (but unrealizable) pattern to define a set of upper and lower masks. A normalized field pattern mask is shown in Fig.2.9-7, expressed in deciBels.

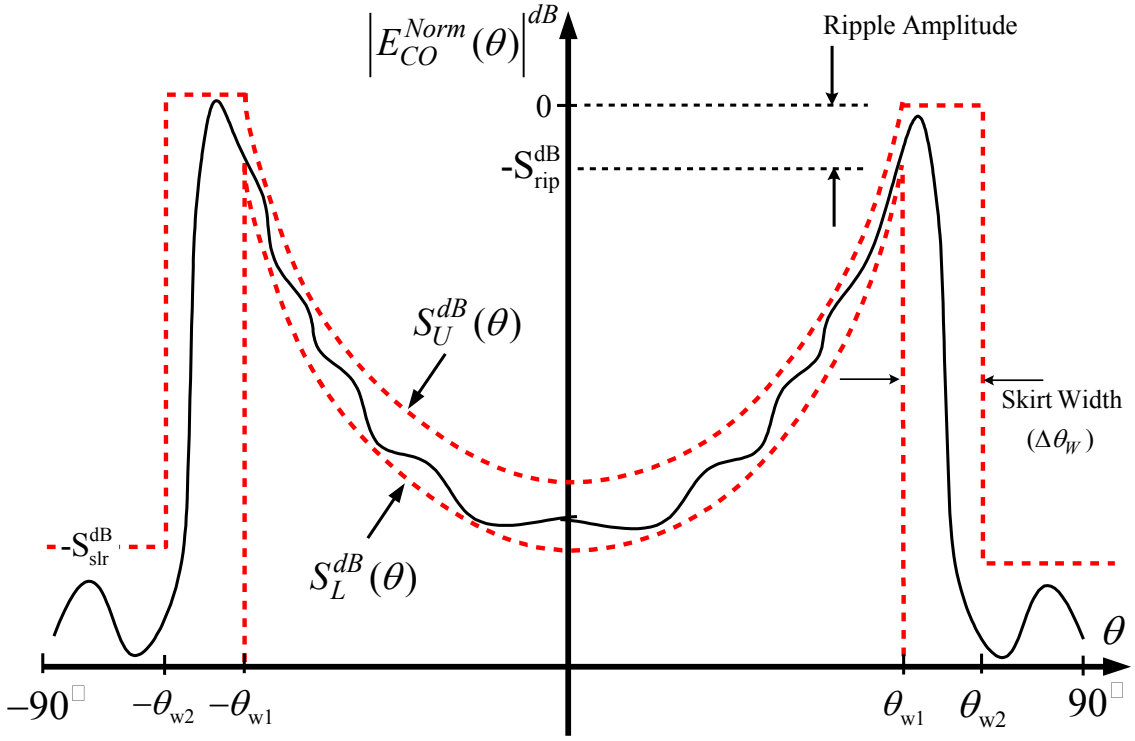

Fig. 2.9-7 : Pattern mask for isoflux pattern. Although the allowable ripple amplitude S^{dB}_{rip} appears to be changing over the angular region $-\theta_{FOV} \le \theta \le \theta_{FOV}$ (note that $\theta_{FOV} = \theta_{w1}$), quantitative inspection would show that this is not actually so.

These masks can be written as

$$\mathrm{S}_{\mathrm{U}}^{\mathrm{dB}}(\theta)=\begin{cases} -S_{\mathrm{slr}}^{\mathrm{dB}} & -90^{\mathrm{o}}<\theta\le-\theta_{w2} \\ 0 & -\theta_{w2}\le\theta\le-\theta_{w1} \\ \mathrm{S}_{\mathrm{Ideal}}^{\mathrm{dB}}(\theta) & -\theta_{w1}\le\theta\le\theta_{w1} \\ 0 & \theta_{w1}<\theta\le\theta_{w2} \\ -S_{\mathrm{slr}}^{\mathrm{dB}} & \theta_{w2}<\theta\le 90^{\mathrm{o}} \end{cases} \tag{2.9-14}$$

and

$$\mathrm{S}_{\mathrm{L}}^{\mathrm{dB}}(\theta)=\begin{cases} -\infty\, dB & -90^{\mathrm{o}}\le\theta\le-\theta_{w2} \\ -\infty\, dB & -\theta_{w2}\le\theta\le-\theta_{w1} \\ \mathrm{S}_{\mathrm{Ideal}}^{\mathrm{dB}}(\theta)-S_{\mathrm{rip}}^{\mathrm{dB}}=\mathrm{S}_{\mathrm{U}}^{\mathrm{dB}}(\theta)-S_{\mathrm{rip}}^{\mathrm{dB}} & -\theta_{w1}\le\theta\le\theta_{w1} \\ -\infty\, dB & \theta_{w1}\le\theta\le\theta_{w2} \\ -\infty\, dB & \theta_{w2}\le\theta\le 90^{\mathrm{o}} \end{cases} \tag{2.9-15}$$

where, as before, a "- ∞ dB" over some angular region indicates that there is in fact no lower bound over that specific angular region. Quantity $S_{\mathrm{rip}}^{\mathrm{dB}}$ specifies the allowable pattern ripple amplitude over the main beam region, whereas $S_{\mathrm{slr}}^{\mathrm{dB}}$ sets the maximum allowable sidelobe level relative to the main beam maximum.

Execution of the synthesis procedure might fail to provide this required pattern shape. It is important to realise that this might not be the fault of the synthesis process. Since the idealized pattern is derived from directivity considerations the "user" of the synthesis procedures might have chosen an array size that is too small or too large. It may be necessary to re-run the synthesis procedure for arrays of different size and examine the trends. As in most cases of antenna engineering one cannot simply "crank the handle". Although synthesis procedures are most useful tools, insight on the part of the designer remains essential.

2.9.5 Cosecant-Squared Beam Pattern Masks

Cosecant-squared beams have been required for air surveillance radars, ground-mapping radars, and wireless networks. We consider the *air surveillance* application first, and refer to Fig.2.6-8 that depicts an airport radar antenna and an approaching aircraft. The radar cross-

section of the aircraft is denoted by σ, the aircraft is assumed to be approaching at a constant height *h*, and the distance between the antenna and the aircraft is R.

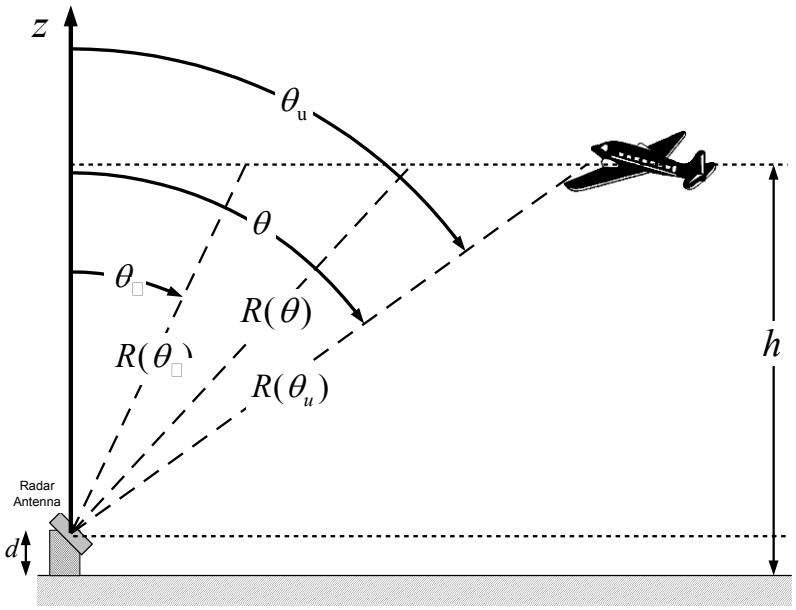

Fig.2.9-8 : Surveillance radar antenna and approaching aircraft.

The well-known radar equation [78] gives the received power P_r at the radar antenna output terminals as

$$P_r = \frac{\sigma \lambda^2 P_t}{(4\pi)^3}\left(\frac{G_t(\theta)}{R^2(\theta)}\right)\left(\frac{G_r(\theta)}{R^2(\theta)}\right) = \frac{\sigma \lambda^2 P_t}{(4\pi)^3}\left(\frac{G_t(\theta)}{R^2(\theta)}\right)^2 \qquad (2.9\text{-}16)$$

In the above equation $G_t(\theta)$ is the gain pattern of the radar antenna as a function of θ, the elevation angle being $(\pi/2-\theta)$. Quantity P_t is the total power delivered to the antenna by the radar transmitter. As it is usually the case, the same antenna is assumed to be used for receiving purposes, so that the gain of the receiving antenna is identical to that of the transmitting antenna, namely $G_r(\theta) = G_t(\theta)$. System designers of such radars often want [78,pp.59-60; 80,pp.170-171] the return signal from the aircraft to be almost constant as it approaches, at least until the aircraft is very close, say over the range of angles $\theta_l \le \theta \le \theta_u$. For this to be so requires that $G_t(\theta)$ be shaped in a way that

$$\frac{G_t(\theta)}{R^2(\theta)} = \frac{G_t(\theta_u)}{R^2(\theta_u)} = \text{Constant} \tag{2.9-17}$$

Since $R(\theta) = (h-d)/\sin(\pi/2-\theta) = (h-d)\,\text{cosec}(\pi/2-\theta)$ this condition can be written as

$$G_t(\theta) = \frac{G_t(\theta_u)}{\text{cosec}^2(\pi/2-\theta_u)}\,\text{cosec}^2(\pi/2-\theta) \tag{2.9-18}$$

If we denote the maximum gain of the antenna by $G_{\max} = G_t(\theta_u)$, and use the fact that $1/\text{cosec}^2(\pi/2-\theta_u) = \sin^2(\pi/2-\theta_u)$, we can rewrite expression (2.9-18) as

$$G_t(\theta) = G_{\max}\sin^2(\pi/2-\theta_u)\,\text{cosec}^2(\pi/2-\theta) = A^2\text{cosec}^2(\pi/2-\theta) \tag{2.9-19}$$

where $A = \sqrt{G_{\max}}\,\sin(\pi/2-\theta_u)$. A sketch of this pattern is shown in Fig.2.9-9. This is an idealized cosecant pattern; it follows the required shape over the angular range $\theta_l \le \theta \le \theta_u$ and is zero elsewhere.

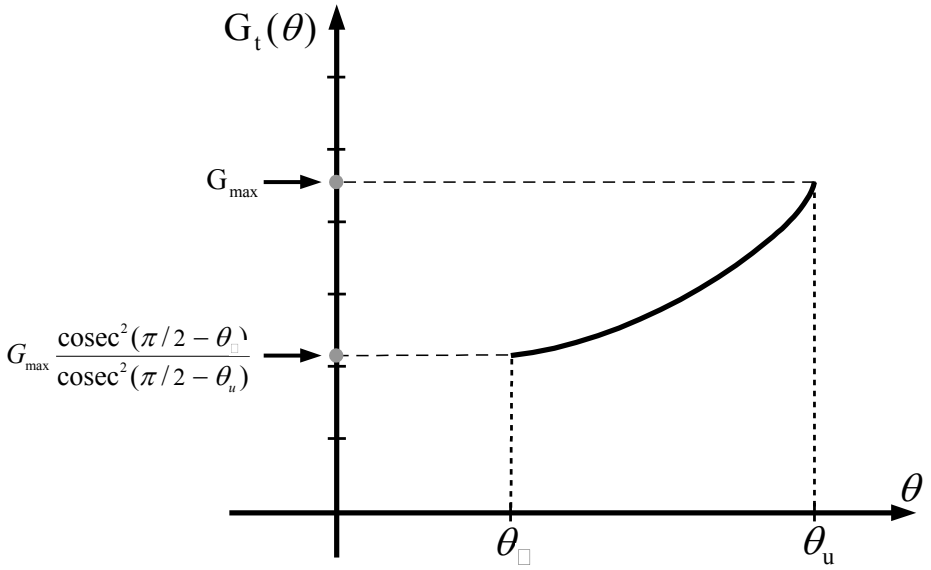

Fig. 2.9-9 : Idealized cosecant pattern for ground-based surveillance radar antenna.

The *wireless network cell* in Fig.2.6-10 is considered next. The Friis transmission equation [78] gives the received power at the receive antenna terminals as

$$P_r = \frac{\lambda^2 P_t G_t(\theta) G_r(\theta)}{(4\pi)^2 R^2(\theta)} \tag{2.9-20}$$

The user receive antennas are low directivity antennas, and in this analysis we assume they are isotropic. This implies that $G_r(\theta) = 1$, and hence that (2.9-20) becomes

$$P_r = \frac{\lambda^2 P_t}{(4\pi)^2} \left(\frac{G_t(\theta)}{R^2(\theta)} \right) \tag{2.9-21}$$

If wireless network designers wish the received signal to be the same at all receive positions in a cell [81] over the range of angles $\theta_l \le \theta \le \theta_u$ then we need $G_t(\theta)$ be shaped such that

$$\frac{G_t(\theta)}{R^2(\theta)} = \frac{G_t(\theta_1)}{R^2(\theta_1)} = \text{Constant} \tag{2.9-22}$$

which at once means that

$$G_t(\theta) = \frac{G_t(\theta_1)}{\text{cosec}^2\theta_1} \text{cosec}^2\theta = \frac{G_{\max}}{\text{cosec}^2\theta_1} \text{cosec}^2\theta \tag{2.9-23}$$

since $R(\theta) = (h-d)\,\text{cosec}\,\theta$. This pattern is sketched in Fig.2.9-10.

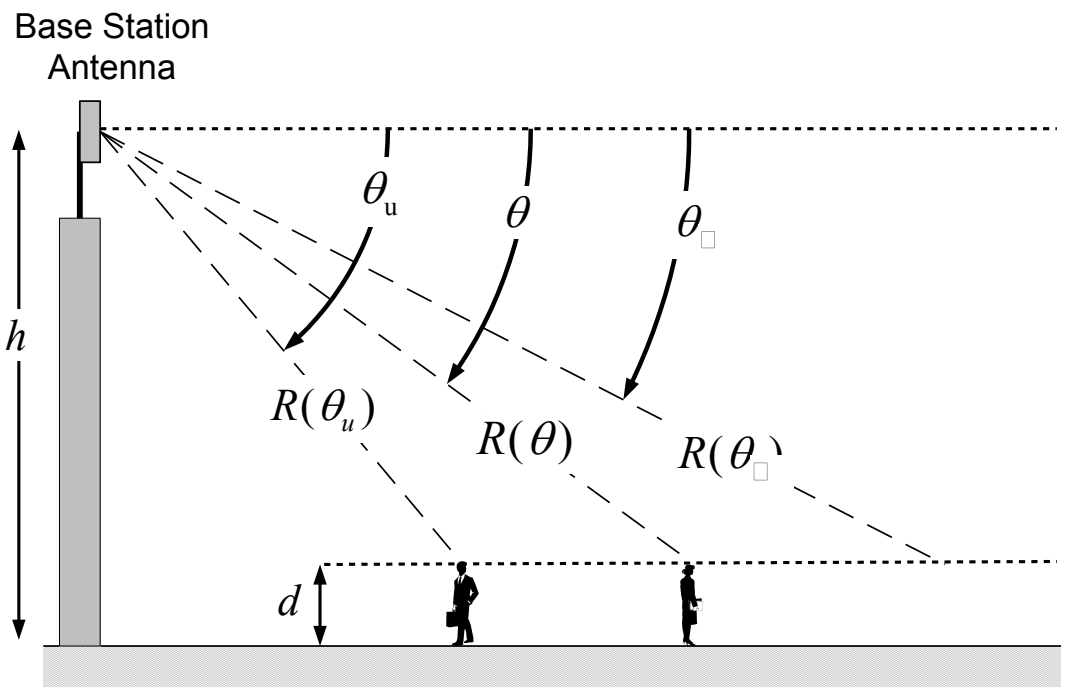

Fig. 2.9-10 : Depiction of a base station antenna, and users at various distances from it, in a wireless network cell. Quantity $R(\theta_l)$ is the range for a user at the cell perimeter, in which direction the base station antenna gain must be at its maximum.

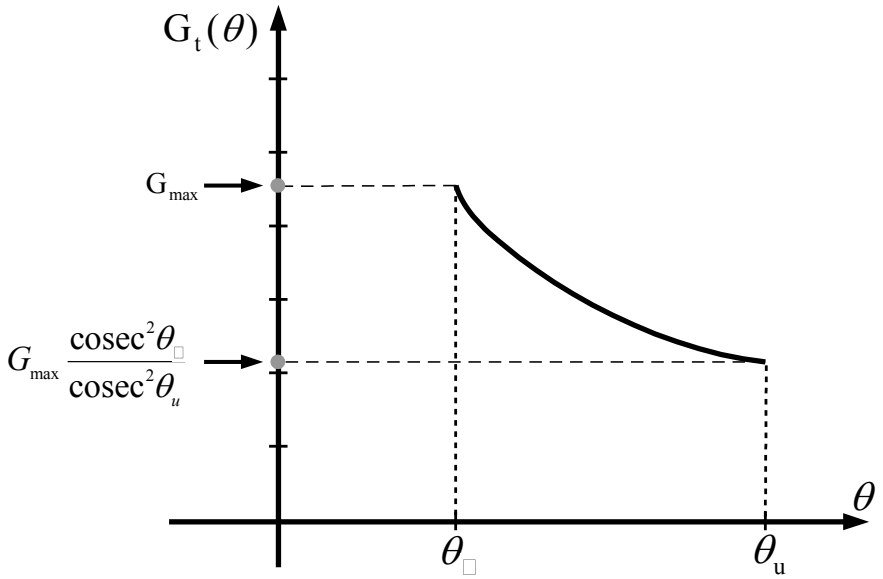

Fig. 2.9-11 : Idealized cosecant pattern for base-station antenna of wireless network cell.

In the above discussions we have implicitly assumed (for the surveillance radar case at least) that the radar cross section of an aircraft is isotropic, and that the ground is flat. In many applications more detailed analysis of the actual scenario may cause systems engineers to specify idealized antenna patterns that are slight perturbations of the above cosecant ones. For instance, in the case of ground mapping radar [79,pp.526] with the antenna on an aircraft the preferred shaped pattern is of the form

$$G_t(\theta) = G_{\max} \frac{\operatorname{cosec}^2\theta \sqrt{\cot\theta}}{\operatorname{cosec}^2\theta_1 \sqrt{\cot\theta_1}} \qquad \theta_1 \le \theta \le \theta_u \tag{2.9-24}$$

Nevertheless the idealized cosecant pattern serves to represent the broad class of patterns of this type. If the synthesis procedure is successful on some pure cosecant pattern it will be so for slight perturbations of this shape as well.

Using (2.9-23) the idealized normalized field pattern over the angular range $\theta_l \le \theta \le \theta_u$ is therefore

$$\mathrm{S}_{\mathrm{Ideal}}(\theta) = \begin{cases} 0 & -90^{\mathrm{o}} \le \theta < \theta_l \\ \sqrt{G(\theta)/G_{\max}} = \dfrac{\operatorname{cosec}\theta}{\operatorname{cosec}\theta_1} = \dfrac{\sin\theta_1}{\sin\theta} & \theta_l \le \theta \le \theta_u \\ 0 & \theta_u < \theta \le 90^{\mathrm{o}} \end{cases} \tag{2.9-25}$$

In order to perform an excitation synthesis we must use this idealized (but unrealizable) pattern to define a set of upper and lower masks. The normalized field pattern mask in this case is shown in Fig.2.9-7, expressed in deciBels. Mathematically it can be expressed as

$$\mathrm{S}_{\mathrm{U}}(\theta) = \begin{cases} -S_{\mathrm{slr}}^{\mathrm{dB}} & -90^{\mathrm{o}} \le \theta \le \theta_1 - \Delta\theta_1 \\ 0 & \theta_1 - \Delta\theta_1 \le \theta \le \theta_1 \\ \mathrm{S}_{\mathrm{Ideal}}^{\mathrm{dB}}(\theta) & \theta_1 \le \theta \le \theta_u \\ \mathrm{S}_{\mathrm{Ideal}}^{\mathrm{dB}}(\theta_u) & \theta_u \le \theta \le \theta_u + \Delta\theta_u \\ -S_{\mathrm{slr}}^{\mathrm{dB}} & \theta_u + \Delta\theta_u \le \theta \le 90^{\mathrm{o}} \end{cases} \tag{2.9-26}$$

and

$$S_L(\theta) = \begin{cases} -\infty & -90^o \le \theta \le \theta_l - \Delta\theta_l \\ -\infty & \theta_l - \Delta\theta_l \le \theta \le \theta_l \\ S^{dB}_{Ideal}(\theta) - S^{dB}_{rip} = S^{dB}_{U}(\theta) - S^{dB}_{rip} & \theta_l \le \theta \le \theta_u \\ -\infty & \theta_u \le \theta \le \theta_u + \Delta\theta_u \\ -\infty & \theta_u + \Delta\theta_u \le \theta \le 90^o \end{cases} \tag{2.9-27}$$

with $S^{dB}_{Ideal}(\theta) = 20\log_{10}\left[S_{Ideal}(\theta)\right]$.

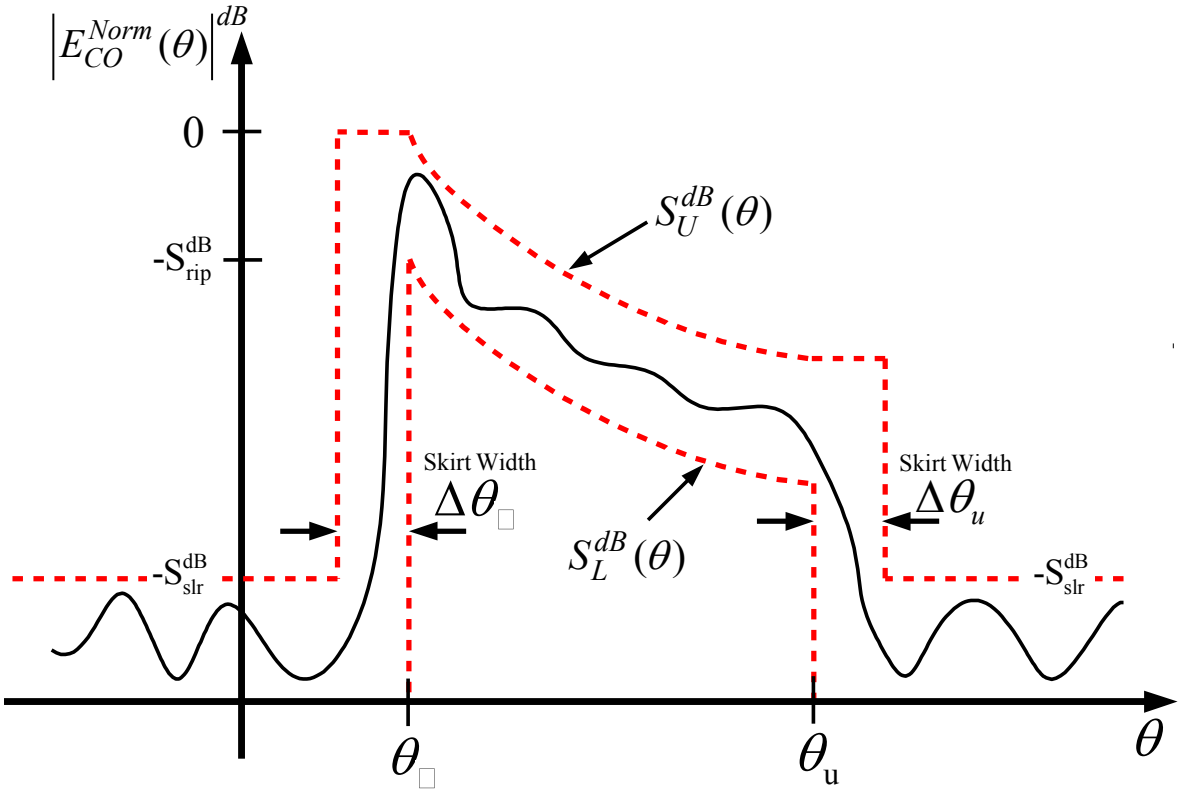

Fig. 2.9-12 : Masks for cosecant pattern. Although the allowable ripple amplitude S^{dB}_{rip} appears to be changing over the angular region $\theta_l \le \theta \le \theta_u$, quantitative inspection would show that this is not so.

2.10 CONCLUSIONS

We began this chapter by recognizing the enormous amount of work that has been published on excitation synthesis in general, but were able to restrict that part of it which we would be reviewing. This was made possible by selecting only those portions that are applicable to what we wish to achieve in this thesis, or were the forerunners upon which such methods are based. It allowed us to classify existing synthesis techniques into four broad classes, namely classical techniques, those based directly on general numerical optimisation algorithms, those that can be formulated as convex programming problems, and ones based on the method of projections. Having argued why generalised projection methods would be used in the present work, we delved into such methods in some detail, in order to lay the groundwork for Chapter 3 and Chapter 4, where these methods are extended and applied to the specific problems at hand.

Although not *the* major contribution of this thesis, this tutorial-like elucidation of the method of projections in a manner that takes it beyond the mathematical framework in which it is usually couched, into an applications-oriented format, does not appear to be available elsewhere. We have also presented, in one place, a systematic derivation and explanation of three specific types of shaped beam, namely sector-beams, isoflux beams and cosecant-squared beams, which are used in practice. This, along with the careful formulation of a way to specify pattern constraints for projection methods that will lead to such beam shapes that has been given, we have not found in other publications.

2.11 REFERENCES FOR CHAPTER 2

[1] R. C. Hansen, *Phased Array Antennas* (Wiley, 1998).

[2] C. A. Balanis, *Antenna Theory* (Wiley, 2005) Fig.6.6.

[3] P. Kildal, "Aperture efficiency and line feed phase center of parabolic cylindrical reflector antenna", IEEE Trans. Antennas Propagat., Vol.32, No.6, pp.553-561, June 1984.

[4] M. Leung, J. S. Kot and B. B. Jones, "Wideband dual polarized line feed development for a cylindrical reflector radio telescope", IEEE Int. AP-S Symp. Digest, pp.1929-1932, 2007.

[5] N. Gagnon, A. Petosa & D. A. McNamara, "Electrically Thin Free-Standing Phase and Amplitude Shifting Surface for Beam Shaping Applications", *Microwave & Optical Technology Letters*, Vol.54, No.7, pp.1566-1571, July 2012.

[6] M. T. Ma, Theory and Application of Antenna Arrays, (John Wiley and Sons, 1974).

[7] D. K. Cheng, "Optimisation techniques for antenna arrays", Proc. IEEE, Vol. 59, pp. 1664-1674, Dec. 1971.

[8] R. L. Pritchard, "Optimum directivity patterns for linear point arrays", J. Acoustical Soc. Amer., Vol.25, No.5, pp. 879-891, Sept.1953.

[9] Y. T. Lo, S. W. Lee and Q. H. Lee, "Optimisation of directivity and signal-to-noise ratio of an arbitrary antenna array", Proc. IEEE, Vol. 54, No. 8, pp. 1033-1045, Aug. 1966.

[10] R. C. Hansen, Chaps.9 & 10. in : A.W.Rudge et.al.(Edits.), *The Handbook of Antenna Design*, Vol.2 (Peter Peregrinus Ltd., 1982).

[11] C. L. Dolph, "A current distribution for broadside arrays which optimises the relationship between beam width and side-lobe level", Proc. IRE, Vol. 34, pp. 335-348, June 1946.

[12] R. C. Hansen, "Fundamental limitations in antennas", Proc. IEEE, Vol. 69, No. 2, pp. 170-182, Feb. 1981.

[13] G. Meinardus, Approximation of Functions : Theory and Numerical Methods (Springer-Verlag, 1967).

[14] R. E. Collin & F. J. Zucker, Antenna Theory, Part I (McGraw-Hill, 1969).

[15] H. J. Riblet, "Discussion on 'A current distribution for broadside arrays which optimises the relationship between beam width and sidelobe level'.", Proc. IRE, Vol. 35, pp. 489-492, June 1947.

[16] R. C. Hansen, “Array pattern control and synthesis”, Proc. IEEE (Special Issue on Antennas), Vol.80, pp.141-151, Jan.1992.

[17] R. C. Hansen (Edit.), Microwave Scanning Antennas Vol.I (Academic Press, 1964).

[18] R. J. Mailloux, Phased Array Antenna Handbook (Artech House, 1994).

[19] R. L. Pritchard, “Optimum directivity patterns for linear point arays”, J. Acoustical Soc. Am., Vol.25, No.5, pp.879-891, Sept.1953.

[20] R. H. DuHamel, “Optimum patterns for endfire arrays”, Proc. IRE, Vol.41, pp.652-659, 1953.

[21] D. A. McNamara, “An Exact Formulation for the Synthesis of Broadside Chebyshev Arrays of 2N Elements with Inter-Element Spacing $d < \lambda/2$”, Microwave & Optical Tech. Letters, Vol.48, No.3, pp.457-463, March 2006

[22] R. J. Stegen, “Gain of Tchebycheff arrays”, IRE Trans. Antennas Propagat., Vol.8, pp.629-631, Nov.1960.

[23] R. C. Hansen, "Aperture efficiency of Villeneuve $\bar{n}$ arrays", IEEE Trans. Antennas Prop., Vol. AP-33, No.6, pp. 668-669, June 1985.

[24] A. T. Villeneuve, "Taylor patterns for discrete arrays", IEEE Trans. Antennas Prop., Vol. AP-32, No. 10, pp.1089-1093, Oct. 1984.

[25] D. A. McNamara, "Generalised Villeneuve $\bar{n}$-distribution", IEE Proc., Vol.136, No.3, pp.245-249, June 1989.

[26] P. M. Woodward, “Method of calculating the field over a plane aperture required to produce a given polar diagram”, J.IEEE, Pt.IIA, Vol.93, pp.1554-1558, 1947.

[27] R. S. Elliott, *Antenna Theory and Design* (Prentice-Hall, 1981).

[28] K. Milne, “Synthesis of power radiation patterns for linear array antennas”, IEE Proc., Pt.H, Vol.134, No.3, pp.285-296, June 1987.

[29] H. J. Orchard, R. S. Eliott, and G. J. Stern, “Optimising the synthesis of shaped antenna patterns”, IEE Proc. Microwave Antennas Propagat., Vol.132, pp.63-68, 1985.

[30] B. D. Carlson & D. Willner, “Antenna pattern synthesis using weighted least squares”, IEE Proc., Vol.139, Pt.H, pp.11-16, Feb.1992.

[31] L. I. Vaskelainen, “Iterative least-squares synthesis methods for conformal array antennas with optimized polarization and frequency properties”, IEEE Antennas Propagat., Vol.45, pp.1179-1185, July 1997.

[32] L. I. Vaskelainen, “Constrained least-squares optimization in conformal array antenna synthesis”, IEEE Antennas Propagat., Vol.55, No.3, pp.859-867, March 2007.

[33] L. I. Vaskelainen, "Phase synthesis of conformal array antennas", IEEE Trans. Antennas Propagat., Vol.48, No.6, pp.987-991, June 2000.

[34] J. F. DeFord and O. P. Gandhi, "Phase-only synthesis of minimum peak sidelobe patterns for linear and planar arrays", *IEEE Trans. Anten. Propag.* **36**(2):191–201 (Feb. 1988).

[35] F. Ares-Pena, "Applications of genetic algorithms and simulated annealing to some antenna problems, in *Electromagnetic Optimization by Genetic Algorithms*, Y.Rahmat-Samii and E. Michielssen (Edits.), pp. 119–155 (Wiley, 1999).

[36] J. M. Johnson and Y. Rahmat-Samii, "Genetic algorithms in engineering electromagnetics", *IEEE Anten. Propag. Mag.* **39**(4):7–21 (Aug. 1997).

[37] R. L. Haupt, "An introduction to genetic algorithms for electromagnetics", *IEEE Anten. Propag. Mag.* **37**(2):7–15 (April 1995).

[38] R. Haupt, "Comparison between genetic and gradient-based optimization algorithms for solving electromagnetics problems", *IEEE Trans. Magn.* **31**(3):1932–1935 (May 1995).

[39] R. L. Haupt, *Antenna Arrays: A Computational Approach* (Wiley, 2010).

[40] R. L. Haupt and D. Werner, *Genetic Algorithms in Electromagnetics* (Wiley, 2007).

[41] R. L. Haupt, "Optimum quantized low sidelobe phase tapers for arrays", *Electron. Lett.* **31**(14):1117–1118 (July 1995).

[42] D. W. Boeringer and D. H. Werner, "Adaptive mutation parameter toggling genetic algorithm for phase-only array synthesis", *Electron. Lett.* **38**(25):1618–1619 (Dec. 2002).

[43] D. W. Boeringer, D. H. Werner, and D. W. Machuga, "A simultaneous parameter adaptation scheme for genetic algorithms with application to phased array synthesis", *IEEE Trans. Anten. Propag*. **53**(1):356–371 (Jan. 2005).

[44] K. K. Yan and Y. Lu, "Sidelobe reduction in array-pattern synthesis using genetic algorithm", *IEEE Trans. Anten. Propag.* **45**(7):1117–1122 (July 1997).

[45] D. Marcano and F. Duran, "Synthesis of antenna arrays using genetic algorithms", *IEEE Anten. Propag. Mag.* **42**(3):12–20 (June 2000).

[46] D. W. Boeringer and D. H. Werner, "Particle swarm optimization versus genetic algorithms for phased array synthesis", *IEEE Trans. Anten. Propag.* **52**(3):771–779 (March 2004).

[47] O. M. Bucci, M. D'Urso & T. Isernia, "Some facts and challenges in array antenna synthesis", 19th Int. Conf. Applied Electromagnetics and Communications (ICECom), Sept.2007.

[48] O. M. Bucci, M. D'Urso & T. Isernia, "Exploiting convexity in array antenna synthesis problems", Proc. IEEE Radar Conf. (RadarCon), Rome, Italy, 2008.

[49] R. R. Kurth, "Optimization of array performance subject to multiple power pattern constraints", IEEE Trans. Antennas Propagat., Vol. AP-22, No.1, pp.103-105, Jan.1974.

[50] O. Einarsson, "Optimization of planar arrays", IEEE Trans. Antennas Propagat., Vol. AP-27, No.1, pp.86-92, Jan.1979.

[51] K. Hirasawa, "The application of a biquadratic programming method for phase-only optimization of antenna arrays", IEEE Trans. Antennas Propagat., Vol. 36, No.11, pp.1545-1550, Nov.1988.

[52] B. P. Ng, M. H. Er and C. Kot, "A flexible array synthesis method using quadratic programming", IEEE Trans. Antennas Propagat., Vol. AP-41, No.11, pp.1541-1550, Nov.1993.

[53] H. Lebret and S. Boyd, "Antenna array pattern synthesis via convex optimization", IEEE Trans. Signal Processing, Vol. AP-45, No.3, pp.526-532, March 1997.

[54] T. Isernia and G. Panariello, "Optimal focusing of scalar fields subject to arbitrary upper bounds", Electronics Letters, Vol.34, No.2, pp.162-164, Jan.1998.

[55] T. Isernia, P. Di Iorio and F. Soldovieri, "An effective approach for the optimal focusing of array fields subject to arbitrary upper bounds", IEEE Trans. Antennas Propagat., Vol. 48, No.12, pp.1837-1847, Dec.2000.

[56] O. M. Bucci, L. Caccavale and T. Isernia, "Optimal far-field focusing of uniformly spaced arrays subject to arbitrary upper bounds in nontarget directions", IEEE Trans. Antennas Propagat., Vol. 50, No.11, pp.1539-1553, Nov. 2002.

[57] R. Torrealba, D. H. Covarubbias and M. Panduro, "Analysis of robustness for convex optimization applied to array antenna pattern synthesis", J. Computer Science, Vol.4, No.12, pp.1036-1041, 2008.

[58] P. Rocca, L. Manica, R. Azaro and A. Massa, "A hybrid approach to the synthesis of subarrayed monopulse linear arrays", IEEE Trans. Antennas Propagat., Vol. 57, No.1, pp.280-283, Jan.2009.

[59] S. Prasad, "Generalized array pattern synthesis by the method of alternating orthogonal projections", IEEE Trans. Antennas Propagat., Vol. AP-28, No.3, pp.328-332, May 1980.

[60] A. Levi & H. Stark, "Image restoration by the method of generalised projections with application to restoration from magnitude", J.Opt.Soc. Am., Pt.A, Vol.1, No.9, pp.932-943, Sept.1984.

[61] G. T. Poulton, "Antenna power pattern synthesis using method of successive projections", Electronics Lett., Vol.22, No.20, pp.1042-1043, Sept.1986.

[62] O. M. Bucci, G. Franceschetti, G. Mazzarella & G. Panariello, "Intersection approach to array pattern synthesis", IEE Proc., Vol.137, Pt.H, No.6, pp.349-357, Dec.1990.

[63] O. M. Bucci & G. D'Elia, "Power synthesis of reconfigurable conformal arrays with phase-only control", IEE Proc.-Microw. Antennas Propag., Vol.145, No.1, pp.131-136, Feb.1998.

[64] E. Botha & D. A. McNamara, "Conformal array synthesis using alternating projections, with maximum likelihood estimation used in one of the projection operators", Electronics Lett., Vol.29, No.20, pp.1733-1734, Sept.1993.

[65] O. M. Bucci, G. D'Elia & G. Romito, "Power synthesis of conformal arrays by a generalised projection method", IEE Proc.-Microw. Antennas Propag., Vol.142, No.6, pp.467-471, Dec.1995.

[66] E. Botha, J. Joubert & D. A. McNamara, "Alternative Formulation & Applications Aspects of the Generalised Projection Method for Array Antenna Synthesis", *International Journal of RF and Microwave Computer-Aided Engineering*, Vol.19, No.6, pp.657-668, Nov.2009.

[67] H. Stark & Y. Yang, *Vector Space Projections : A Numerical Approach to Signal and Image Processing, Neural Nets, and Optics* (Wiley, 1998).

[68] P. L. Combettes, "On the numerical robustness of the parallel projection method in signal synthesis", IEEE Signal Processing Letters, Vol.8, No.2, pp.45-47, Feb.2001.

[69] Y. Censor, N. Cohen, T. Kotzer & J. Shamir, "Summed square distance error reduction by simultaneous multiprojections and applications", Applied Mathematics & Computation, Vol.126, pp.157-179, 2002.

[70] G. Pierra, "Decomposition through formalisation in a product space", *Math. Programming*, Vol.28, pp.96-115, Jan.1984.

[71] T. Swierczynski & D. A. McNamara, "The Solution of 'Switched Element' Array Synthesis Problems Using the Parallel Generalised Projection Algorithm", Microwave & Optical Technology Letters, Vol.40, No.6, pp.465-471, March 2004.

[72] R. J. Marks, "Alternating Projections onto Convex Sets", Chapter 14 in P.A.Jansson (Edit.), Deconvolution of Images and Spectra (Academic Press, 1997) Second Edition.

[73] P. L. Combettes, "Inconsistent signal feasibility problems : Least-squares solutions in a product space", IEEE Trans. Signal Processing, Vol.42, pp.2955-2966, Nov.1994.

[74] IMSL Math Library, Routine *LSGRR*.

[75] Routine *pinv*, MATLAB, The Mathworks Inc., Natick, Massachussetts, USA.

[76] E. Botha, J. Joubert & D .A. McNamara, "The Selection of Starting Points for Array Synthesis Using the Method of Generalised Projections", *URSI* National Radio Science Meeting *Digest*, Boston, Massachusetts, USA, July 2001, p.85.

[77] L. J. Ricardi, "Satellite Antennas", Chapter 36 in : R.C. Johnson, *Antenna Engineering Handbook* (3rd Edition), McGraw-Hill, 1993.

[78] G. Thiele and W. Stutzman, *Antenna Theory & Design* (Wiley, 1998) Chap.8

[79] M. I. Skolnik, *Introduction to Radar Systems* (McGraw-Hill, 1962).

[80] S. Drabowitch, A. Papiernik, H. D. Griffiths, J. Encinas & B. L. Smith, *Modern Antennas* (Springer, 2005) 2nd Edition.

[81] E. Holzman, "Pillbox antenna design for millimeterwave base-station applications", IEEE Antennas & Propagation Magazine, Vol.45, No.1, pp.27-37, Feb.2003.

CHAPTER 3

Modified Method of Projections for Transmission Coefficient Synthesis of Cylindrical Printed Lens Antennas

3.1 GOALS

A number of reasons were identified in Section 1.1 as to why printed lenses for shaped beams have been found to not perform as well as expected. It is believed that if the range of amplitude and phase values of the printed lens element transmission coefficients could be made to satisfy certain constraints then, for reasons of practical implementation, it might be possible to improve such performance. These constraints include the use of a pre-dominantly phase-based synthesis to have less back-scatter from the input surface of the lens. Another possibility is to not require that just any transmission coefficients be dictated by the synthesis process, but only ones that are members of some database. In this chapter we develop a synthesis method that makes such constraints possible. It is based on the method of generalized projections.

Section 3.2 discusses a feed field model needed for the developments in this chapter. In Section 3.3 we derive a forward operator that allows the projection method to operate in the lens element transmission coefficient space; in other words the transmission coefficients are directly the variables in the synthesis process. Section 3.4 gives an appropriate reverse operator. Projection operators that allow a variety of transmission coefficient constraints to be applied are provided in Sections 3.5 through 3.8. Some are adaptations of ones quoted in the existing literature, albeit expressed directly in terms of the transmission coefficient. Those in Sections 3.7 and 3.8 have not been used by others; they are new. Both a serial and a parallel projection synthesis algorithm are stated in Section 3.9. These will be implemented in Chapter 4. A parallel projection algorithm has not yet been used for shaped beam synthesis by anyone; we will demonstrate some of its advantages over the serial form in Section 4.3. We mentioned in Section 2.7 that a reasonable estimation of starting values for the element phases is essential when using the projection method for the synthesis of shaped beams in order to avoid so-called traps. It was also noted that there is no general scheme that will provide such starting points. In Section 3.10

we describe the details of a general method for doing this; this is also not available elsewhere. Section 3.11 provides concluding remarks, and some references are given in Section 3.12.

3.2 MODEL FOR THE NORMALIZED FEED FIELD $E_y^{in}(x_n)$

The background for the discussion of this section has been given in Section 2.3. If we have a specific feed in mind it is always possible to determine $E_y^{in}(x_n)$ through measurement or some detailed electromagnetic model. Here we will adopt an approximate model that is nevertheless realistic, and widely used in studying reflector antennas and reflectarray antennas. It has the advantage that it quite accurately describes realistic feed patterns in the feed main lobe region (which illuminates the printed lens). It is of course not accurate over angular regions far from the feed main lobe. We refer to the situation shown in Fig.3.2-1.

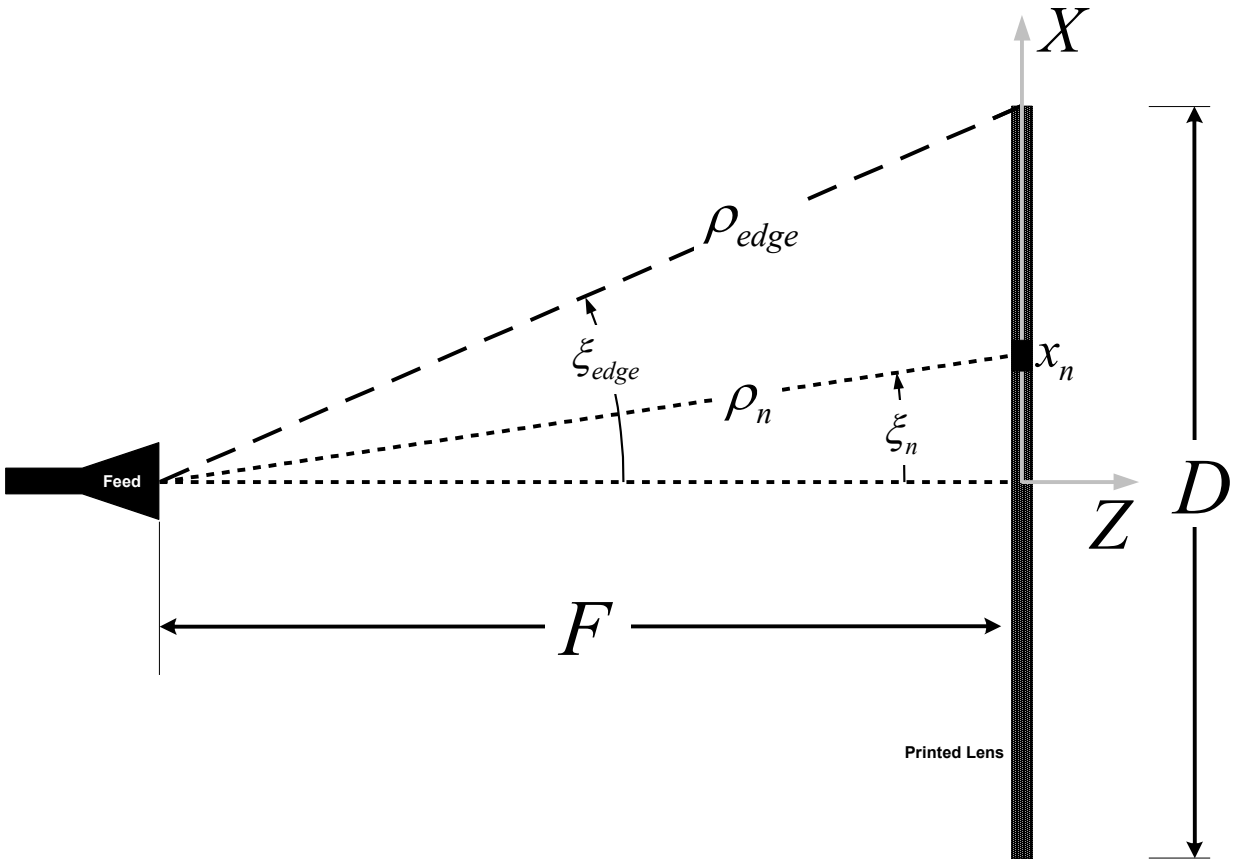

Fig.3.2-1 : Relationship between the feed model and printed lens geometries.

Simple geometry allows us to write

$$\rho_n = \sqrt{x_n^2 + F^2} \tag{3.2-1}$$

$$\xi_n = \tan^{-1}(x_n / F) \tag{3.2-2}$$

$$\xi_{edge} = \tan^{-1}\left\{\frac{D/2}{F}\right\} = \tan^{-1}\left\{\frac{1}{2(F/D)}\right\} \tag{3.2-3}$$

and

$$\rho_{edge} = \sqrt{(D/2)^2 + F^2} \tag{3.2-4}$$

Using a raised-cosine feed pattern model [1], we have

$$E_y(x_n) = \cos^q(\xi_n)\frac{e^{-jk\rho_n}}{\rho_n} \tag{3.2-5}$$

This implies that

$$\left|E_y\right|^{\max} = \frac{1}{F} \tag{3.2-6}$$

and so the normalised feed field on the input surface of the printed lens is

$$E_y^{in}(x_n) = \frac{E_y(x_n)}{\left|E_y\right|^{\max}} = F\cos^q(\xi_n)\frac{e^{-jk\rho_n}}{\rho_n} \tag{3.2-7}$$

If we wish to have a feed illumination taper[50] of C_0 dB say, this means we need to select *m* such that

$$C_0 = -20\log\left|E_y^{in}(D/2)\right| = -20\log\left\{\frac{F}{\rho_{edge}}\cos^q(\xi_{edge})\right\} \tag{3.2-8}$$

[50] This means that, since the normalised feed field on axis is 0 dB, that at the edge of the lens is $-C_0$ dB.

which gives

$$q = \frac{-(C_0 / 20) + \log(\rho_{edge} / F)}{\log\left\{\cos(\xi_{edge})\right\}} \tag{3.2-9}$$

For example, if we have a printed lens with aperture dimension D = 152.4 mm with an $F/D = 0.5$. This means that F = 76.2mm. Thus we have $\xi_{edge} = 45^{o}$ and $\rho_{edge} = 107.76\,\text{mm}$. If we want $C_0 = 10\text{dB}$, then we must have q = 2.4.

If we wish to examine the synthesis process (that follows) without the feed effects we can simply set m = 0 and make F large relative to D. The determination of $E_y^{in}(x_n)$ could be more sophisticated than the raised cosine feed model used here. It could be extracted from the output of a detailed computational electromagnetics model of the feed, or it could be found from a near-field measurement of the feed fields back-projected to the plane with which the printed less input surface eventually coincides.

3.3 FORWARD OPERATOR WITH LENS ELEMENT TRANSMISSION COEFFICIENTS AS SYNTHESIS VARIABLES

Recall that the radiation pattern analysis model in expression (2.2-19) is

$$E_{CO}(\theta) = \sum_{n=1}^{N_e} a_n F_n(\theta) \tag{3.3-1}$$

where

$$F_n(\theta, \phi) = e^{jkx_n \sin\theta} \tag{3.3-2}$$

Using expression (2.3-9) from Section 2.3 that relates the effective complex excitation of the n-th lens element (at the output surface of the lens) to the complex transmission coefficient b_n of the element and the feed field $E_y^{in}(x_n)$ incident on the n-th element (at the input surface of the lens), to the allows us to rewrite (3.3-1) in the form

$$E_{CO}(\theta) = \sum_{n=1}^{N_e} b_n \, E_y^{in}(x_n) F_n(\theta) \tag{3.3-3}$$

A finite-dimensional discrete pattern vector $[E_{CO}]$ can again be obtained by selecting pattern points $\{\theta_1, \theta_2, ..., \theta_m, ...\theta_M\}$ at which $E_{CO}(\theta)$ in (3.3-3) is sampled, giving

$$[E_{CO}] = \begin{bmatrix} E_{CO}(\theta_1) \\ E_{CO}(\theta_2) \\ \bullet \\ \bullet \\ \bullet \\ \bullet \\ E_{CO}(\theta_m) \\ \bullet \\ \bullet \\ \bullet \\ E_{CO}(\theta_M) \end{bmatrix} = [T_{EB}][B] \tag{3.3-4}$$

where in this case

$$[T_{EB}] = \begin{bmatrix} F_1(\theta_1) E_y^{in}(x_1) & F_2(\theta_1) E_y^{in}(x_2) & \bullet & \bullet & F_{N_e}(\theta_1) E_y^{in}(x_{N_e}) \\ F_1(\theta_2) E_y^{in}(x_1) & F_2(\theta_2) E_y^{in}(x_2) & & & F_{N_e}(\theta_2) E_y^{in}(x_{N_e}) \\ \bullet & \bullet & \bullet & & \bullet \\ \bullet & \bullet & & \bullet & \bullet \\ \bullet & \bullet & & & \bullet \\ F_1(\theta_M) E_y^{in}(x_1) & F_2(\theta_M) E_y^{in}(x_2) & \bullet & \bullet & F_N(\theta_M) E_y^{in}(x_{N_e}) \end{bmatrix} \tag{3.3-5}$$

and

$$[B] = \begin{bmatrix} b_1 \\ b_2 \\ \bullet \\ \bullet \\ b_{N_e} \end{bmatrix} \tag{3.3-6}$$

is vector of lens element transmission coefficients.

By defining the new forward operator in (3.3-5) we are now able to use the vector of element transmission coefficients $[B]$ directly in the projection synthesis technique as the synthesis variable. Any constraint projection operators used in the application of the method are now directly constraints on the transmission coefficients, which is what we really want. One "sees" the transmission coefficient amplitudes and phases explicitly. The synthesis process is brought a step closer to the practical design issues. It is possible to examine the effect of the feed pattern beamwidth (in the present model, by changing the value of the index m), and hence the effect of the amplitude and phase taper across the input surface of the lens. One can also observe the influence of the F/D ratio on the range of transmission coefficient values required.

It is understood that the definition of $[T_{EB}]$ implicitly includes normalisation of the resultant pattern vector $[E_{CO}]$.

3.4 REVERSE OPERATOR WITH LENS ELEMENT TRANSMISSION COEFFICIENTS AS SYNTHESIS VARIABLES

The reverse operator will be some generalized inverse of the forward operator, and so we can use the result in Section 2.7.5 to write

$$[T_{BE}] = \left([T_{EB}]^H [W][T_{EB}]\right)^{-1} [T_{EB}]^H [W] \qquad (3.4\text{-}1)$$

which is the same as that used in [2], except here it will map from the pattern space directly to the transmission coefficient space.

3.5 PROJECTION OPERATORS FOR TRANSMISSION COEFFICIENT AMPLITUDE DYNAMIC RANGE RESTRICTIONS

3.5.1 Excitation Amplitude Dynamic Range Restriction

This was extracted from [2], and has already been defined in Section 2.7.8 where, in order to explain the various projection synthesis algorithm types, we needed to define at least one excitation constraint operator in order to show in concrete terms what is meant by such an operator. However, here we write it in terms of the element transmission coefficient vector. In order to be able to easily distinguish between the various transmission coefficient constraint operators we will introduce, we will call the present constraint operator P_{B1}; subsequent operators will be labeled P_{Bm} for m = 2,3,…,7.

Dynamic range is defined as the ratio of the maximum transmission coefficient magnitude to the minimum transmission coefficient magnitude, namely $B_{\max} / B_{\min}$. We will always normalize the transmission coefficient magnitudes before applying the dynamic ratio constraint, and so we will can use $B_{\max} = 1$. Then a projection operator that enforces an amplitude dynamic range constraint ($B_{\min} \le |b_n| \le 1$) on the transmission coefficient vector $[B]$ is

$$P_{B1}\left\{[B]\right\} = \left[b_1', b_2', ..., b_n', ..., b_{N_e}'\right]^T \tag{3.5-1}$$

where[51]

$$b_n' = \begin{cases} b_n & if\ B_{\min} \le |b_n| \le 1 \\ \dfrac{b_n}{|b_n|} B_{\min} & if\ |b_n| < B_{\min} \end{cases} \tag{3.5-2}$$

This class of transmission coefficient constraint does not place any constraint on the transmission coefficient phases. The operation described (3.5-1) can be described in words as follows :

- The transmission coefficient (b_n) of each of the $n = 1, 2, ..., N_e$ elements is examined in turn.

[51] We have shown the bounds as being the same for all elements. They could of course be set such they are dependent on the element index. In other words the bounds could be different for each element. Similar comments can be made for the remaining transmission coefficient constraints that will be discussed.

- If the magnitude of b_n is larger than the maximum value it is set equal to the maximum value, but its phase is left unaltered.
- If the magnitude of b_n lies within the bounds B_{max} and B_{min} then a_n is left unaltered in both amplitude and phase.
- If the magnitude of b_n is smaller than the minimum value it is set equal to the minimum value, but its phase is left unaltered.
- It is understood that, as an integral part of the application of P_{B1} the resultant excitations are always normalized with respect to that which has the largest magnitude.

3.5.2 Excitation Restricted to be Symmetric in Amplitude and Phase

$$P_{B2}\left\{\left[B\right]\right\} = \left[b_1', b_2', ..., b_n', ..., b_{N_e}'\right]^T \tag{3.5-3}$$

where

$$b_n' = \frac{1}{2}\left(b_n + b_{N_e-n+1}\right) \tag{3.5-4}$$

The operation described (3.5-3) can be described in words as follows :

- The complex transmission coefficient of each of the $n = 1, 2, ..., N_e$ elements is obtained by taking the average of each b_n and the transmission coefficient of the corresponding element (namely b_{N_e-n+1}) in the other half of the array.
- This gives a projected set of excitations that is symmetrical in both amplitude and phase.

Expression (3.5-3) is applicable whether the number of array elements N_e is even or odd. We devised this transmission coefficient constraint projection operator because we initially thought it would be needed to ensure symmetry when symmetrical shaped beam patterns are synthesized. In the numerical experiments conducted (to be reported in Chapter 4) we observed that this is not needed if the starting values of the transmission coefficients to be discussed in Section 3.10 are themselves symmetrical. So use of this projection operator was actually not needed; we have nevertheless documented it here for the sake of completeness.

3.5.3 Transmission coefficient Restricted to be Purely Real

$$P_{B3}\left\{\left[B\right]\right\} = \left[b_1', b_2', ..., b_n', ..., b_{N_e}'\right]^T \tag{3.5-5}$$

where

$$b_n' = |b_n| \, sign\{\mathrm{Re}(b_n)\} \tag{3.5-6}$$

where $\mathrm{Re}(b_n)$ means "real part of", and the sign function performs precisely what it's names says, namely take the sign of its argument.

The operation described (3.5-5) can be described in words as follows :

- The magnitude of each complex transmission coefficient is retained.
- The transmission coefficient phase is set to 0° if the phase of b_n is such that $\angle b_n \in (-90^o, 90^o)$.
- The transmission coefficient phase is set to -180° if the phase of b_n is such that $\angle b_n \in (90^o, 270^o)$.
- This gives a projected set of transmission coefficients that is real.

We devised this transmission coefficient constraint projection operator because in the literature review we noticed that real distributions are often required for pencil beam patterns; such a projection operator would be useful if using the synthesis methods described here for pencil beam work. However, we did not utilize this projection operator in the work of this thesis as (with the benefit of hindsight) it is inappropriate for shaped beam synthesis.

3.6 PROJECTION OPERATORS FOR TRANSMISSION COEFFICIENT AMPLITUDE & PHASE RESTRICTIONS

If, as illustrated in Fig.3.6-1, we wish to bound the range of both the amplitude and phase of the transmission coefficients within intervals $[B_{min},1]$ and $[\alpha_{min},\alpha_{max}]$, respectively, then[52]

$$P_{B4}\left\{\left[B\right]\right\}=\left[b_1',b_2',.....,b_n',...,b_{N_e}'\right]^T \tag{3.6-1}$$

where the b_n' are found by applying first the rule

$$\mathrm{b}_\mathrm{n}''=\begin{cases}\left|\mathrm{b}_\mathrm{n}\right|\cos(\angle b_\mathrm{n}-\alpha_{\max})e^{j\alpha_{\max}} & if\ \angle b_\mathrm{n}>\alpha_{\max}\\ \mathrm{b}_\mathrm{n}\ if\ \alpha_{\min}\le\angle b_\mathrm{n}\le\alpha_{\max} & \\ \left|\mathrm{b}_\mathrm{n}\right|\cos(\angle b_\mathrm{n}-\alpha_{\min})e^{j\alpha_{\min}} & if\ \angle b_\mathrm{n}<\alpha_{\min}\end{cases} \tag{3.6-2}$$

followed by the rule

$$\mathrm{b}_\mathrm{n}'=\begin{cases}\mathrm{b}_\mathrm{n}'' & if\ B_{\min}\le\left|\mathrm{b}_\mathrm{n}''\right|\le 1\\ \dfrac{\mathrm{b}_\mathrm{n}''}{\left|b_\mathrm{n}''\right|}B_{\min} & if\ \left|\mathrm{b}_\mathrm{n}''\right|<B_{\min}\end{cases} \tag{3.6-3}$$

Observe that one determines the set of b_n'' first, and then the set of b_n'. In other words the phase constraint is applied first and then the amplitude constraint, The order is important. Swapping them around would not result in a projection onto the correct set of constrained transmission coefficients [3]. The operation described (3.6-1) can be described in words as follows:

- The transmission coefficient (b_n) of each of the $n=1,2,.....,N_e$ elements is examined in turn.
- The phase of each b_n is restrained to the range $[\alpha_{\max},\alpha_{\min}]$.
- The amplitude dynamic range restriction is then applied to the resultant transmission coefficient (namely b_n'') as in Section 3.5.1.

[52] As always, the element excitation magnitudes must be normalized prior to implementation of the constraint rule that follows. Note that this constraint operator was described in [3]; here we express it in terms of the element transmission coefficient vector [B].

- It is understood that, as an integral part of the application of P_{B4} the resultant transmission coefficients are always normalised with respect that which has the largest magnitude.

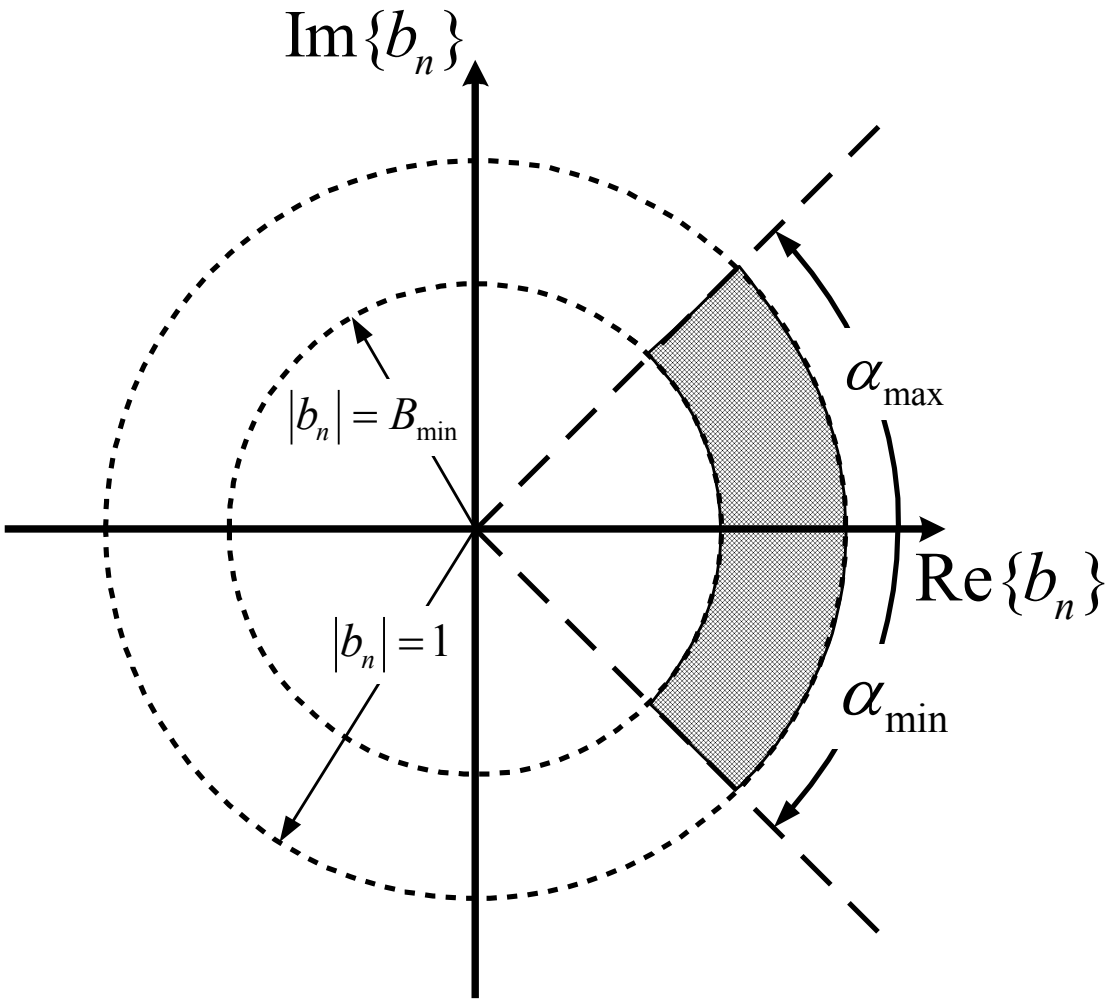

Fig.3.6-1 : Illustration of the Amplitude and Phase Constraint Restriction Operator

3.7 PROJECTION OPERATORS FOR PHASE-ONLY SYNTHESIS

3.7.1 True Phase-Only Synthesis

We have deduced, from the operator describe din Section 3.6, a "phase-only synthesis" constraint operator, namely

$$P_{B5}\left\{\left[B\right]\right\}=\left[b_1',b_2',....,b_n',...,b_{N_e}'\right]^T \tag{3.7-1}$$

where

$$\mathrm{b}_n'=\frac{\mathrm{b_n}}{|b_\mathrm{n}|} \tag{3.7-2}$$

We observe the following:

- The projected (that is, constrained) transmission coefficient amplitudes are all unity. They are not allowed to vary.
- The projected transmission coefficient phases are retained with each projection, and the range of transmission coefficient phase values is not restricted in any way.
- All transmission coefficients are constrained in a homogeneous manner over the array aperture.

The phase-only synthesis of shaped beam patterns has not been described in the literature. In spite of the title of [5] it is not a phase-only synthesis that is described there. In [5] the element amplitudes are not uniform; the "phase-only" phrase in the title indicates that the beam shape is slightly reconfigured using only the element phase values.

3.7.2 True Phase-Only Synthesis with Limited Phase Range

If we not only want to have a uniform transmission coefficient amplitude distribution but also want to bound the phase of the transmission coefficients within intervals $[\alpha_{\min},\alpha_{\max}]$, then the constraint projection operator is

$$P_{B6}\left\{\left[B\right]\right\}=\left[b_1',b_2',....,b_n',...,b_{N_e}'\right]^T \tag{3.7-3}$$

where the b_n' are given by

$$\mathrm{b}_\mathrm{n}''=\begin{cases}|\mathrm{b_n}|\cos(\angle b_\mathrm{n}-\alpha_{\max})e^{j\alpha_{\max}} & if\ \angle b_\mathrm{n}>\alpha_{\max}\\ \mathrm{b_n}\ if\ \alpha_{\min}\le\angle b_\mathrm{n}\le\alpha_{\max} & \\ |\mathrm{b_n}|\cos(\angle b_\mathrm{n}-\alpha_{\min})e^{j\alpha_{\min}} & if\ \angle b_\mathrm{n}<\alpha_{\min}\end{cases} \tag{3.7-4}$$

$$b'_n = \frac{b''_n}{|b''_n|} \qquad (3.7\text{-}5)$$

Observe that one determines the set of b''_n first, and then the set of b'_n, otherwise it will not be a projection operator.

3.8 PROJECTION OPERATOR FOR TRANSMISSION COEFFICIENT CONSTRAINTS SUBJECT TO MEMBERSHIP OF A RESTRICTED DATABASE

When we wish to synthesize a printed lens with a shaped beam we usually set up a database of complex transmission coefficients. Then we separately perform a synthesis to find the required transmission coefficients of each of the cells of the lens. Thereafter we fit the required transmission coefficients to the database values in some "best" way. Here we are proposing an alternative approach, namely that we use our knowledge of the database values as an integral part of the synthesis procedure, rather than completing the synthesis and only then seeing how well we can do (using the database values) as far as achieving these ideal transmission coefficients are concerned. It might be called an "opportunistically based" synthesis method, and is an approach that has not yet been used by others "in the loop" of a synthesis method.

We consider the database to be a set of complex transmission coefficients τ_q, $q = 1, 2, ..., Q$ where usually $Q > N_e$, and assume that only these are available to the lens antenna designer. This set then defines the transmission coefficient space. Suppose that, at the end of some iteration (not necessarily the final iteration) of the projection synthesis method formulated directly in terms of the lens element transmission coefficients, we arrive at a set of "recommended" transmission coefficients $\{b_1, b_2, ..., b_n, ..., b_{N_e}\}$. Precisely these transmission coefficient values are not all available. Only the Q database values are available. We can then map the set $\{b_1, b_2, ..., b_n, ..., b_{N_e}\}$ onto the set of database values. But this must be done using a projection operator; we listed in Section 2.7.2 what properties a projection operator must satisfy. Thus we define a projection operator

$$P_{B7}\{[B]\} = \left[b'_1, b'_2, ..., b'_n, ..., b'_{N_e}\right]^T \qquad (3.8\text{-}1)$$

where the b_n' are found by applying the following set of rules :

- Consider each b_n in turn.
- Search the database to determine the particular τ_q that minimizes $\left|b_n - \tau_q\right|$. In other words,

$$b_n' = \min_{q=1,2,.....,Q} \left|b_n - \tau_q\right| \tag{3.8-2}$$

In other words, the operation (3.8-1) considers each b_n in turn, and sets it equal to the database value τ_q from which its Euclidean distance is the smallest. It is therefore obvious that this is a projection; if we apply such an operation to the result of the projection we get the same result (which is a required property of a projection operator). The simultaneous implementation of amplitude dynamic range and/or phase range constraints is easily done. We simply delete from the database all those values that may not be used. A transmission coefficient constraint projector such as this has not been published elsewhere.

3.9 PROJECTION ALGORITHMS WITH PATTERN AND TRANSMISSION COEFFICIENT CONSTRAINTS

3.9.1 Preliminary Remarks

Projection algorithms acting in the transmission coefficient space were selected rather than in the pattern space. The resulting transmission coefficients then always satisfy the constraints specified for them, whereas we can observe by how much the resulting patterns exceed the pattern masks. This was one of the aims of the thesis, namely to observe what price must be paid as far as pattern performance is concerned when we have restrictions on the lens element transmission coefficients that are desirable to use in practice,

3.9.2 Serial Projection Algorithm

The effort made in presenting the projection method in tutorial form in Section 2.7.9 next allows us to easily write down the serial algorithm (in transmission coefficient space) that will be used in Chapter 4, namely:

Recursion Algorithm

$$\left[B\right]_{k+1} = P_1\left\{P_2\left[B\right]_k\right\} \tag{3.9-1}$$

Projection Operators

$$P_1\left\{\left[B\right]\right\} = P_{Bm}\left\{\left[B\right]\right\} \tag{3.9-2}$$

$$P_2\left\{\left[B\right]\right\} = [T_{BE}]P_E\left\{[T_{EB}][B]\right\} \tag{3.9-3}$$

where P_{Bm} may be any one of the transmission coefficient constraint operators defined in the preceding sections for m = 1,2,3,…,7. Operator P_E was defined in Section 2.7.6.

3.9.3 Parallel Projection Algorithm

Similarly, from Section 2.7.10 we can specify the parallel algorithm (in transmission coefficient space) that will be used in this thesis, namely:

Recursion Algorithm

$$\left[B\right]_{k+1} = (1-r_k)\left[B\right]_k + r_k\left(\alpha_1 P_1\left\{\left[B\right]_k\right\} + \alpha_2 P_2\left\{\left[B\right]_k\right\}\right) \tag{3.9-4}$$

$$\alpha_1 + \alpha_2 = 1 \tag{3.9-5}$$

with the value of α_1 specified, and then α_2 calculated as $\alpha_2 = 1-\alpha_1$. Quantity r_k is the relaxation parameter mentioned in Section 2.7.2.

Projection Operators

$$P_1\left\{\left[B\right]\right\} = [T_{BE}]P_E\left\{[T_{EB}][B]\right\} \tag{3.9-6}$$

$$P_2\left\{\left[B\right]\right\} = P_{Bm}\left\{\left[B\right]\right\} = \left[b_1', b_2', ..., b_n', ..., b_{N_e}'\right]^T \qquad (3.9\text{-}7)$$

3.10 STARTING VALUE ESTIMATION OF THE EXCITATION PHASES FOR PROJECTION SYNTHESIS OF SHAPED BEAM PATTERNS

3.10.1 General Considerations

We explained in Section 2.7 that a reasonable estimation of starting values of the excitation phases is essential when using the projection method for the excitation synthesis of shaped beams. It was also noted that there is no general scheme that will provide such starting points. However, we have in this work found that, for linear arrays, an approximate analytical technique published more than 30 years ago [6,7] can serve this purpose quite satisfactorily. The technique itself was published as a synthesis method in its own right, but would no longer be considered appropriate for excitation synthesis purposes, since it is not able to impose even sidelobe constraints (let alone excitation constraints). Its use as a possible means of obtaining starting points for numerically based synthesis methods has been suggested by others, but no details have been given on how to do this for specific shaped beams. We will demonstrate how it can be used to rapidly provide starting excitation phase values for superior modern synthesis techniques such as the method of projections. It is a good example of how earlier analytical methods can be fruitfully used in novel ways to make modern numerically-based approaches more usable. Whenever a new beam shape is required there is some minor analytical work needed on the part of the engineer. Although this might be considered a disadvantage, the benefit is that one can perform such derivations for a class of beam shapes once, and then very rapidly generate starting phase values for any size array by simply solving a resulting differential equation numerically. We show that this can be easily done using Matlab-based routines irrespective of the array size.

The reader is referred to [6,7] for the background to the method. We will here summarise the procedure, and how we have applied it in this work[53] :

- A continuous linear source of length 2L is assumed to be lying on the x-axis, with $-L \le x \le L$.

[53] The notation used will be that of this thesis rather than that in references [6,7].

• The amplitude distribution along the linear source is denoted by $A(x)$, and is assumed to be known. We have found, through the copious numerical experimentation of which the results in Chapter 4 are a sample, that taking $A(x)=1$ gives suitable starting values for the projection synthesis method to proceed for the three shaped beams considered.

• The goal is to find the phase distribution $\Psi(x)$ along the linear source in order to obtain a radiation pattern described in normalised field form by $F_{norm}(\theta)$ over the angular range $-\pi/2 \le \theta \le \pi/2$.

• Instead of using x and θ directly, the formulation uses normalised coordinates. These are defined as

$$\xi = x/L \qquad -1 \le \xi \le 1 \tag{3.10-1}$$

and

$$u = \sin\theta \qquad -1 \le u \le 1 \tag{3.10-2}$$

• The *first step* is to evaluate

$$g(\xi) = \frac{\int_{-L}^{x} A^2(x)\,dx}{\int_{-L}^{L} A^2(x)\,dx} = \frac{\int_{-1}^{\xi} A^2(\eta)\,d\eta}{\int_{-1}^{1} A^2(\eta)\,d\eta} \tag{3.10-3}$$

where $\eta = x/L$ has been used as a normalised dummy variable.

• The *second step* is to use the ideal required pattern to evaluate

$$h(u) = \frac{\int_{-1}^{u} \left|F_{norm}(\tau)\right|^2 d\tau}{\int_{-1}^{1} \left|F_{norm}(\tau)\right|^2 d\tau} \tag{3.10-4}$$

• The *third step* is to equate $h(u)$ and $g(\xi)$, namely

$$h(u) = g(\xi) \tag{3.10-5}$$

and use this to obtain an expression for variable $u(\xi)$, in other words an expression for the normalised pattern angle u in terms of the normalised position ξ on the linear source.

• The *fourth step* is to use the expression for $u(\xi)$ in the differential equation

$$\frac{d\Psi(\xi)}{d\xi} = -\frac{2\pi}{\lambda} L u(\xi) \qquad -1 \le \xi \le 1 \tag{3.10-6}$$

whose solution gives the required phase distribution $\Psi(\xi)$ of the continuous source. Phase is always a relative quantity, and so without loss of generality we can use

$$\Psi(\xi)\big|_{\xi=0} = 0 \tag{3.10-7}$$

as the "initial condition" . In this thesis the above ordinary differential equation is solved using a variable step Runge-Kutta method as implemented in the MATLAB routine *ODE45* except for the one instance for which the solution can be found in closed form.

• The starting values of the excitation phases for the linear array of discrete elements is then obtained by a simple sampling of the continuous starting phase distribution. It is well-known that such direct sampling of continuous distributions does not provide a linear array with exactly the same pattern as that of the continuous source. Indeed, even if the goal were actually the synthesis of a continuous linear source the approach described here would not be considered sufficient, as inspection of the results in [6,7] would show. But since we simply wish to have a set of "warm" starting values that will be changed by the actual synthesis procedure none of the above two issues need to concern us here. The values of the sampling points x_n, in other words the array element locations, are given in Section 2.3. The phase values $\Psi(x_n)$ at these points are found from the solution of the ordinary differential equation (3.10-6) by evaluating $\Psi(\xi_n)$ with

$$\xi_n = \begin{cases} \left(\text{n-N-}\frac{1}{2}\right)\frac{\text{d}}{\text{L}} & \text{2N Elements} \\ \left(\text{n-N-1}\right)\frac{\text{d}}{\text{L}} & \text{2N+1 Elements} \end{cases} \tag{3.10-8}$$

and

$$x_n = \xi_n L \tag{3.10-9}$$

In what follows we will simply write this as $\Psi(x_n)$.

Finally, the starting transmission coefficient values can be found as $b_n = a_n / E_y^{in}(x_n)$. However, we have found that it is even sufficient to use the starting a_n values directly for the starting values of b_n.

3.10.2 Flat-Topped Patterns : Estimation of the Starting Values of the Excitation Phases

A. Idealized Pattern

Flat-topped pattern constraints were shown in Section 2.6.3. The flat-topped pattern is defined over the range $-u_o \le u \le u_o$, where $u_o = \cos\theta_{w1}$, θ_{w1} is defined in Fig.2.9-4 in Section 2.9.3. The normalized field pattern amplitude is equal to unity over the interval $-u_o \le u \le u_o$ and is zero elsewhere. So we can write the normalized ideal flat-topped beam pattern as

$$F_{norm}(u) = \begin{cases} 0 & -1 \le u < -u_0 \\ 1 & -u_0 \le u \le u_0 \\ 0 & u_0 < u \le 1 \end{cases} \qquad (3.10\text{-}10)$$

B. General Case

Using (3.10-1) the expression (3.10-4) becomes

$$h(u) = \frac{\int_{u_a}^{u} |F_{norm}(\tau)|^2 \, d\tau}{\int_{u_a}^{u_b} |F_{norm}(\tau)|^2 \, d\tau} = \frac{\int_{-u_0}^{u} d\tau}{\int_{-u_0}^{u_0} d\tau} = \frac{u + u_0}{2u_0} \qquad (3.10\text{-}11)$$

and so we can write

$$\frac{u + u_0}{2u_0} = g(\xi) \qquad (3.10\text{-}12)$$

and hence

$$u(\xi) = u_0 \{2g(\xi) - 1\} \qquad (3.10\text{-}13)$$

Expression (3.10-6) then allows us to write the differential equation as

$$\frac{d\Psi(\xi)}{d\xi} = -\frac{2\pi}{\lambda} L u_0 \{2g(\xi) - 1\} \qquad -1 \le \xi \le 1 \qquad (3.10\text{-}14)$$

Using the normalized dummy variable is $\eta = x/L$, we have $A(\eta) = \left|E_y^{in}(\eta)\right|$, with E_y^{in} defined in Section 2.3. Thus

$$g(\xi) = \frac{\int_{-1}^{\xi} \left| E_y^{in}(\eta) \right|^2 d\eta}{\int_{-1}^{1} \left| E_y^{in}(\eta) \right|^2 d\eta} \qquad (3.10\text{-}15)$$

In general this will need to be evaluated numerically during numerical solution of the differential equation for the starting phase distribution $\Psi(\xi)$, since closed-form expressions for E_y^{in} might not be available.

C. Differential Equation for Uniform Amplitude Distribution

If we assume a uniform amplitude over the source, then (3.10-15) gives

$$g(\xi) = \frac{\xi + 1}{2} \qquad (3.10\text{-}16)$$

and (3.10-14) reduces to

$$\frac{d\Psi(\xi)}{d\xi} = -\frac{2\pi}{\lambda} L u_o \xi \qquad -1 \le \xi \le 1 \qquad (3.10\text{-}17)$$

whose solution can be found in closed form to be

$$\Psi(\xi) = -\frac{2\pi}{\lambda} L u_o \left(\frac{\xi^2}{2} \right) \qquad -1 \le \xi \le 1 \qquad (3.10\text{-}18)$$

The starting values of the excitation phase are then $\Psi(x_n)$.

D. Numerical Example

We next show the starting values for an example of an array of $N_e = 32$ elements with a half-wavelength inter-element spacing. As stated in Section 3.10.1, we assume the starting amplitude values are all unity. The starting phase values calculated from (3.10-18) as shown in Fig.3.10-1. Throughout the thesis we will represent phases in the range [-180°,180°], although [0°,360°] could equally well be used. Note that what appears like a sudden jump in the phase values is not actually so. The resulting radiation pattern obtained if we use the starting values as the actual transmission coefficients are as shown in Fig.3.10-2. It clearly does not satisfy the radiation pattern masks, but then it is not expected to do so. Using the said starting values of the

transmission coefficients the projection method is responsible for finding the transmission coefficients that will satisfy the required pattern constraints and transmission coefficient constraints.

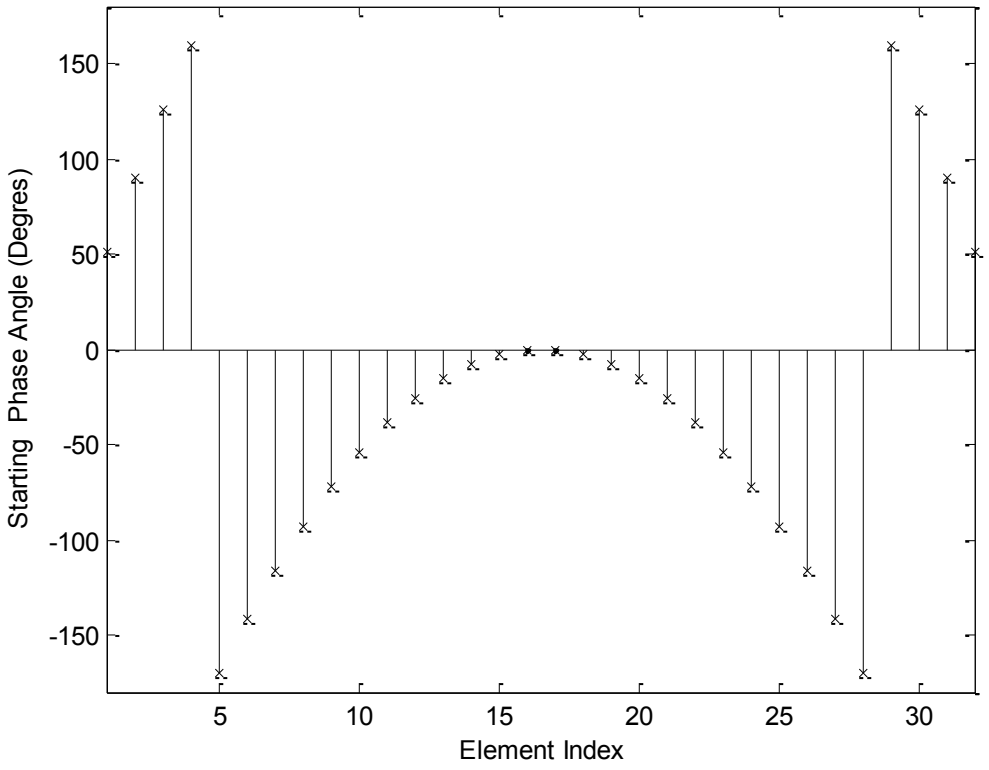

Fig.3.10-1 : Starting Phase of the Excitations for a Flat-Topped Beam Pattern

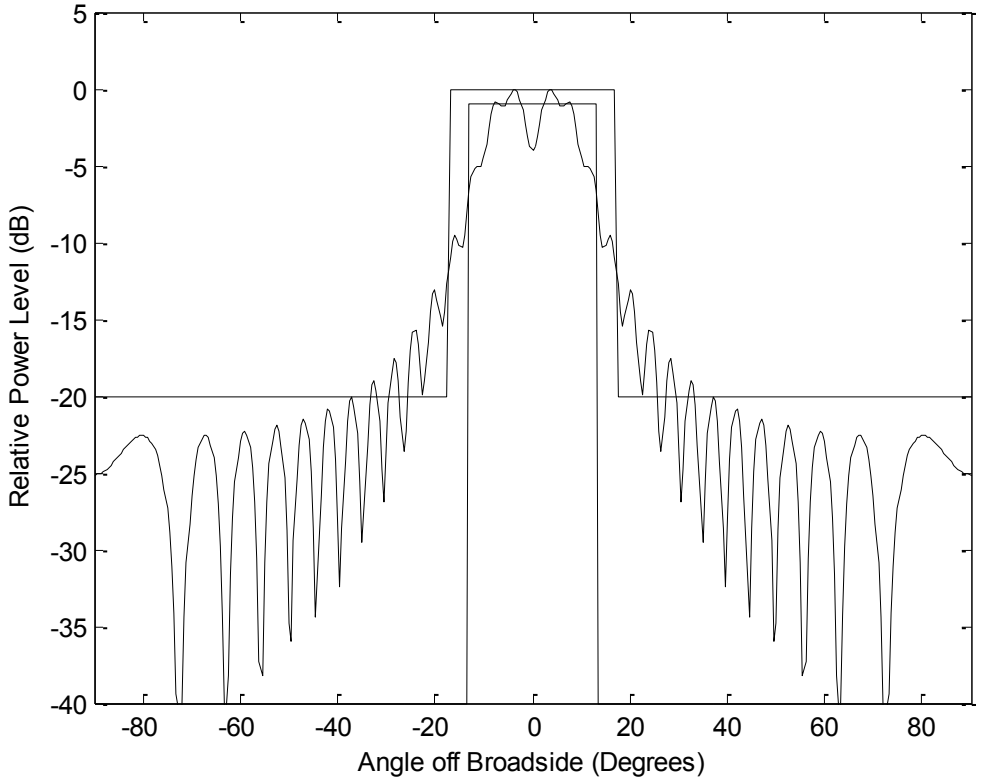

Fig.3.10-2 : Radiation Pattern Using the Excitation Starting Phase Values in Fig.3.10-1

3.10.3 Isoflux Patterns : Estimation of the Starting Values of the Excitation Phases

A. Idealized Pattern

The pattern constraints for this case were explained in Section 2.6.4. The isoflux pattern is defined over the range $-u_o \le u \le u_o$, where $u_o = \cos\theta_{w1}$, with θ_{w1} is defined in Fig.2.9-7 in Section 2.9.4. The normalized field pattern amplitude is equal to unity at u = ± u_o, and is equal to A at u = 0. The precise idealized pattern cannot be written in closed form but must be determined using the recipe provided in Section 2.6.4. We have found that, certainly for the purposes of determining starting excitation phases, the secant function is a sufficiently good approximation to such isoflux patterns derived in this way. So we can write the normalized ideal isoflux beam pattern as

$$F_{norm}(u) = \begin{cases} 0 & -1 \le u < -u_0 \\ A\sec(\alpha u) & -u_0 \le u \le u_0 \\ 0 & u_0 < u \le 1 \end{cases} \qquad (3.10\text{-}19)$$

where[54]

$$\alpha = \frac{1}{u_0}\sec^{-1}(1/A) = \frac{1}{u_0}\cos^{-1}(A) \qquad (3.10\text{-}20)$$

B. General Case

Using (3.10-19) the expression (3.10-4) becomes

$$\frac{\int_{u_a}^{u} |F_{norm}(\tau)|^2 \, d\tau}{\int_{u_a}^{u_b} |F_{norm}(\tau)|^2 \, d\tau} = \frac{\int_{-u_0}^{u} \sec^2(\alpha\tau)\, d\tau}{\int_{-u_0}^{u_0} \sec^2(\alpha\tau)\, d\tau} = \frac{\tan(\alpha u) + \tan(\alpha u_0)}{2\tan(\alpha u_0)} \qquad (3.10\text{-}21)$$

and so we can write

$$\frac{\tan(\alpha u) + \tan(\alpha u_0)}{2\tan(\alpha u_0)} = g(\xi) \qquad (3.10\text{-}22)$$

and hence

$$u(\xi) = \frac{1}{\alpha}\tan^{-1}\left[\{2g(\xi) - 1\}\tan\alpha u_0\right] \qquad (3.10\text{-}23)$$

Use of expression (3.10-6) then results in the differential equation

$$\frac{d\Psi(\xi)}{d\xi} = -\frac{2\pi}{\lambda} L \frac{1}{\alpha}\tan^{-1}\left[\{2g(\xi) - 1\}\tan\alpha u_0\right] \qquad -1 \le \xi \le 1 \qquad (3.10\text{-}24)$$

C. Differential Equation for Uniform Amplitude Distribution

If we assume a uniform amplitude over the source, then $g(\xi)$ is given by (3.10-22) and (3.10-6) becomes

$$\frac{d\Psi(\xi)}{d\xi} = -\frac{2\pi}{\lambda} L \frac{1}{\alpha}\tan^{-1}\{\xi\tan(\alpha u_o)\} \qquad -1 \le \xi \le 1 \qquad (3.10\text{-}25)$$

[54] M.R.Spiegel, *Mathematical Handbook* (McGraw-Hill, 1968) gives $\sec^{-1}\tau = \cos^{-1}(1/\tau)$.

The differential equation (3.10-25) is solved numerically using ODE45 for specific values of x, namely $x = x_n$, to give the starting values $\Psi(x_n)$ of the excitation phases.

D. Numerical Example

The starting values for the same size antenna as that in Part D of Section 3.10.2 is used here as well, and the same comments are appropriate.

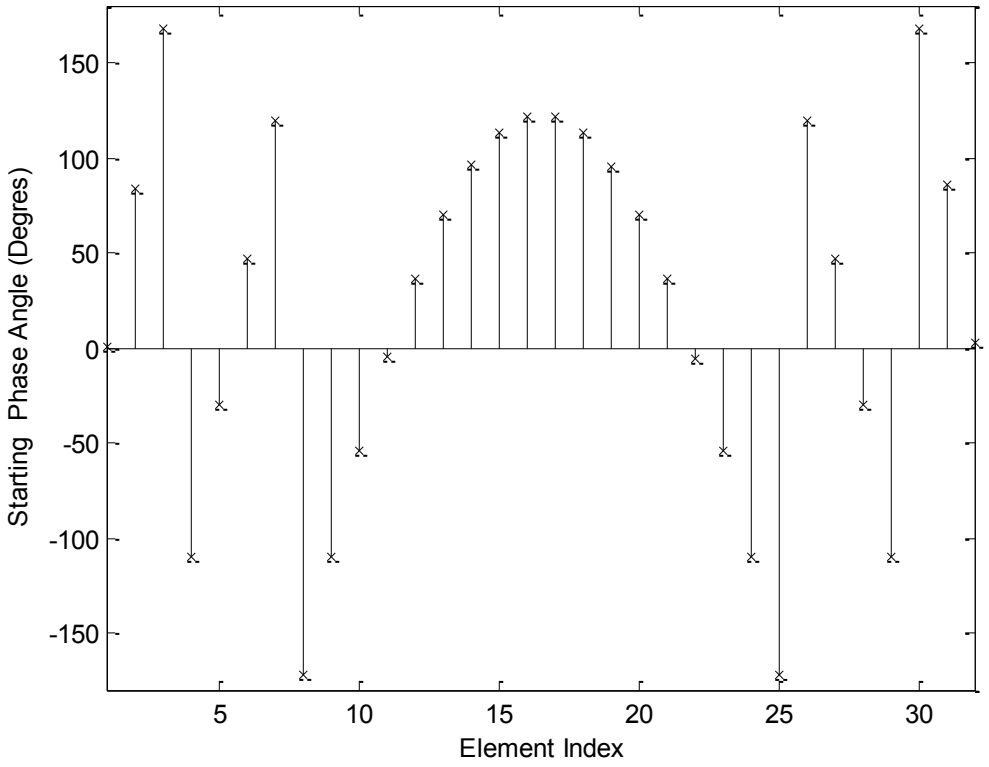

Fig.3.10-3 : Starting Phase of the Excitations for an Isoflux Beam Pattern

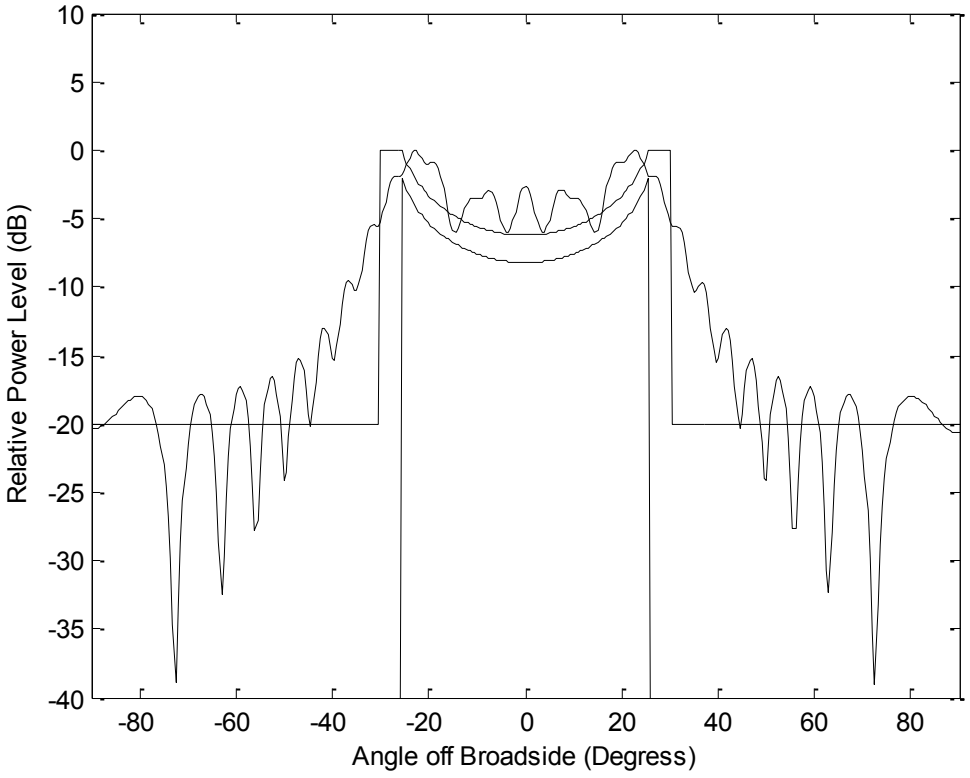

Fig.3.10-4 : Radiation Pattern Using the Excitation Starting Phase Values in Fig.3.10-3

3.10.4 Cosecant Patterns : Estimation of the Starting Values of the Excitation Phases

A. Idealized Pattern

These pattern constraints were discussed at some length in Section 2.6.5. Recall that the ideal beam shape was shown to be $F_{norm}(\theta) = A\,\mathrm{cosec}\,\theta = A/\sin\theta$ over the angular range $\theta_l \le \theta \le \theta_u$ and zero elsewhere. This is shown in Fig.2.9-12. Under the transformation $u = \sin\theta$ this becomes $F_{norm}(u) = A/u$ over the range $u_o \le u \le u_1$ with $u_0 = \sin\theta_l$ and $u_1 = \sin\theta_u$. The normalized field pattern amplitude is unity at $u = u_0$ and hence $A = u_0$, although we will continue to write it as A. The normalized ideal cosecant beam pattern is thus

$$F_{norm}(u) = \begin{cases} 0 & -1 \le u < u_0 \\ A/u & u_0 \le u \le u_1 \\ 0 & u_1 < u \le 1 \end{cases} \qquad (3.10\text{-}26)$$

B. General Case

Using (3.10-26) in expression (3.10-4) yields

$$\frac{\int_{u_a}^{u}\left|F_{norm}(\tau)\right|^2 d\tau}{\int_{u_a}^{u_b}\left|F_{norm}(\tau)\right|^2 d\tau}=\frac{\int_{u_0}^{u}(1/\tau)^2 d\tau}{\int_{u_0}^{u_1}(1/\tau)^2 d\tau}=\frac{\frac{1}{u_0}-\frac{1}{u}}{\frac{1}{u_0}-\frac{1}{u_1}} \qquad (3.10\text{-}27)$$

and so we can write

$$\frac{\frac{1}{u_0}-\frac{1}{u}}{\frac{1}{u_0}-\frac{1}{u_1}}=g(\xi) \qquad (3.10\text{-}28)$$

and hence

$$u=\frac{1}{\frac{1}{u_o}+\left(\frac{1}{u_1}-\frac{1}{u_o}\right)g(\xi)} \qquad -1\le\xi\le 1 \qquad (3.10\text{-}29)$$

Use of expression (3.10-6) then provides the differential equation

$$\frac{d\Psi(\xi)}{d\xi}=-\frac{2\pi}{\lambda}L\frac{1}{\frac{1}{u_o}+\left(\frac{1}{u_1}-\frac{1}{u_o}\right)g(\xi)} \qquad -1\le\xi\le 1 \qquad (3.10\text{-}30)$$

C. Differential Equation for Uniform Amplitude Distribution

If we assume a uniform amplitude over the source, then $g(\xi)$ is given by (3.10-28), and hence (3.10-30) becomes

$$\frac{d\Psi(\xi)}{d\xi}=-\frac{2\pi}{\lambda}L\frac{1}{\frac{1}{u_o}+\left(\frac{1}{u_1}-\frac{1}{u_o}\right)\left(\frac{\xi+1}{2}\right)} \qquad -1\le\xi\le 1 \qquad (3.10\text{-}31)$$

The differential equation (3.10-31) is solved numerically using ODE45 at locations $x = x_n$ to give the starting values $\Psi(x_n)$ of the excitation phases.

D. Numerical Example

The starting values for the same size antenna as that in Part D of Section 3.10.2 is used here as well, and the same comments are appropriate.

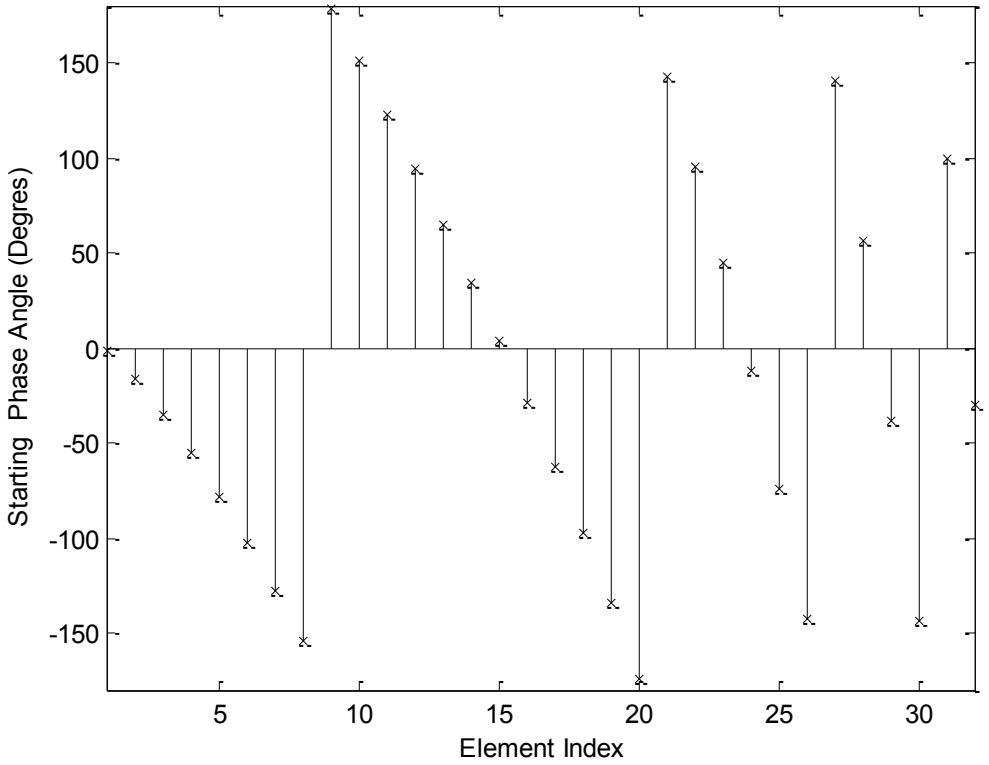

Fig.3.10-5 : Starting Phase of the Excitations for a Cosecant Beam Pattern

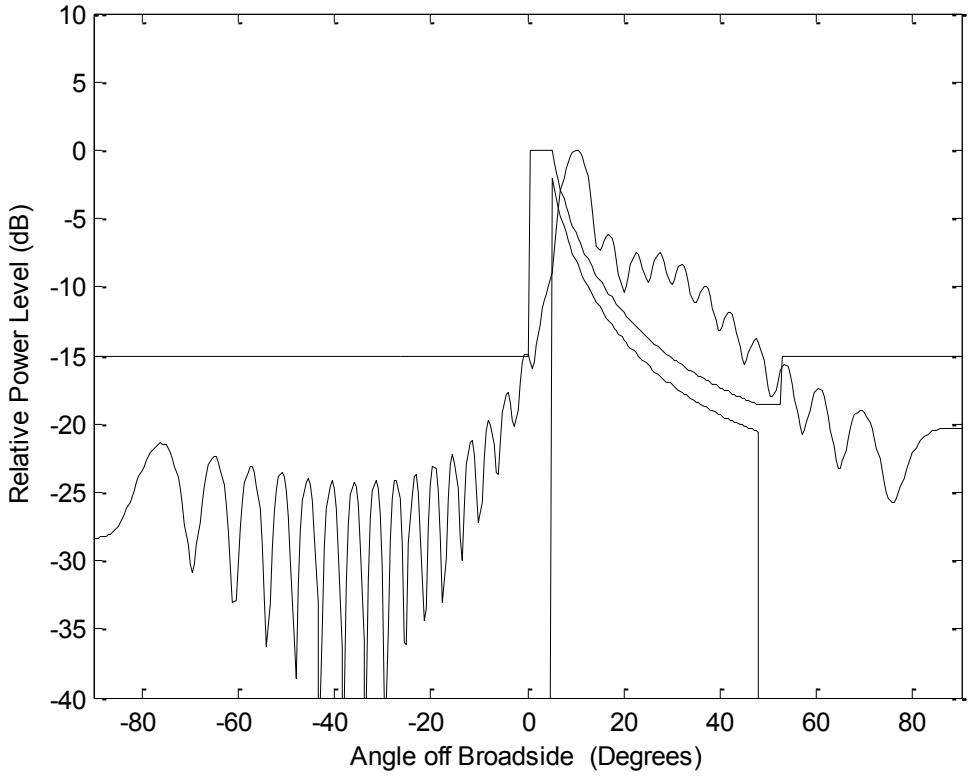

Fig.3.10-6 : Radiation Pattern Using the Excitation Starting Phase Values in Fig.3.10-5

3.11 CONCLUDING REMARKS

The key new contributions offered in this chapter are as follows :

(a). We have developed both serial and parallel projection methods (for the synthesis of shaped beams) that operate in transmission coefficient space. Thus the transmission coefficients of the lens elements are directly the variables in the synthesis process. This was achieved by appropriately defining an altered forward and reverse operator.

(b). We have defined a new projection operator that constrains the transmission coefficient to values that must be selected from a set of available transmission coefficients. This allows what we have referred to as an "opportunistic synthesis". We believe this approach, as straightforward as it appears with hindsight, offers a multitude of possibilities for printed

lens antennas / transmitarrays. Transmission coefficient constraints of any kind can be effectively imposed by simply removing from the database[55].

(c). A very useful approach has been written in structured form for determining the starting points for a shaped beam synthesis via the projection method. Although the possibility of using the approach to find starting excitation phase values has been hinted at in at least one previous publication, details have never actually been given elsewhere. Those provided here should prove helpful to anyone wishing to use projection synthesis methods[56].

3.12 REFERENCES FOR CHAPTER 3

[1] G. Thiele and W. Stutzman, *Antenna Theory & Design* (Wiley, 1998)

[2] E. Botha & D. A. McNamara, "Conformal array synthesis using alternating projections, with maximum likelihood estimation used in one of the projection operators", Electronics Lett., Vol.29, No.20, pp.1733-1734, Sept.1993.

[3] G. Franceschetti, G. Mazzarella & G. Panariello, "Array synthesis with excitation constraints", IEE Proc., Vol.135, Pt.H, No.6, pp.400-407, Dec.1988.

[4] O. M.Bucci, G. Franceschetti, G. Mazzarella & G. Panariello, "Intersection approach to array pattern synthesis", IEE Proc., Vol.137, Pt.H, No.6, pp.349-357, Dec.1990.

[5] O. M. Bucci, G. Mazzarella & G. Panariello, "Reconfigurable arrays by phase-only control", IEEE Trans. Antennas Propagat., Vol.39, No.7, pp.919-925, July 1991.

[6] A. K. Chakraborty, B. N. Das and G. S. Sanyal, "Determination of phase functions for a desired one-dimensional pattern", IEEE Trans. Antennas Propagat., Vol. AP-29, No.3, pp.502-506, May 1981.

[7] A. Chakraborty, B. N. Das and G. S. Sanyal, "Beam shaping using nonlinear phase distribution in a uniformly spaced array", IEEE Trans. Antennas Propagat., Vol.30, pp.1031-1034, Sept.1982.

[55] They of course do not actually have to be removed. Coding statements can simply prevent the constraint projection operator from "seeing" them in the transmission coefficient space. In this way the constraints can be altered without changing the database in anyway. An example is given in Section 4.2.4.

[56] This will be further enhanced using the "trap navigation approach" proposed in Section 4.2.4. It is described there because it was devised while the numerical experiments that are the subject of Chapter 4 were being performed.

CHAPTER 4

Application of the Constrained Transmission Coefficient Synthesis Methods to Shaped Beam Problems

4.1 PRELIMINARY REMARKS

The purpose of this chapter is to implement the formulations developed in Chapter 3. This involved the creation of the appropriate software, which was composed in a MATLAB [1] environment. This will be done for the three shaped beam types of interest, in Sections 4.2, 4.3 and 4.4 respectively. It will be conducted systematically, starting with no transmission coefficient constraints and building up to situations with such constraints. As the transmission coefficient constraints are tightened the given array will be less able to completely satisfy all the required pattern constraints. By beginning with no transmission coefficient constraints we can determine precisely how well the given printed lens can come to the desired beam shape. We will be able to gauge how much such constraints are responsible for our not exactly achieving the shaped patterns we want, and by how much we have to relax these pattern specifications. The penultimate Section 4.5 offers concluding remarks on the chapter, and references are listed in Section 4.6.

Although a wide range of cases have been executed, unless otherwise stated the examples whose results are shown apply to the following cylindrical printed lens antennas:

- D = 152.4 mm, F/D = 0.5, N_e = 32
- D = 191.1 mm, F/D = 0.5, N_e = 40
- D = 1112.7 mm, F/D = 0.5, N_e = 24

at an operating frequency of 30 GHz. We need not specify all the pattern mask parameters in each case (unless some special emphasis is needed) since the masks are included whenever a pattern is plotted.

In order to apply excitation constraints using the projection synthesis method the pattern projection operator described in Section 2.7 is applied, irrespective of the particular pattern mask. The pattern masks for the three canonical shaped beam types of interest in this thesis were discussed in Section 2.6. The SDE used to track the convergence of the projection synthesis

algorithm is that defined in expression (2.7-25). Unless otherwise stated, the serial form of the projection synthesis method should be assumed.

4.2 FLAT-TOPPED PATTERN SYNTHESIS

4.2.1 Synthesis without Constraints on the Transmission Coefficients

If we use $|b_n| = 1$ and $\phi_n = 0^o$ for all elements n = 1 2,3,…..,N_e as the starting values the projection method does not achieve a successful synthesis. However, if we use starting values obtained as described in Section 3.10.2, we obtain the radiation pattern result shown in Fig.4.2-1 below. This can be taken as a reference pattern; we should not expect as perfect a satisfaction of the pattern mask once transmission coefficient constraints are applied. The SDE in Fig.4.2-2 shows that the synthesis converges very rapidly, in fact in less than 20 iterations[57]. The required transmission coefficient amplitudes are depicted in Fig.4.2-3 and Fig.4.2-4, respectively. The pattern mask[58] in this example had an SLR = 20 dB, S_{rip} = 1dB, θ_{w1} = 13° and θ_{w2} = 17° (so that $\Delta\theta_w$ = 4°). We have found the synthesis results relatively insensitive to the specific value of the feed "raised cosine" power between 0 and 3 in the flat-topped beam case, and so have used q = 0.1 throughout.

[57] The SDE should always be monitored. Some problems require many more iterations than others.
[58] Defined in Fig.2.9-4.

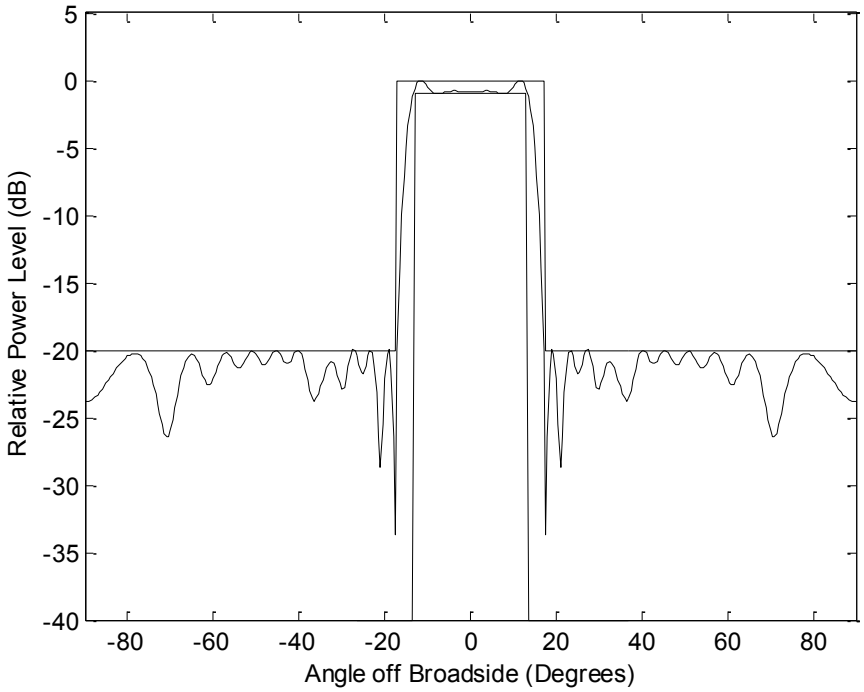

Fig.4.2-1 : Synthesized Flat-Topped Beam Pattern (No Transmission Coefficient Constraints) with $N_e = 32$.

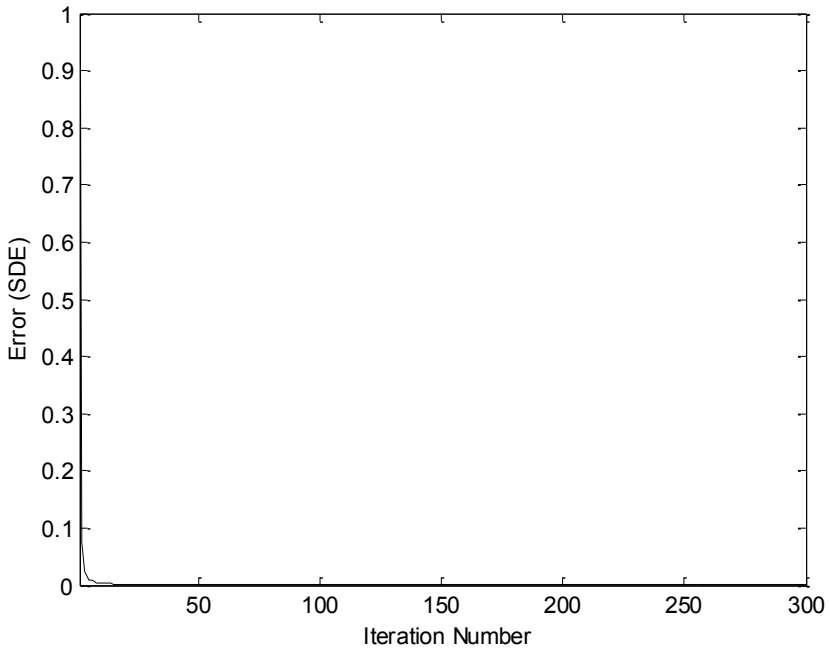

Fig.4.2-2 : SDE for Synthesized Flat-Topped Beam Pattern (No Transmission Coefficient Constraints) with $N_e = 32$.

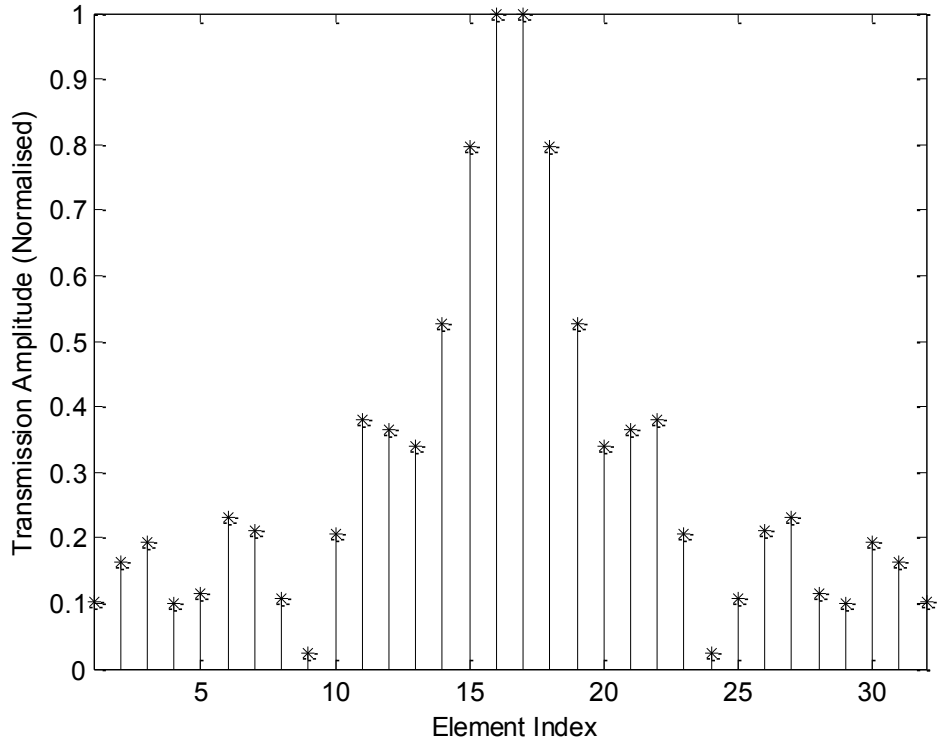

Fig.4.2-3 : Transmission Coefficients Amplitudes of the Synthesized Flat-Topped Beam Pattern (No Transmission Coefficient Constraints) with $N_e = 32$.

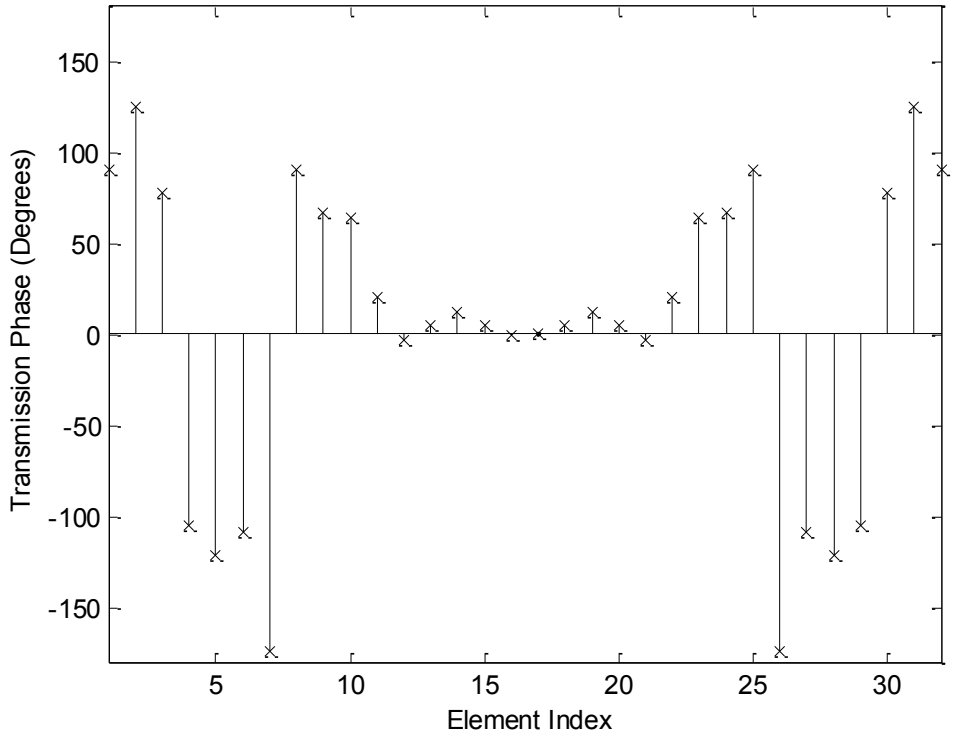

Fig.4.2-4 : Transmission Coefficients Phase of the Synthesized Flat-Topped Beam Pattern (No Transmission Coefficient Constraints) with $N_e = 32$.

In light of the apparent ease with which the 32-element lens is able to satisfy the pattern constraints, the designer might wish to know whether a smaller lens might not be able to perform just as well. If we consider a smaller cylindrical printed lens with aperture dimension D = 112.7 mm and $F/D = 0.5$, composed of N_e = 24 elements[59] we obtain the radiation pattern in Fig.4.2-5. One might be tempted to decide on this lens instead of the larger one. However, we will see that when transmission coefficient constraints are applied in what follows the performance of this smaller lens will suffer more since it has fewer degrees of freedom. What if we increase the lens size to D = 191.1 mm and $F/D = 0.5$, with N_e = 40 elements? The radiation pattern in Fig.4.2-6 is now possible. A lens of this size, with an increased number of degrees of freedom, is clearly able to provide a smaller S_{rip} in the shaped beam region and still give maximum sidelobes of 20dB. Some of these "spare" degrees of freedom might be used in accommodating transmission coefficient constraints.

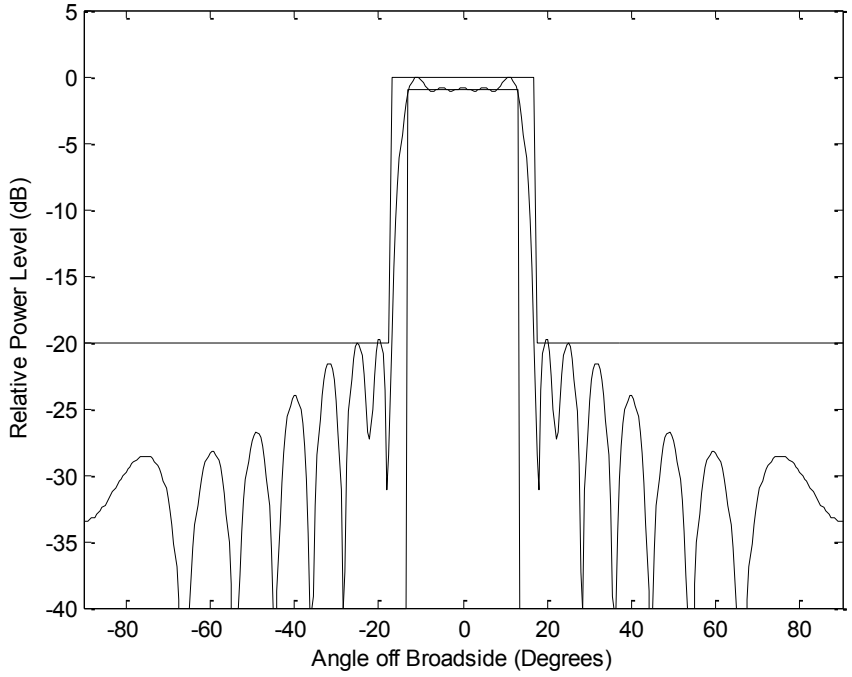

Fig.4.2-5 : Synthesized Flat-Topped Beam Pattern (No Transmission Coefficient Constraints) with N_e = 24.

[59] If the number of elements changes a new set of starting values for the transmission coefficients must of course be calculated. This is routine for any type of shaped beam if we use the method described in Section 3.10.

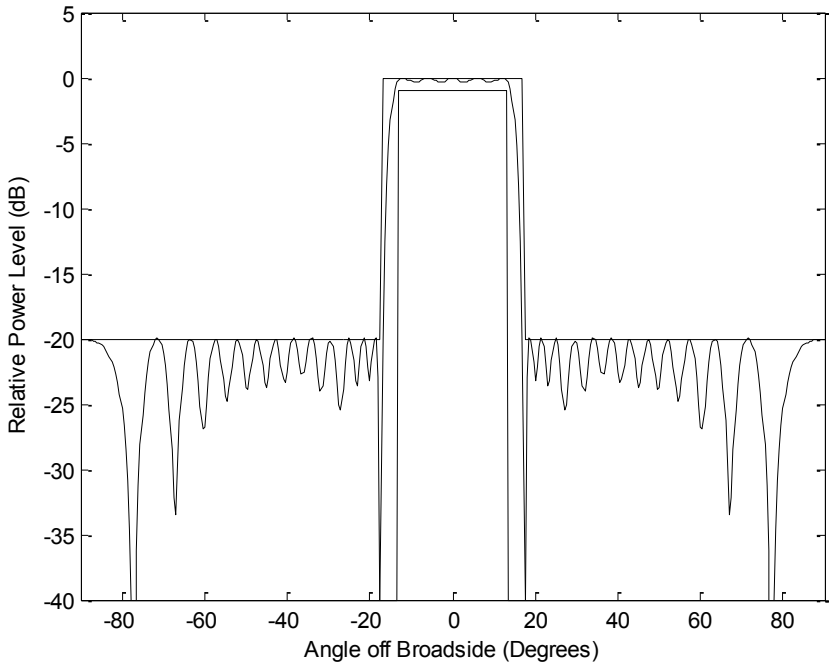

Fig.4.2-6 : Synthesized Flat-Topped Beam Pattern (No Transmission Coefficient Constraints) with $N_e = 40$.

4.2.2 Synthesis with Constraints on the Transmission Coefficient Amplitude

We next impose a constraint on the amplitude of the transmission coefficients ($|b_n|$), namely $-1dB \le |b_n| \le 0dB$. The resulting pattern in Fig.4.2-7 is clearly not able to fit inside the mask; this is the price to pay for the severe dynamic range restriction on $|b_n|$. This inability to satisfy the pattern mask constraints is evident from the SDE plot in Fig.4.2-8; additional iterations do not improve the situation. The transmission coefficient amplitudes and phases are shown in Fig.4.2-9 and Fig.4.2-10.

The designer might then wonder how the pattern might be improved in spite of the dynamic range restriction on $|b_n|$. One possibility is clearly to relax it to say $-3dB \le |b_n| \le 0dB$. The improved pattern is shown in Fig.4.2-11. Note from Fig.4.2-12 that the wider range of $|b_n|$ values has been exploited by the synthesis method.

Another design variable that could be tried is the lens size (or equivalently number of elements). Results for $N_e = 40$ and $N_e = 24$ elements are shown in Fig.4.2-13 and Fig.4.2-14,

respectively. We notice that the $N_e = 40$ lens more closely fits the pattern mask than the $N_e = 32$ case in Fig.4.2-7; it has used its additional degrees of freedom to do so. The $N_e = 24$ lens, on the other hand, exceeds the mask quite markedly, in spite of its good performance in Fig.4.2-5 when there were no transmission coefficient constraints.

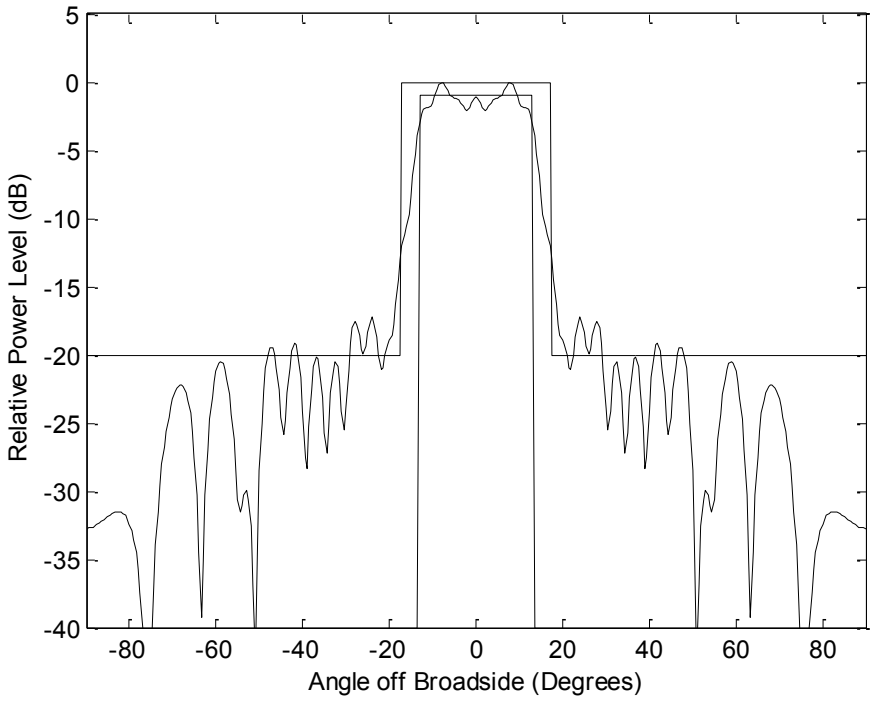

Fig.4.2-7 : Synthesized Flat-Topped Beam Pattern (Transmission Coefficient Amplitude Constrained to be Larger Than -1dB) with $N_e = 32$.

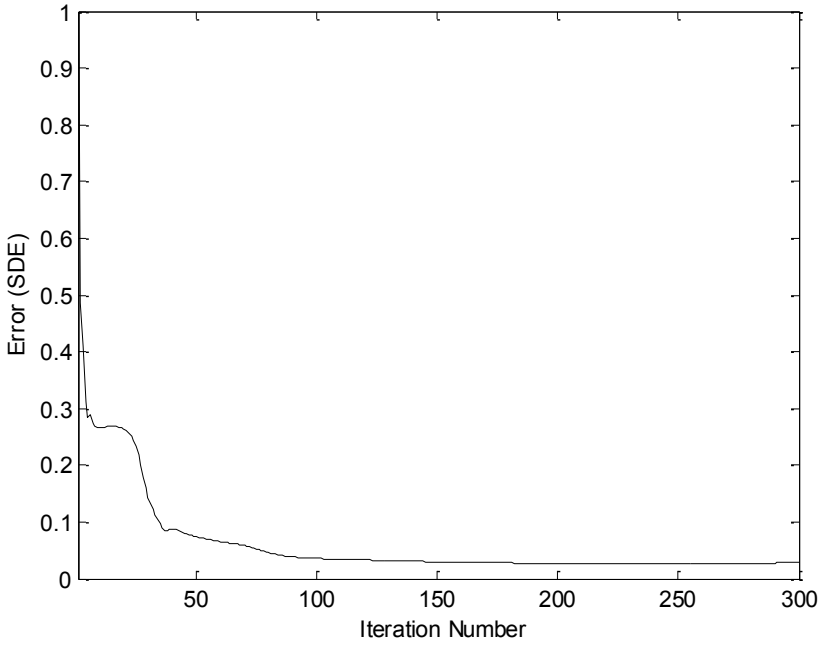

Fig.4.2-8 : Synthesized Flat-Topped Beam Pattern (Transmission Coefficient Amplitude Constrained to be Larger Than -1dB) with $N_e = 32$.

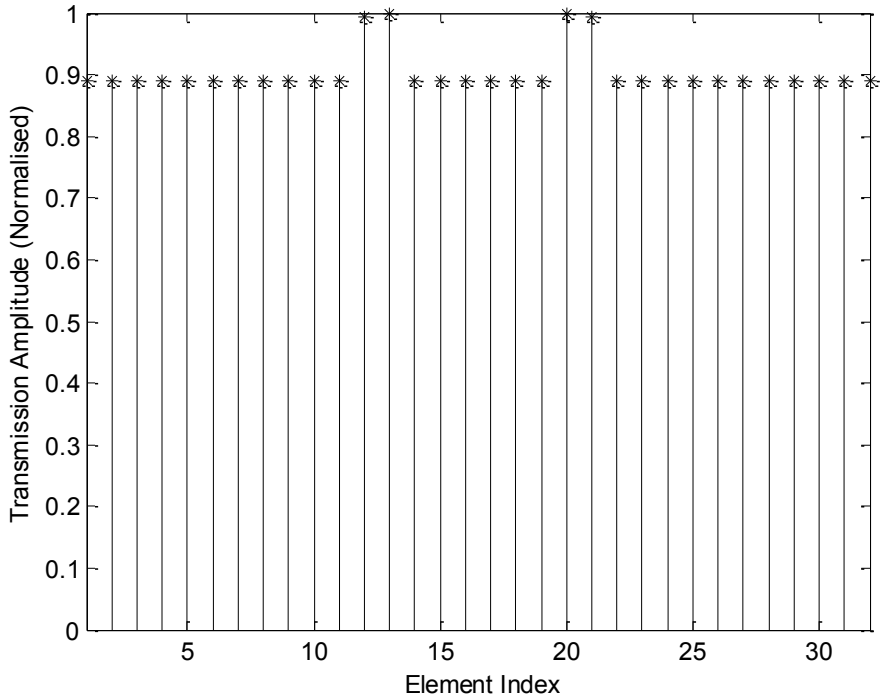

Fig.4.2-9 : Synthesized Flat-Topped Beam Pattern (Transmission Coefficient Amplitude Constrained to be Larger Than -1dB) with $N_e = 32$.

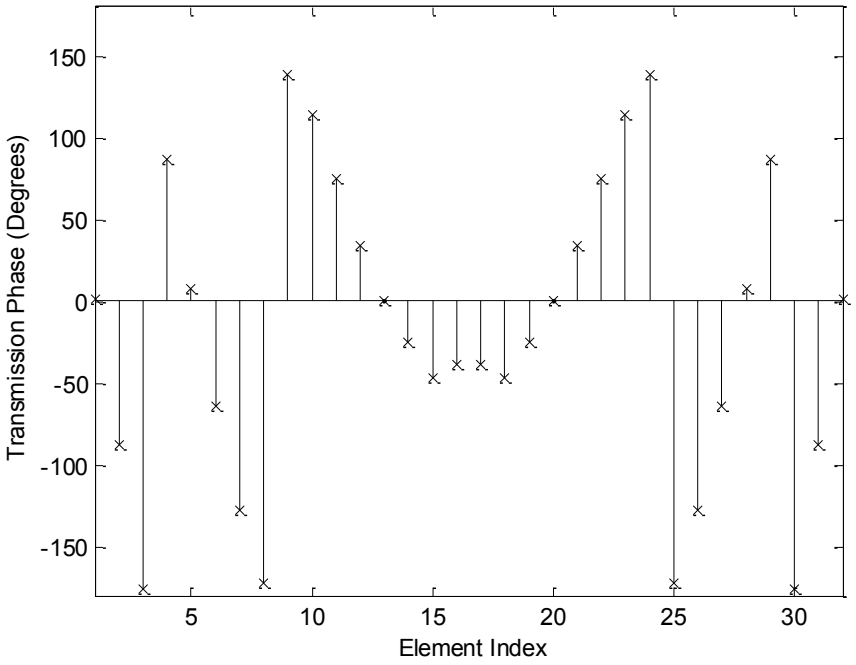

Fig.4.2-10 : Synthesized Flat-Topped Beam Pattern (Transmission Coefficient Amplitude Constrained to be Larger Than -1dB) with $N_e = 32$.

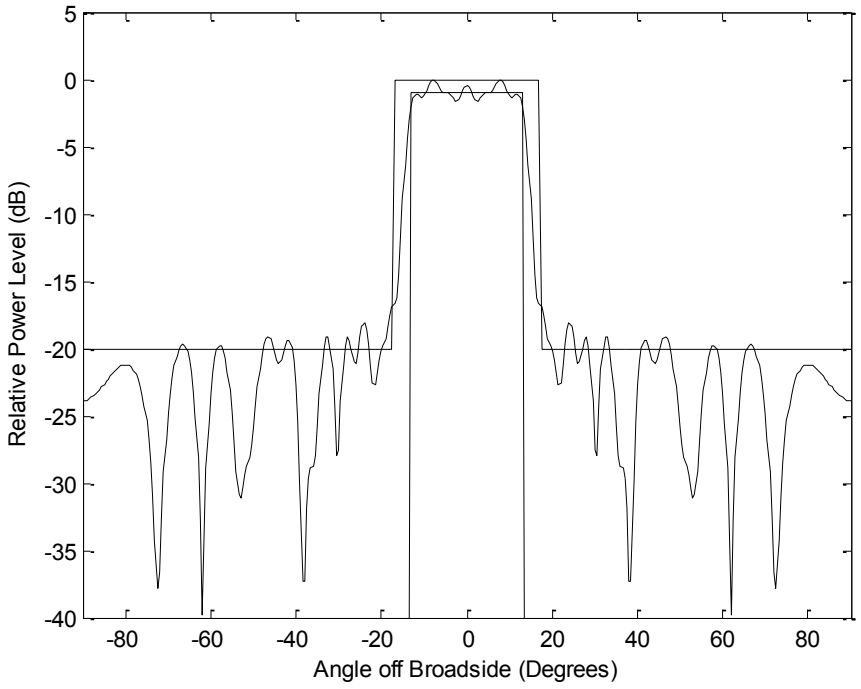

Fig.4.2-11 : Synthesized Flat-Topped Beam Pattern (Transmission Coefficient Amplitude Constrained to be Larger Than -3dB) with $N_e = 32$.

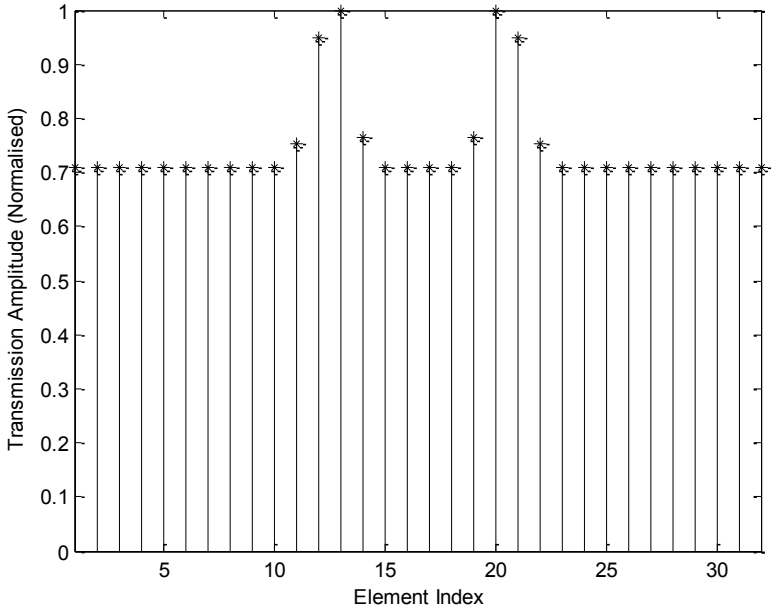

Fig.4.2-12 : Synthesized Flat-Topped Beam Pattern (Transmission Coefficient Amplitude Constrained to be Larger Than -3dB) with $N_e = 32$.

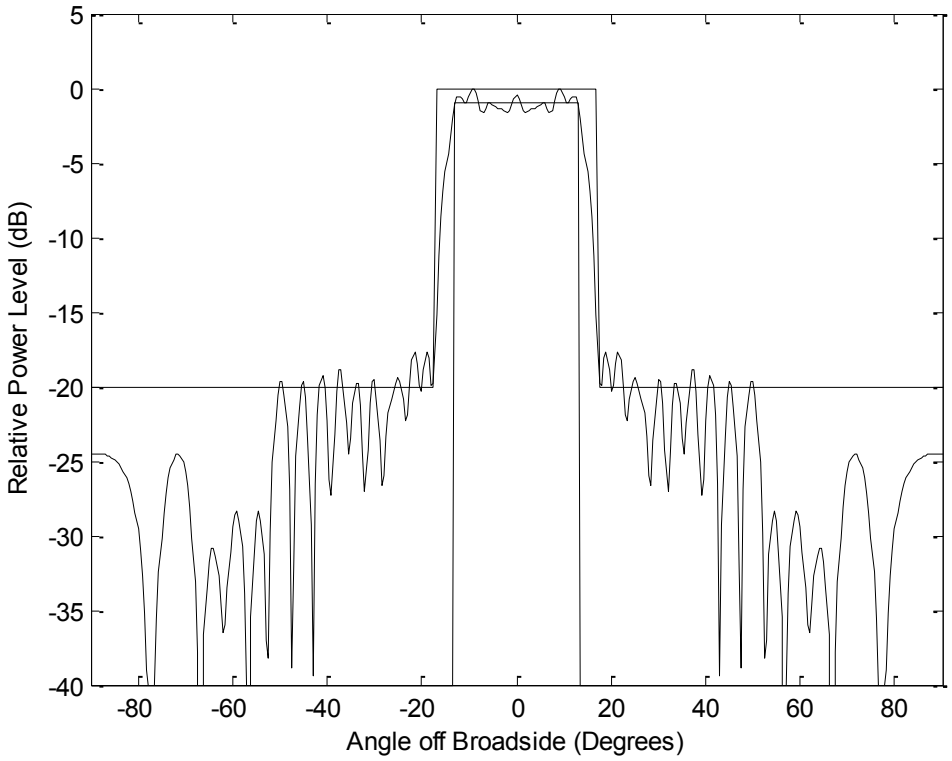

Fig.4.2-13 : Synthesized Flat-Topped Beam Pattern (Transmission Coefficient Amplitude Constrained to be Larger Than -1dB) with $N_e = 40$.

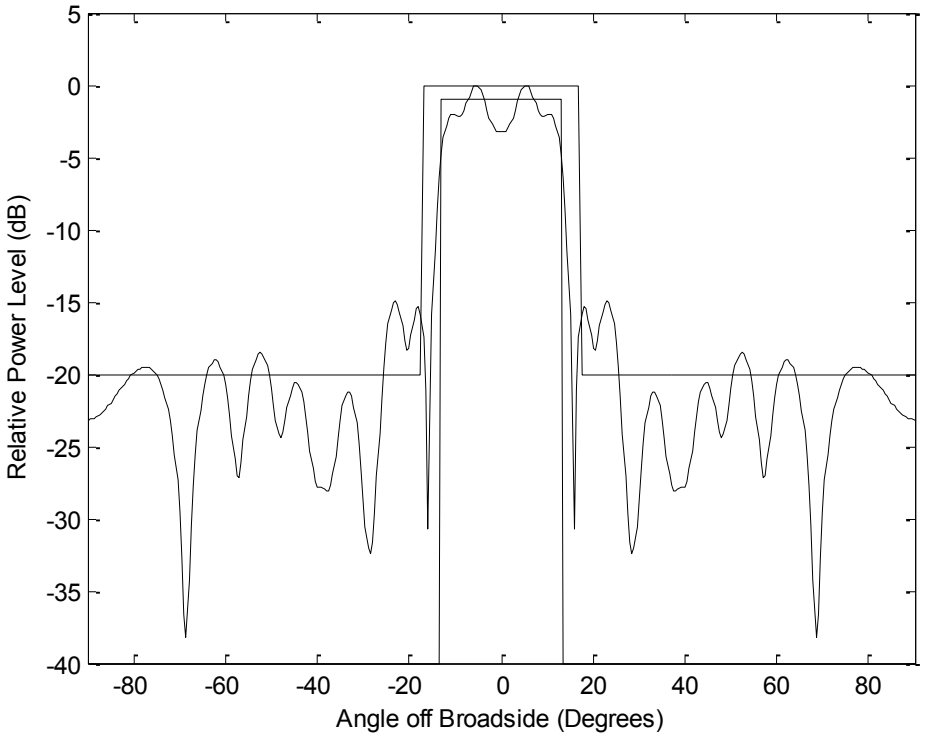

Fig.4.2-14 : Synthesized Flat-Topped Beam Pattern (Transmission Coefficient Amplitude Constrained to be Larger Than -1dB) with $N_e = 24$.

4.2.3 Synthesis with the Transmission Coefficient Amplitude Equal to Unity (Phase-Only Synthesis)

This is the so-called true phase-only case, for which the transmission coefficient is unity for all lens elements (cells), but its phase is allowed to vary from element to element. Although phase-only synthesis has already been done by several authors, the majority of their work assumes that excitation amplitude synthesis can be performed (once), and excitation phase-only control subsequently used to reconfigure the antenna from one shaped beam to another. Some authors (albeit relatively few) have done a true phase-only synthesis with the same excitation amplitude assigned to all array elements, but only for the sidelobe control of pencil beam patterns. There has been no examination of what shaped beams can be achieved with true phase-only synthesis.

It is apparent that the pattern in Fig.4.2-15, resulting from the "phase-only" constraint on the transmission coefficients, is not as satisfactory as its counterpart in Fig.4.2-1 (where no constraints were imposed on the transmission coefficients). This is also perceived from the SDE behavior in Fig.4.2-16. The Fig.4.2-17 confirms the fact that this is a "phase-only" result (all the transmission coefficient amplitudes are unity), and Fig.4.2-18 shows what the phases of the transmission coefficients need to be. If we for some reason do not wish to alter the lens size, we might investigate whether relaxing some pattern specification might bring the pattern closer to compliance. For instance, if we allow S_{rip} to increase to 2dB, and the sidelobe level (SLR) to rise to 12 dB, we obtain the result in Fig.4.2-19 with its SDE in Fig.4.2-20 showing that the pattern mask is satisfied more closely. The designer would need to decide whether this is preferred or whether to adopt some other tactic. Thus far we have used the same flat-topped pattern width in all the examples shown. If we widen this region so that $\theta_{w1} = 18°$ and $\theta_{w2} = 22°$ (with SLR = 20 dB, S_{rip} = 1dB, and $\Delta\theta_w = 4°$ as before) the phase-only synthesis yields the pattern shown in Fig.4.2-21. This is far worse than the result in Fig.4.2-15, even though the only change has been that of widening the shaped beam region. This is a cased where the size of the lens would need to be changed to increase the number of degrees of freedom.

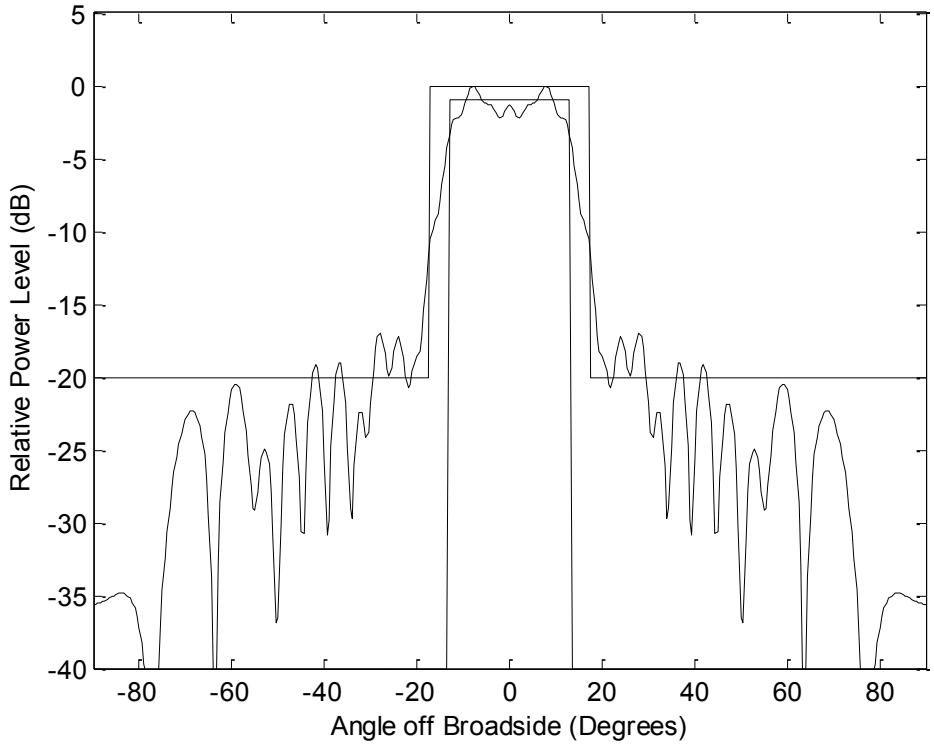

Fig.4.2-15 : Synthesized Flat-Topped Beam Pattern (Phase-Only Constraint) with $N_e = 32$.

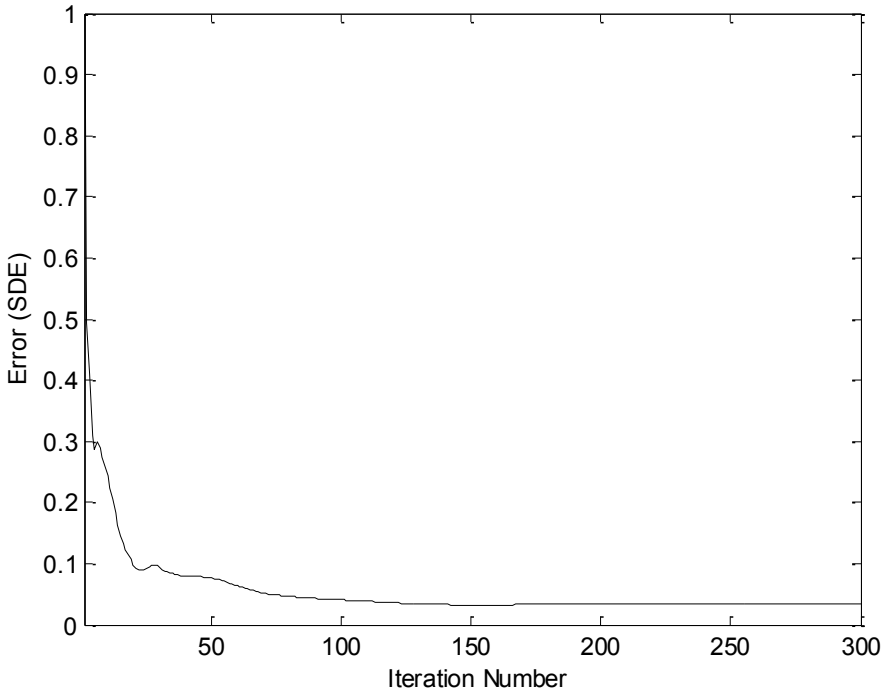

Fig.4.2-16 : SDE for Flat-Topped Beam Synthesis (Phase-Only Constraint) with $N_e = 32$.

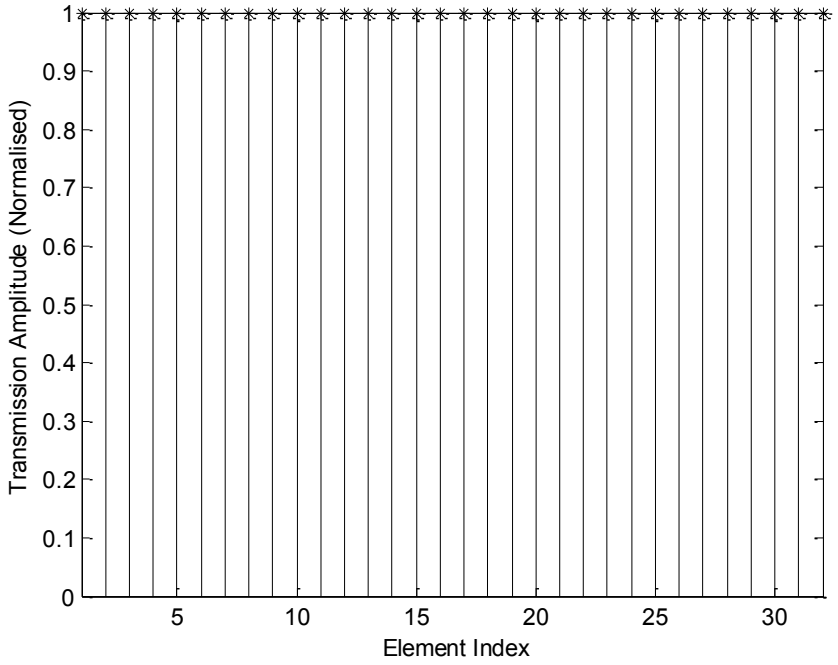

Fig.4.2-17 : Synthesized Flat-Topped Beam Transmission Coefficient Amplitudes (Phase-Only Constraint) with $N_e = 32$.

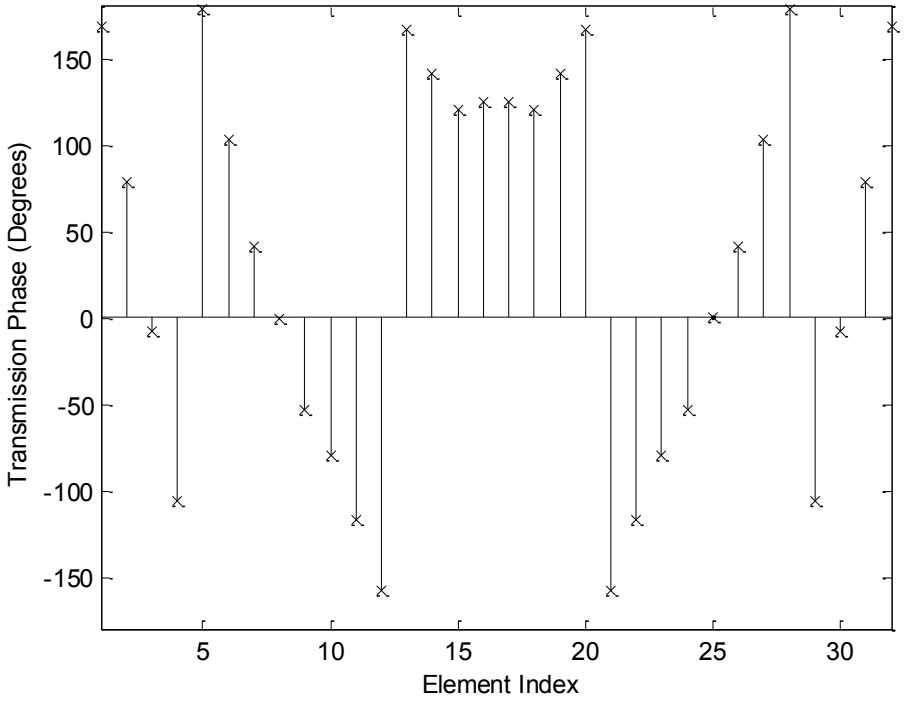

Fig.4.2-18 : Synthesized Flat-Topped Beam Pattern Transmission Coefficient Phase (Phase-Only Constraint) with $N_e = 32$.

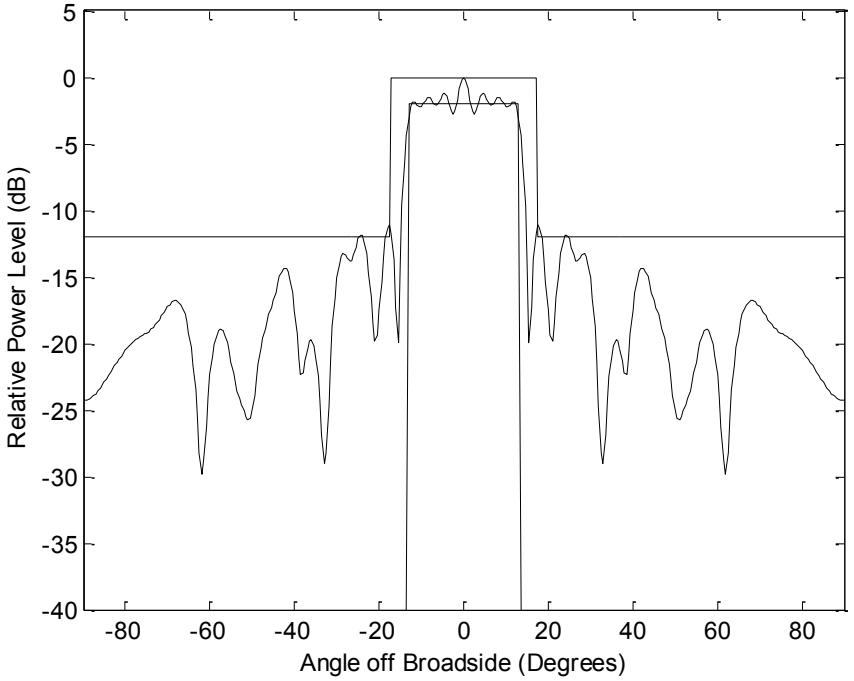

Fig.4.2-19 : Synthesized Flat-Topped Beam Pattern (Phase-Only Constraint) with $N_e = 32$ and S_{rip} increased from 1 dB to 2dB.

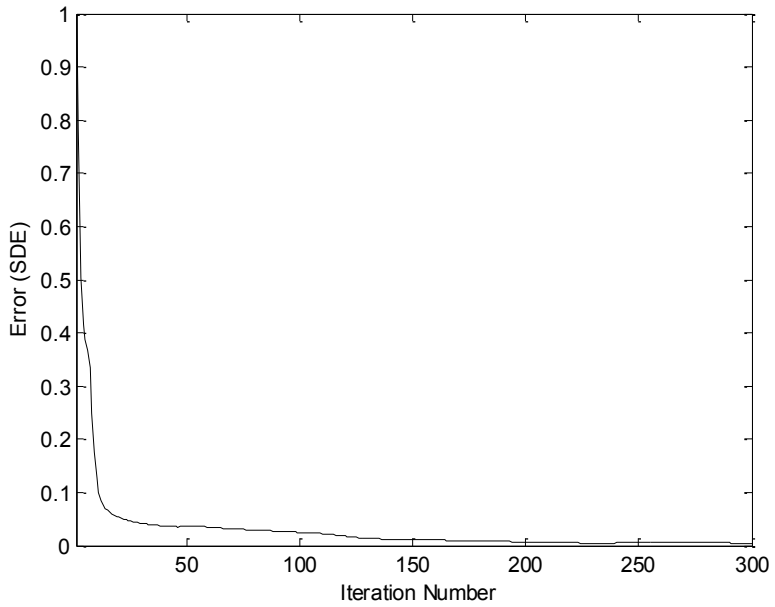

Fig.4.2-20 : SDE for Synthesis of Flat-Topped Beam Pattern (Phase-Only Constraint) with $N_e = 32$ and S_{rip} increased from 1 dB to 2dB.

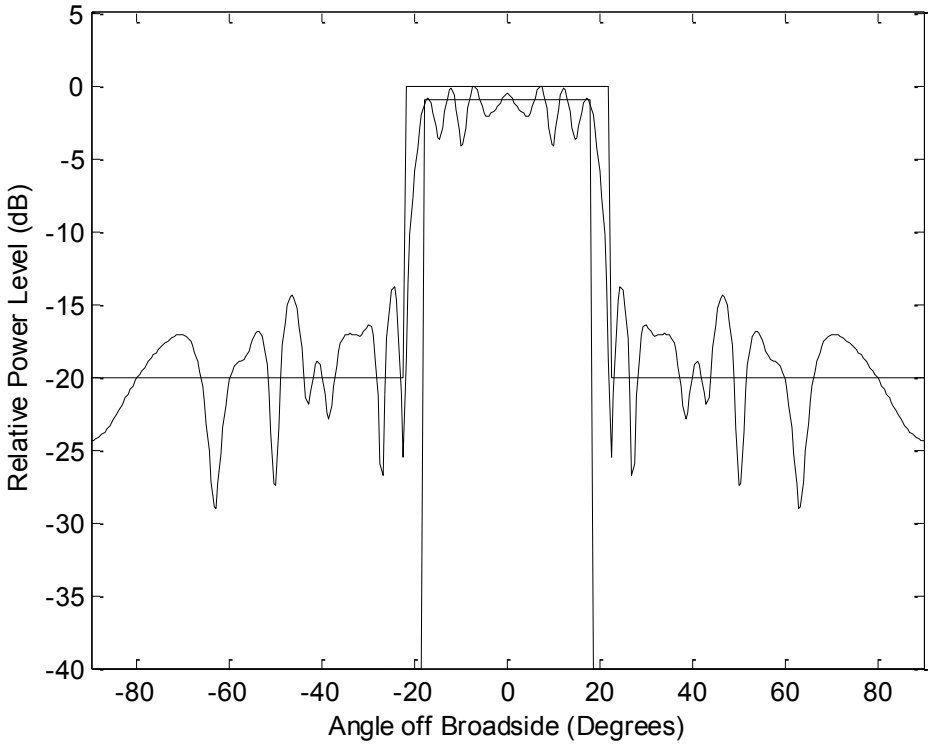

Fig.4.2-21 : Synthesized Flat-Topped Beam Pattern (Transmission Coefficient Amplitude Constrained to be Larger Than -1dB) with $N_e = 32$.

4.2.4 Synthesis Using Database-Constrained Transmission Coefficients

We next show the results obtained when using the "opportunistic" transmission coefficient synthesis approach devised in Section 3.8. A complete set of database[60] values [2] is shown by the asterisks (∗) in Fig.4.2-22. If the complete set of database values is used in the synthesis process the radiation pattern is as shown in Fig.4.2-23. The starting transmission coefficient values for the opportunistic synthesis procedure were those found in Section 3.7 for the unconstrained synthesis[61]. We observe in Fig.4.2-23 that the sidelobe constraints are not met when the transmission coefficient space is only the set of database values; but we are now aware of the effect of constraining the transmission coefficients in this manner. In this case the weights were increased to a large value in the shaped beam region in setting up the weight vector [W] used in determining the reverse operator. This forced the satisfaction of the pattern constraints over the shaped beam region at the expense of the sidelobe region. These weights could be used differently depending on the importance of the shaped beam details compared to those of the sidelobe region in some application. The actual transmission coefficients selected by the synthesis procedure are indicated by the circles in Fig.4.2-22. The transmission coefficient amplitudes and phases of specific elements are shown in Fig.4.2-24 and 4.2-25, respectively.

Next we suppose that only those database values for which the transmission coefficient amplitude is greater than -2dB are retained in the database. This is equivalent to restricting the amplitude dynamic range of the database values, so that the allowed transmission coefficient space is that denoted by the asterisks (∗) in Fig.4.2-26. The resulting pattern is that in Fig.4.2-27; the price to pay for so severely constraining the transmission coefficient amplitude is clear. The actual transmission coefficients used are indicated by the circles in Fig.4.2-26. The transmission

[60] We are simply using this as representative of a typical database. The one being used was not established for the purposes of realizing a cylindrical lens. Nevertheless it is sufficient to demonstrate the technique.

[61] We have found that it is advantageous to progress from a weaker to stronger excitation constraint, using the synthesized transmission coefficients from one step as the starting values for the next step (with the stricter constraint). This does not appear to have been done by others. It might be referred to as a "trap navigation approach". In other words, it is advantageous to gradually increase the transmission coefficient and pattern constraints to the desired levels in successive executions of the complete projection method (each execution consisting of the required number of iterations). One would begin with the starting values derived via the method in Chapter 3, and execute the projection method without transmission coefficient constraints. The resulting transmission coefficients are then used as the starting values for the next execution of the projection method (which uses less stringent versions of the final transmission coefficient constraints), and so on, until the final execution of the projection method that imposes the full values of the transmission coefficient constraints.

coefficient amplitudes and phases of specific elements are those in Fig.4.2-28 and 4.2-29, respectively. It is noted that the database values have some "gaps" in the transmission coefficient phase range [0°,50°] for transmission coefficient amplitudes higher than -2dB. Using the synthesis method being discussed one could add some artificial database values in this region and establish what improvements in the radiation pattern would result if such values were available.

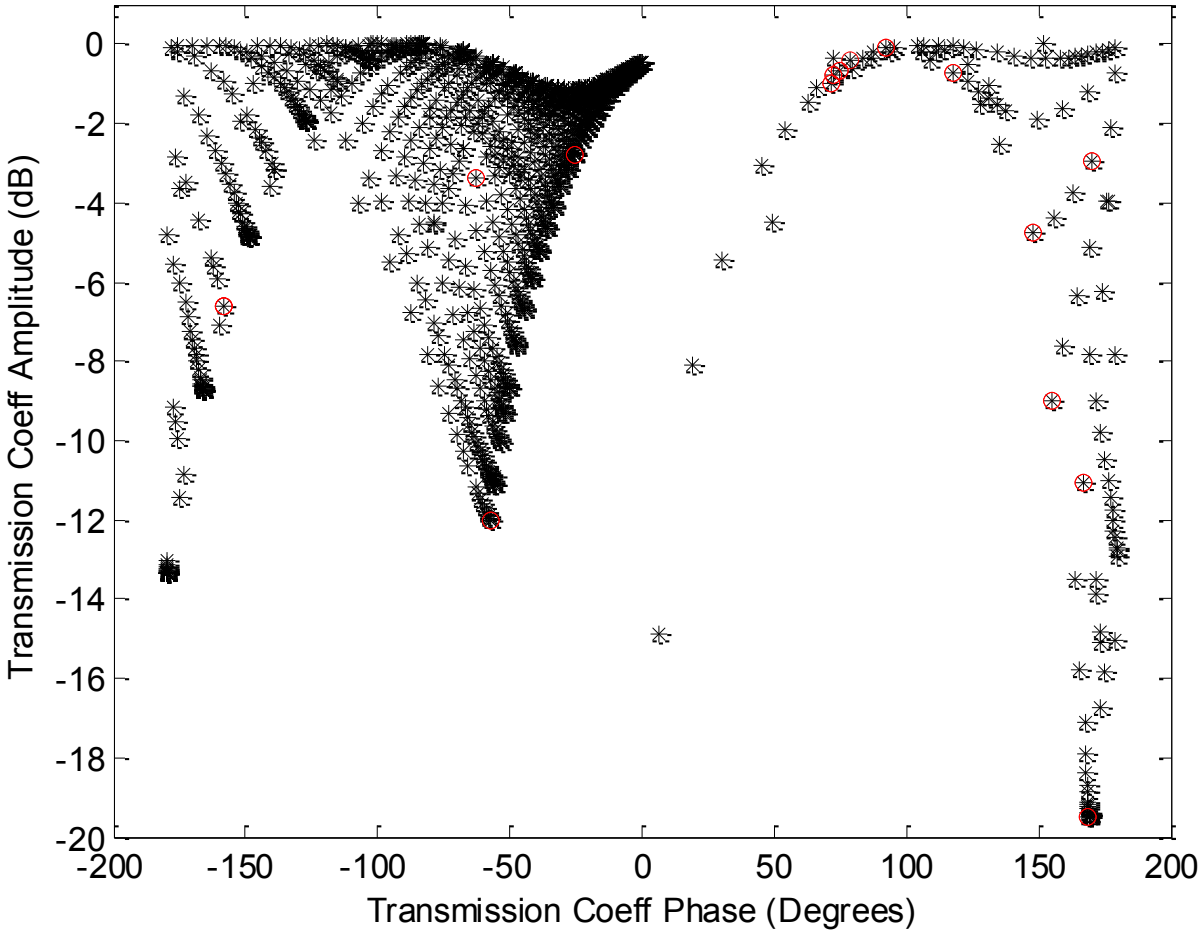

Fig.4.2-22 : Database of Lens Element Transmission Coefficients

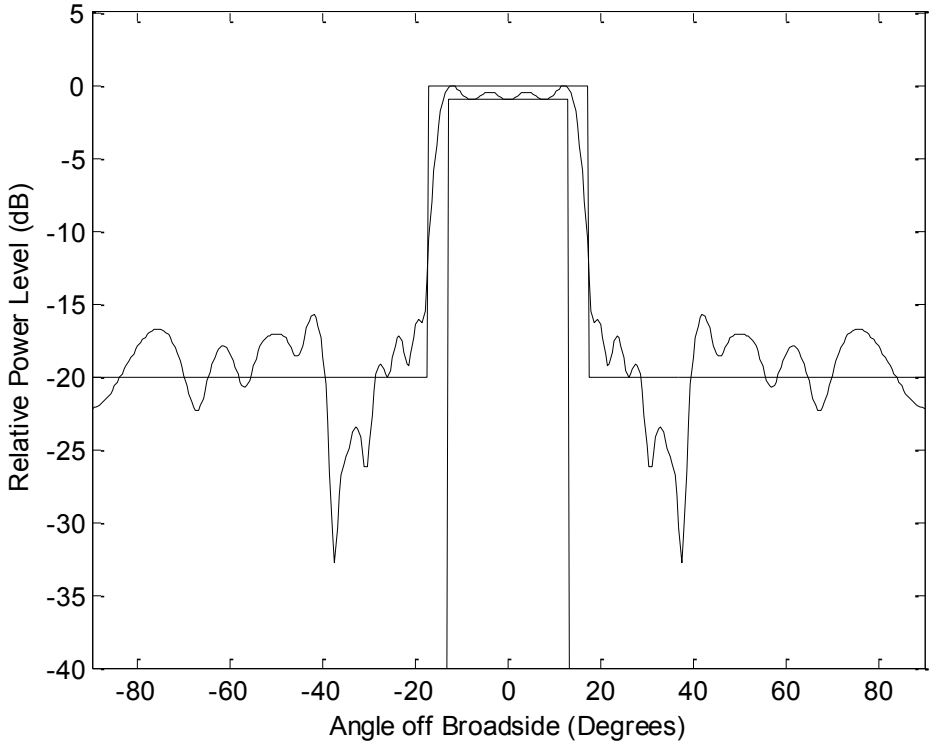

Fig.4.2-23 : Synthesized Flat-Topped Beam for Transmission Coefficients Constrained to be Members of the Database in Fig.4.2-22 (with $N_e = 32$).

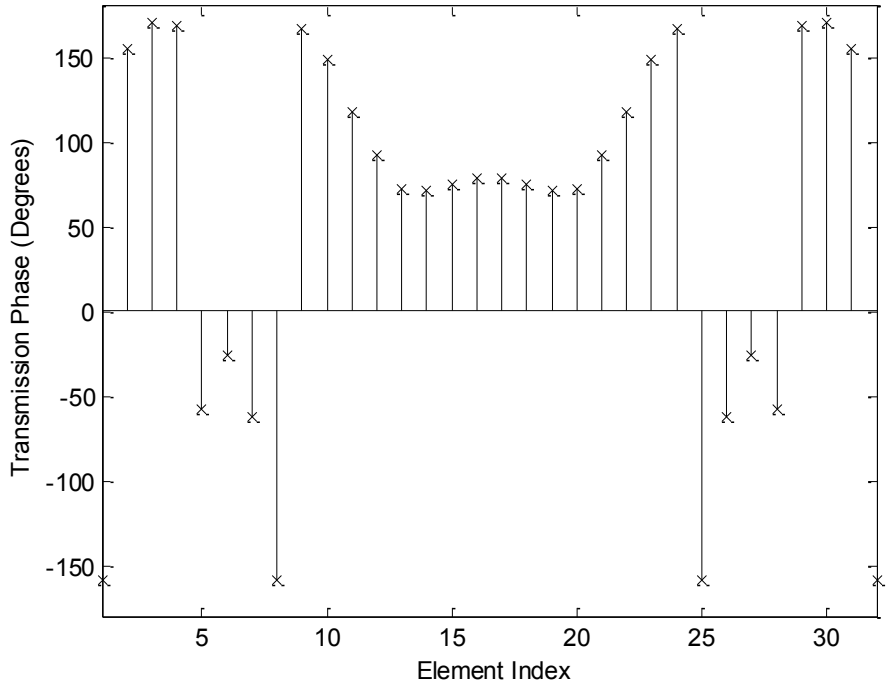

Fig.4.2-24 : Synthesized Flat-Topped Beam Transmission Coefficient Phases for the Pattern in Fig.4.2-23 (with $N_e = 32$).

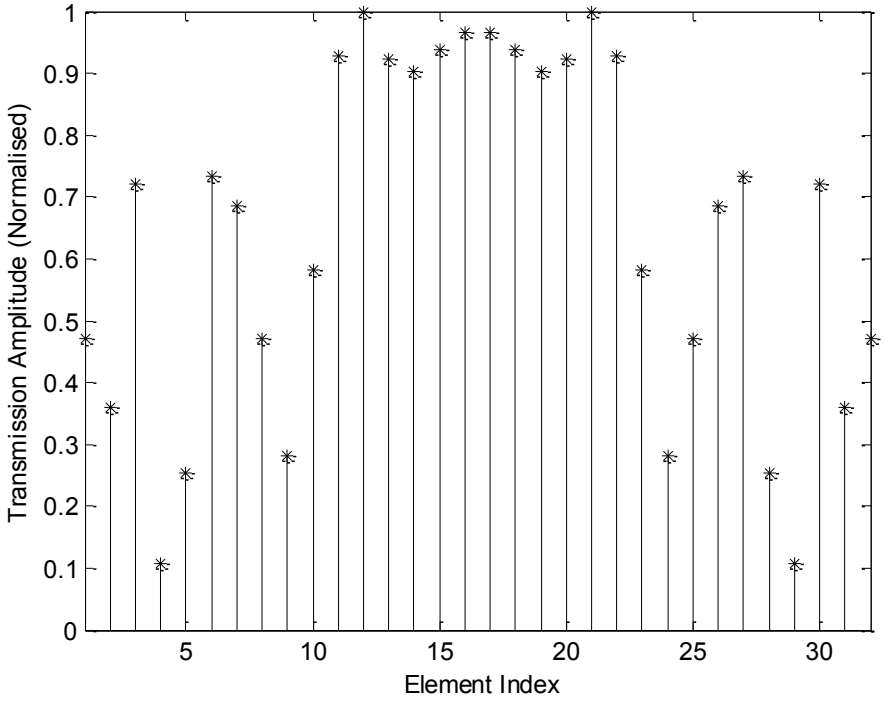

Fig.4.2-25 : Synthesized Flat-Topped Beam Transmission Coefficient Amplitudes for the Pattern in Fig.4.2-23 (with $N_e = 32$)

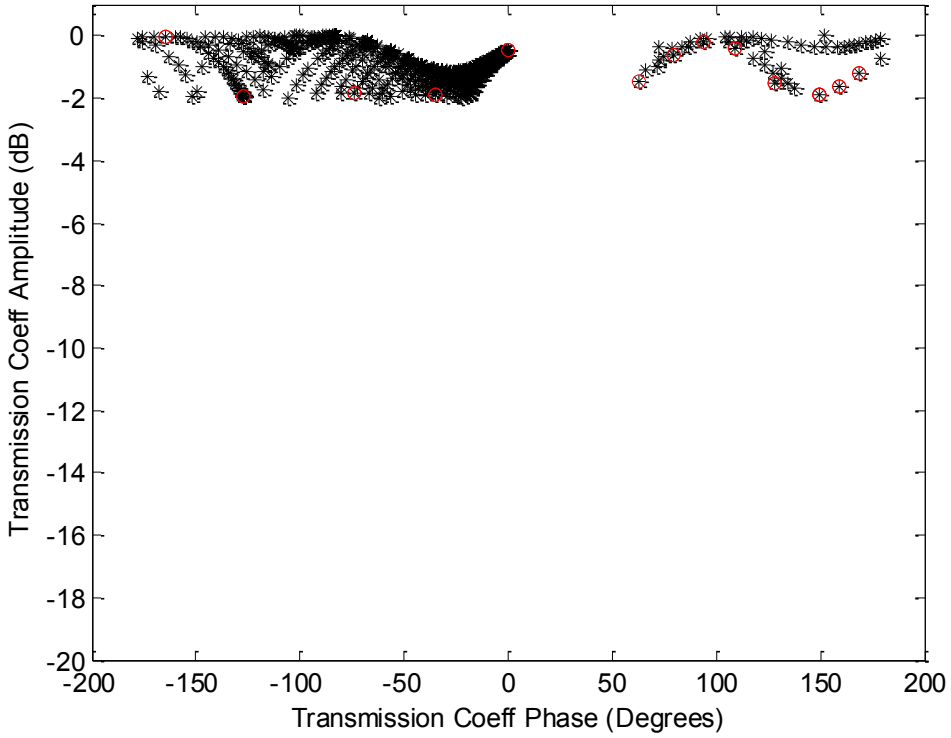

Fig.4.2-26 : Database of Lens Element Transmission Coefficients, Restricted to Transmission Coefficient Greater Than -2dB

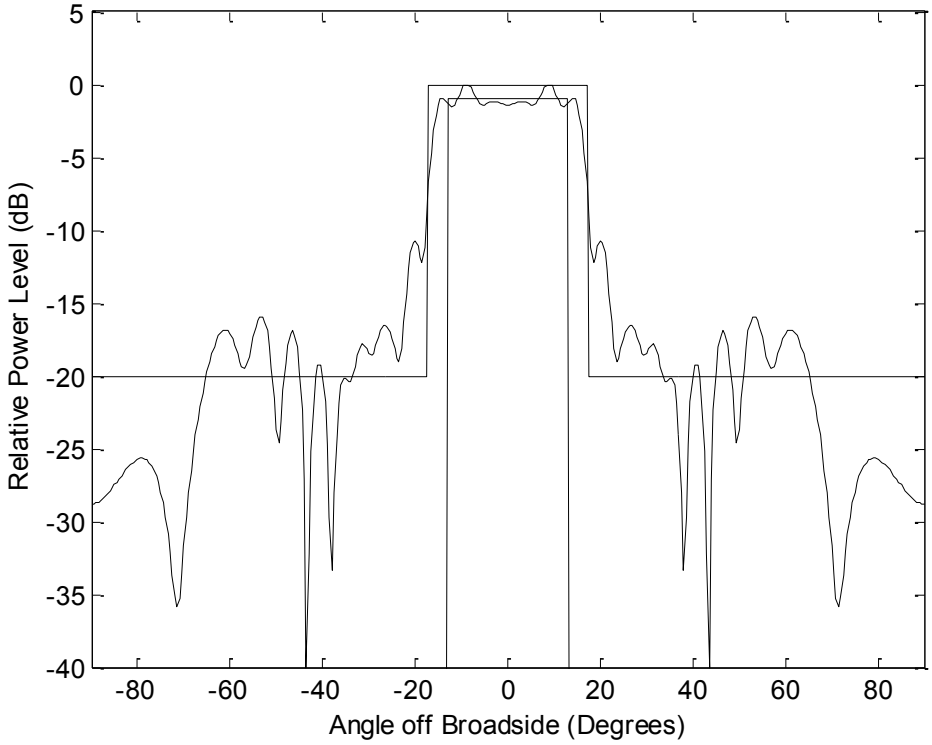

Fig.4.2-27 : Synthesized Flat-Topped Beam Pattern for Transmission Coefficients Constrained to be Members of the Database in Fig.4.2-26 (with $N_e = 32$)

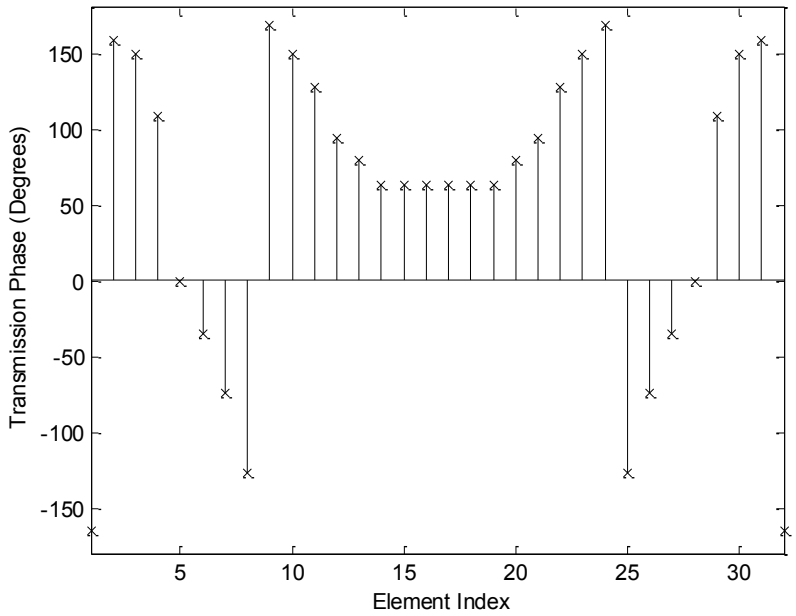

Fig.4.2-28 : Synthesized Flat-Topped Beam Transmission Coefficient Phases for the Pattern in Fig.4.2-27 (with $N_e = 32$)

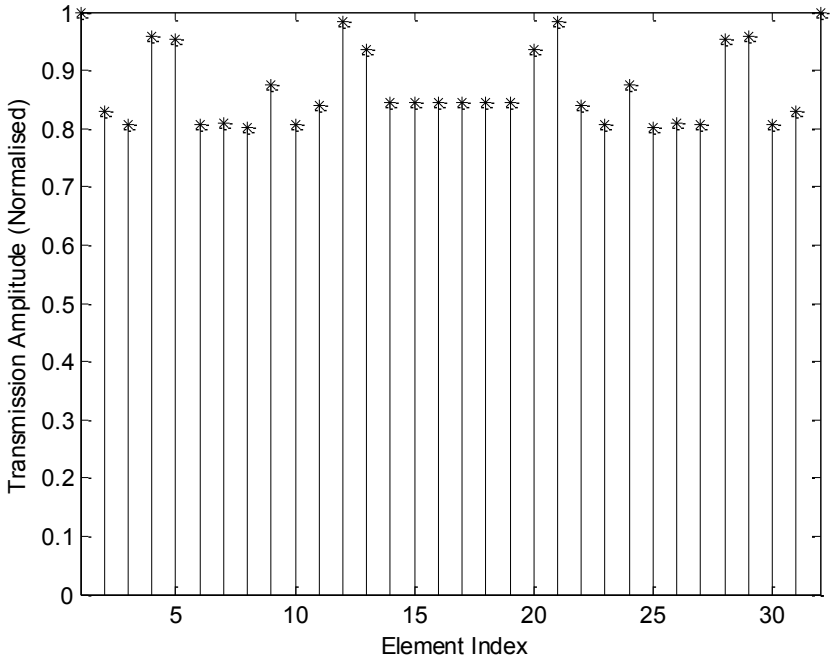

Fig.4.2-29 : Synthesized Flat-Topped Beam Transmission Coefficient Amplitudes for the Pattern in Fig.4.2-27 (with $N_e = 32$)

4.3 ISOFLUX PATTERN SYNTHESIS

The isoflux pattern is, like the flat-top case of Section 4.2, symmetrical. We will therefore show fewer examples than was done for the flat-top case. We selected an isoflux pattern[62] for the case R = 6378 km, H = 8000 km, and $\theta_{FOV} = 25.5°$. In addition we use SLR = 15 dB, S_{rip} = 1dB, $\Delta\theta_w = 5°$. The resultant pattern when there are no constraints on the transmission coefficients is that in Fig.4.3-1. The "phase-only" result is given in Fig.4.3-2; it is surprisingly close to satisfying the pattern mask in spite of the fact that all the $|b_n|$ are the same value. Finally, Fig.4.3-3 shows what one achieves if the dynamic range constraint $-2dB \le |b_n| \le 0dB$ is applied. The isoflux pattern is 'forgiving' as far as the amplitude constraints on the transmission coefficients are concerned.

[62] Described in Section 2.9.4, with all parameters being used for the mask specification being shown in Fig.2.9-7.

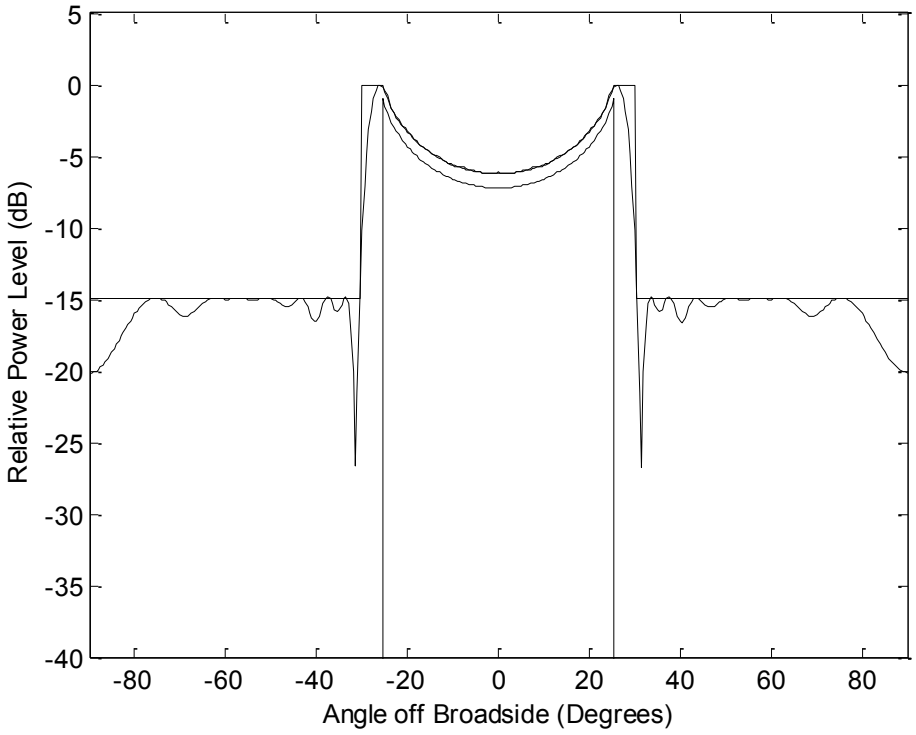

Fig.4.3-1 : Synthesized Isoflux Beam Pattern (No Transmission Coefficient Constraints) with $N_e = 32$.

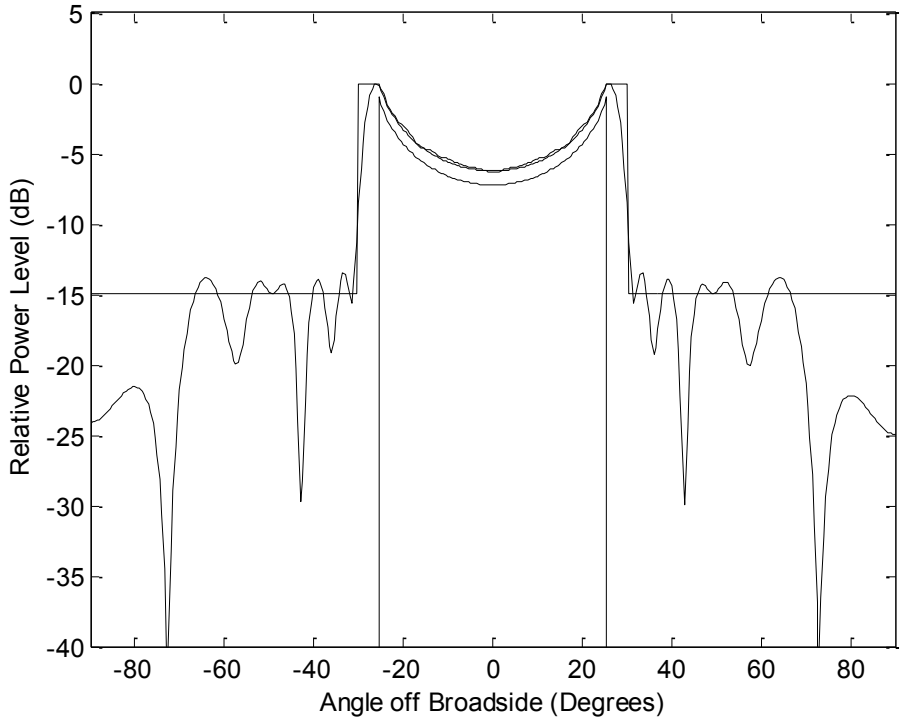

Fig.4.3-2 : Synthesized Isoflux Beam Pattern (Phase-Only Constraint) with $N_e = 32$.

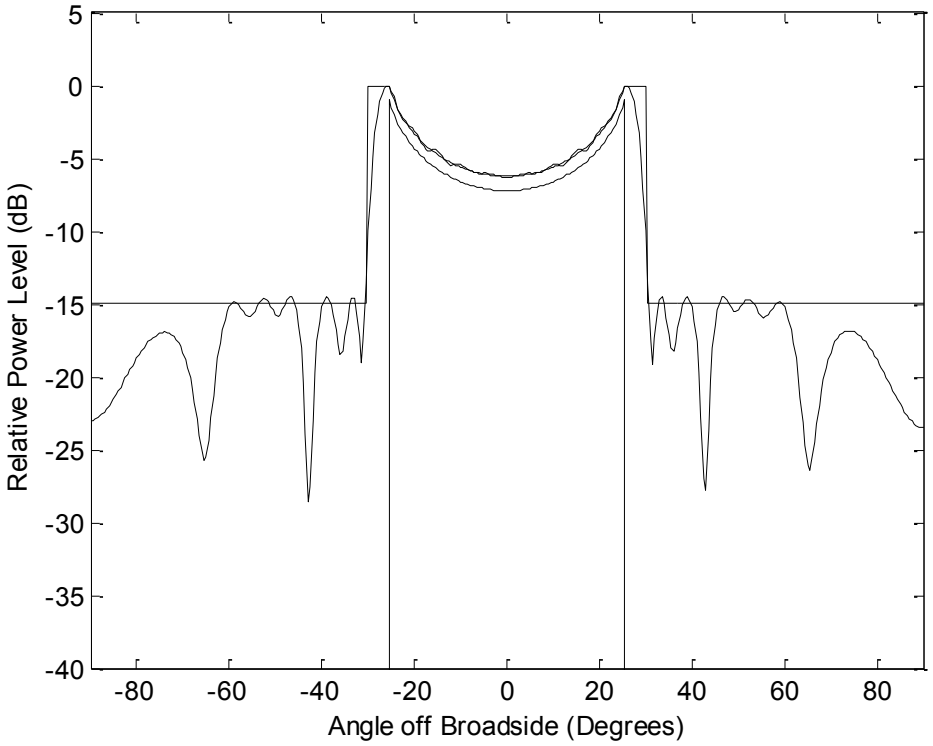

Fig.4.3-3 : Synthesized Isoflux Beam Pattern (Dynamic Range Constraints $-2dB \le |b_n| \le 0dB$) with $N_e = 32$.

4.4 COSECANT PATTERN SYNTHESIS

The flat-topped and isoflux beams discussed in the previous two sections are symmetrical about the boresight direction. The cosecant pattern[63] is asymmetrical. The pattern mask parameters are $\theta_l = 15^o$, $\theta_u = 58^o$, $\Delta\theta_l = \Delta\theta_u = 6^o$, SLR = 20 dB and S_{rip} = 2dB. Without constraints on the b_n, the synthesized pattern is as shown in Fig.4.4-1. The b_n amplitudes and phases are shown in Fig.4.4-2 and Fig.4.4-3, and are asymmetrical, as expected.

Since the constraint that restricts the phase of the b_n but leaves the amplitudes $|b_n|$ free was not discussed for the previous shaped beams, for completeness we show the result in Fig.4.4-4, obtained when we restrict the range of the transmission coefficient phases to $-130^o \le \angle b_n \le 130^o$. This constraint has relatively little effect on the final pattern's ability to satisfy the mask even

[63] Described in Section 2.9.5, with all the pattern mask parameters being shown in Fig.2.9-12.

though there were (in Fig.4.4-3) several elements whose transmission coefficient phases were outside the restricted range used to achieve Fig.4.4-4.

In light of the ease with which the mask is satisfied by the pattern in Fig.4.4-1, we tightened the specification to $\Delta\theta_l = \Delta\theta_u = 4^o$, SLR = 20 dB and S_{rip} = 1dB. The cost of doing this is that the SLR is now violated, but only slightly, as shown in Fig.4.4-6. If this were allowable, it might be possible to use a smaller lens; whether such trade-offs are acceptable would depend on the particular situation.

Up to this point in the chapter all results are for application of the serial form of the projection algorithm described in Section 3.9.2. We next also apply the parallel form that has been described in Section 3.9.3 to cosecant beam synthesis. A value q = 3 (the raised cosine power in the feed model, as discussed in Section 3.2) was selected. The serial algorithm now gives the result in Fig.4.4-7 for a phase-only synthesis. The pattern violates the mask both in the shaped beam region and the sidelobe region. The parallel algorithm gives the much more favourable result shown in Fig.4.4-8, when $\alpha_1 = 0.8$ and $\alpha_2 = 0.2$. There is only a slight violation of the mask in the sidelobe region, and the mask is satisfied in the shaped beam region. An examination of the transmission coefficient phases reveals why this is so. Whereas "phase-only" (and any other transmission coefficient constraints) are strictly imposed by the serial algorithm, in the parallel implementation this would only be so if α_2 were very much larger than α_1. Here the use of $\alpha_1 = 0.8$ and $\alpha_2 = 0.2$ means that more effort is made by the algorithm in meeting the pattern constraint than the transmission coefficient constraints. This is useful. For instance, Fig.4.4-9 shows us that if we are prepared to allow the $|b_n|$ to occupy the range $-2dB \le |b_n| \le 0dB$ then a relatively good pattern can still be obtained[64]. Such a situation might indeed be a favourable compromise for printed lens antennas.

[64] It is not possible to use the serial form in this way.

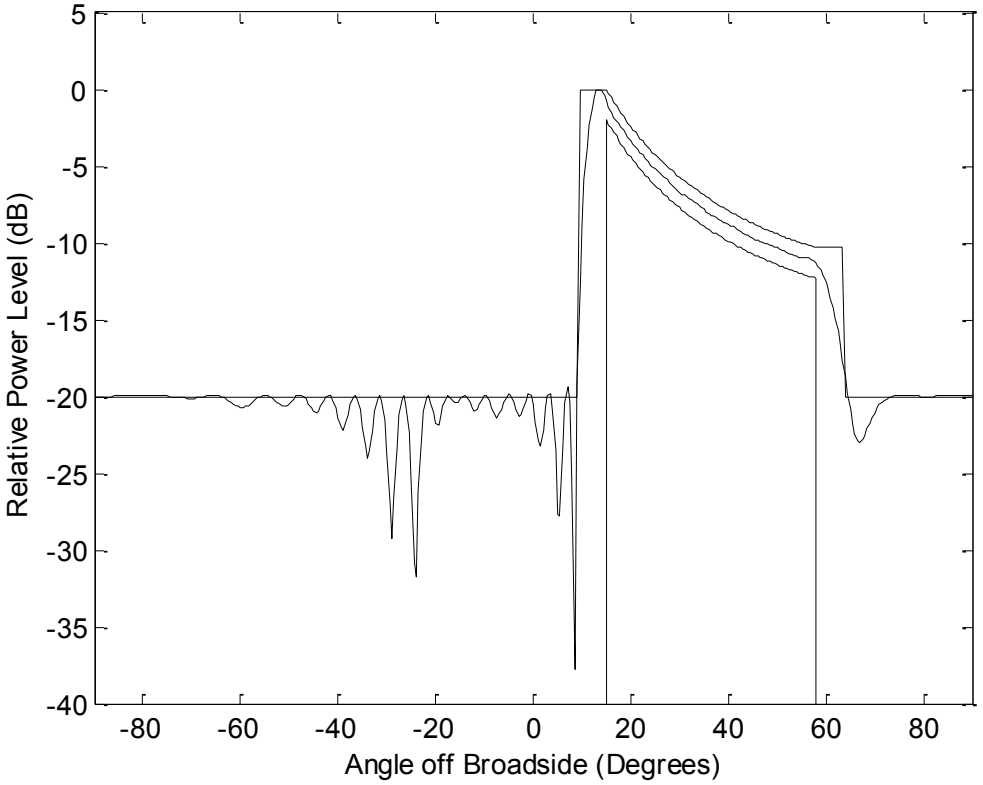

Fig.4.4-1 : Synthesized Cosecant Beam Pattern (No Transmission Coefficient Constraints) with $N_e = 32$.

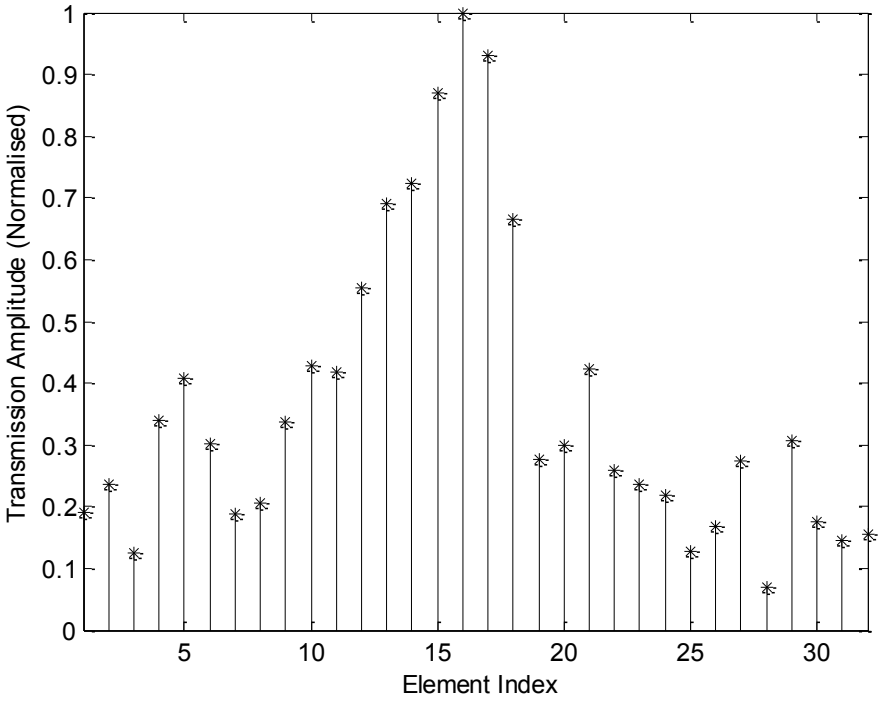

Fig.4.4-2 : Transmission Coefficient Amplitude for the Pattern in Fig.4.4-1

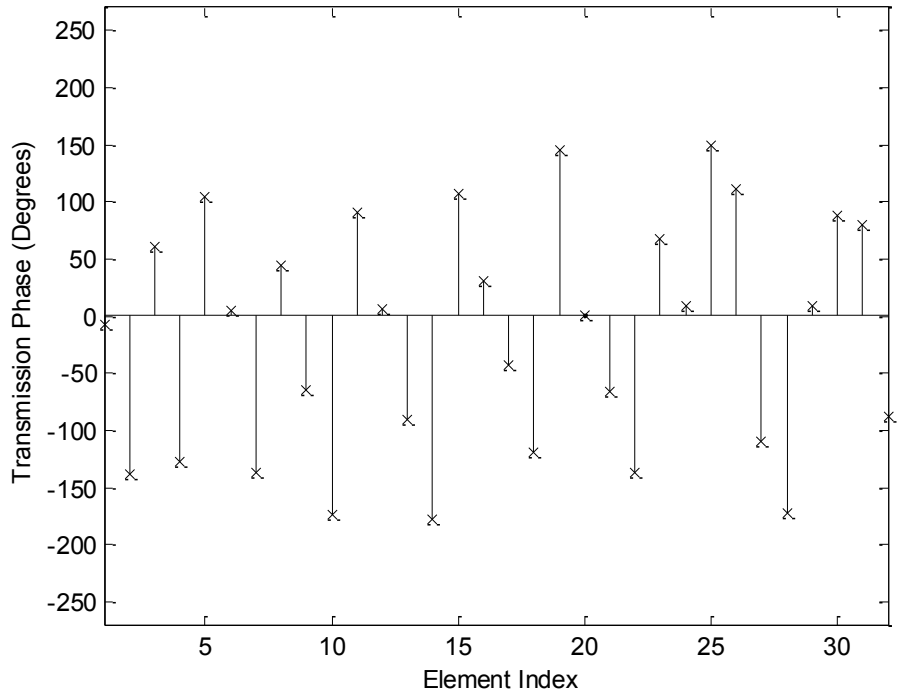

Fig.4.4-3 : Transmission Coefficient Phase for the Pattern in Fig.4.4-1

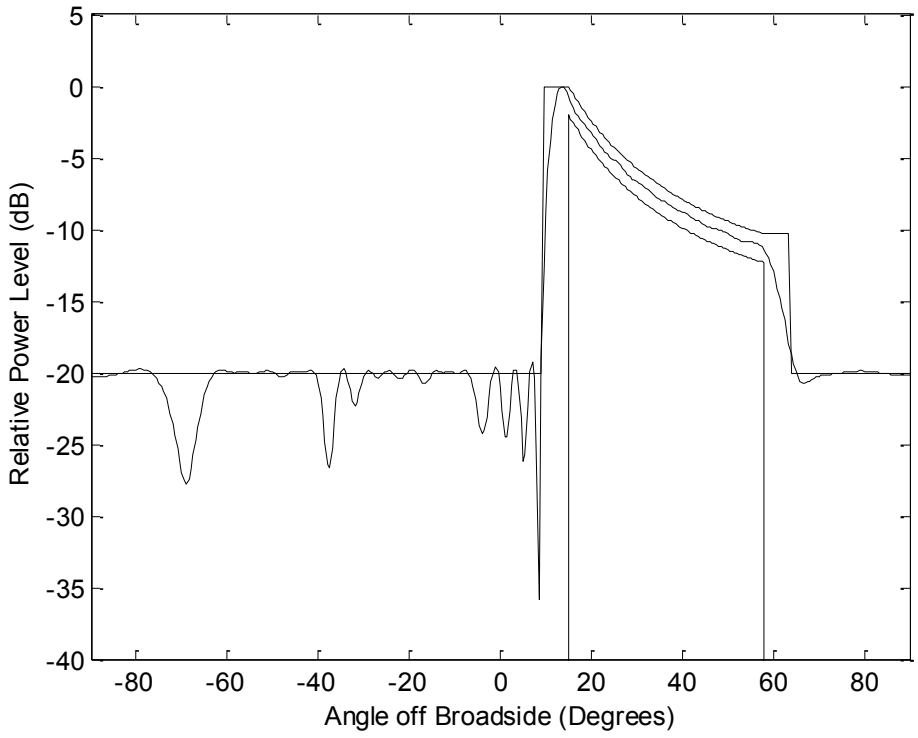

Fig.4.4-4 : Synthesized Cosecant Beam Beam Pattern (Transmission Coefficient Phase Range Constraint $-130^{o} \le \angle b_n \le 130^{o}$) with $N_e = 32$.

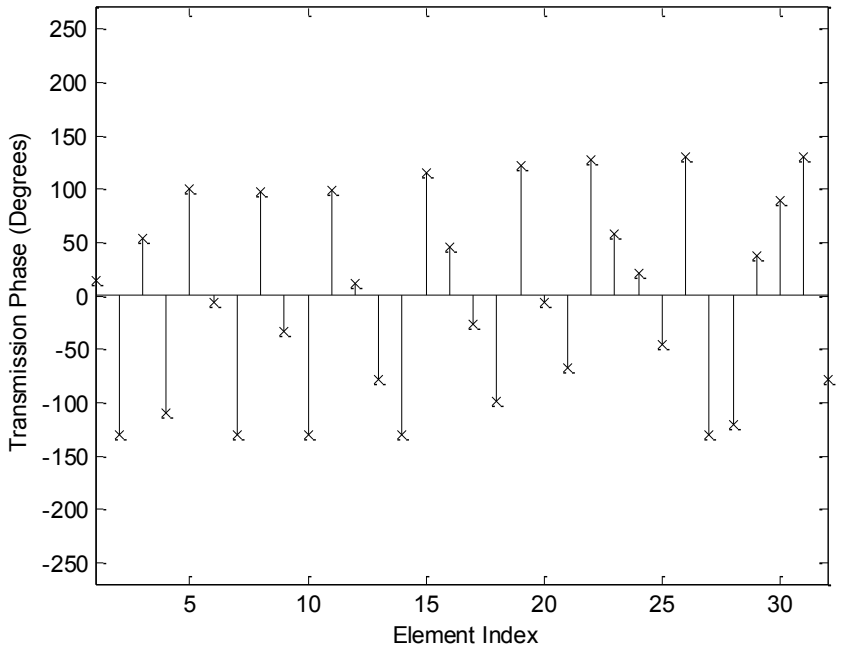

Fig.4.4-5 : Transmission Coefficient Phase for the Pattern in Fig.4.4-4

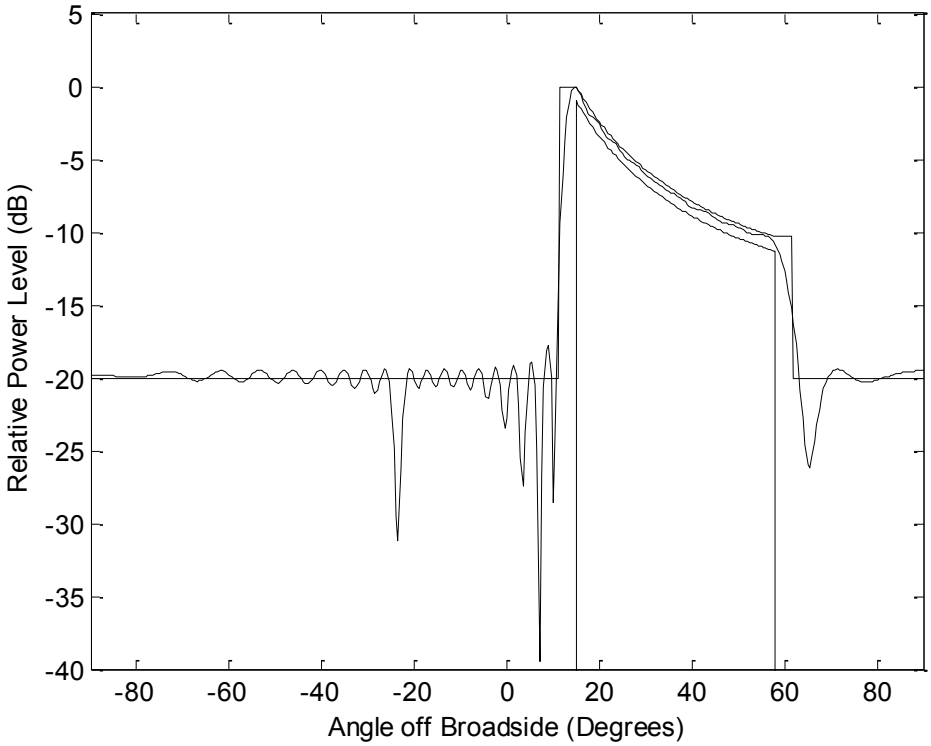

Fig.4.4-6 : Synthesized Cosecant Beam Pattern with Pattern Mask Parameters Tightened to $\Delta\theta_l = \Delta\theta_u = 4^o$ and S_{rip} = 1dB (No Transmission Coefficient Constraints) with N_e = 32

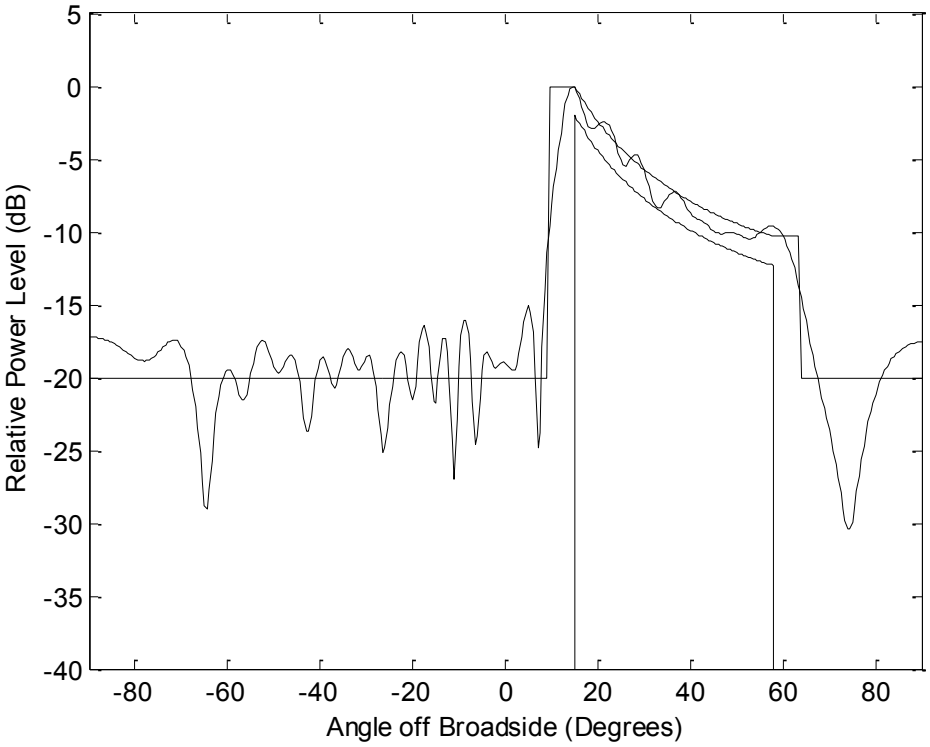

Fig.4.4-7 : Cosecant Beam Pattern from a Phase-Only Synthesis Using the Serial Form of the Projection Algorithm with $N_e = 32$

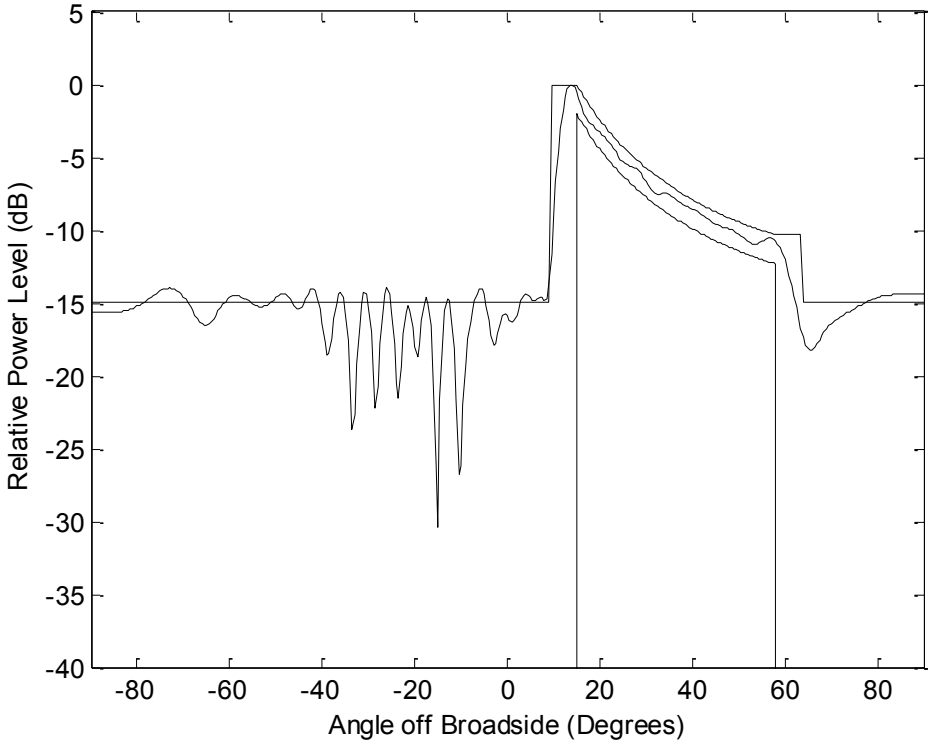

Fig.4.4-8 : Cosecant Beam Pattern from a Phase-Only Synthesis Using the Parallel Form of the Projection Algorithm with $\alpha_1 = 0.8$ and $\alpha_2 = 0.2$, and $N_e = 32$

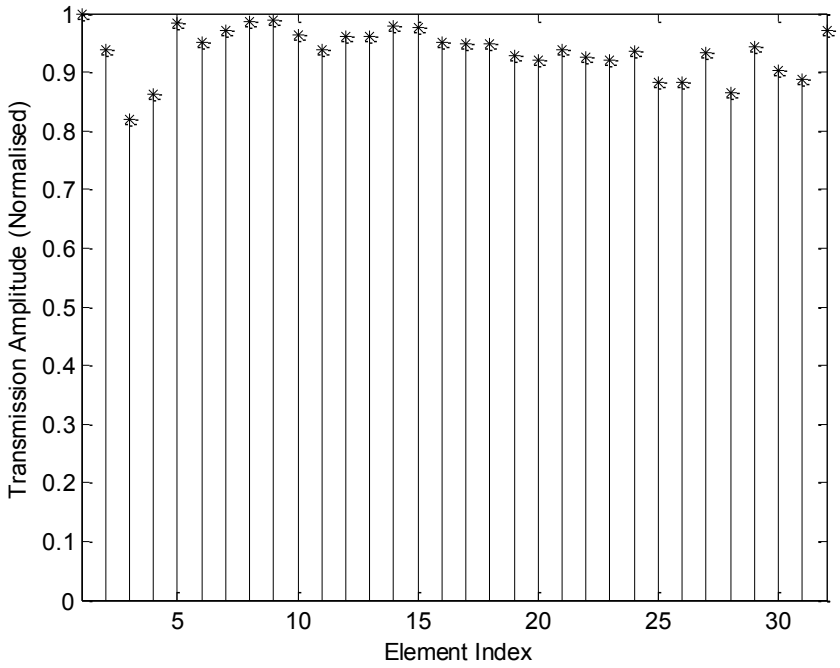

Fig.4.4-9 : Synthesized Transmission Coefficient Amplitude for the Pattern in Fig.4.4-8

4.5 CONCLUDING REMARKS

The best way to demonstrate the effectiveness of a synthesis method is to illustrate its success (or otherwise) for a varied number of examples. This has been accomplished in this chapter, for flat-topped, isoflux and cosecant shaped beam patterns.

In addition, it is clear that, by using the projection synthesis method in the lens element transmission coefficient space the transmission coefficient constraints are made explicit, and it is possible to judge the plausibility of such constraints. Unlike other numerically based excitation synthesis methods, the constraints are not hidden deep within some objective function. During the numerical experimentation used to exercise the method, and from which the specimen examples shown in this chapter were extracted, we devised what we have called the "trap navigation approach" was proposed as a means of allowing the projection method to navigate through traps as it iterates.

It was shown that shaped beams can indeed be synthesized using a phase-only synthesis, or when phase-only synthesis with limited amplitudes range is allowed. By using the projection synthesis method we can obtain the required lens transmission coefficients, subject to such

amplitude and phase constraints, that will provide a pattern that is only slightly degraded compared to the idealized case that is physically possible without such constraints.

There are no commercial software packages for performing synthesis subject to excitation constraints, and none for shaped beam synthesis even without excitation constraints. Thus all the codes used in the generation of the results presented in this chapter have been developed "from scratch" as part of the work of this thesis.

4.6 REFERENCES FOR CHAPTER 4

[1] MATLAB™, Mathworks Inc., USA (www.mathworks.com)

[2] N. Gagnon, RF Technologies, Communications Research Centre Canada, *Private Communication*.

CHAPTER 5

General Conclusions

The principal contributions of this thesis are:

- The development of a means of formulating generalized projection based synthesis methods that directly use the printed lens transmission coefficients as the synthesis variables. This makes it possible to immediately perceive what influence constraints on the actual transmission coefficients have on the possible radiation pattern performance.

- A demonstration of what is physically possible as regards the performance of a cylindrical lens antenna for three different types of widely-used shaped beams (sector beam, cosecant beam, and isoflux beam), when either the transmission coefficient amplitudes, or transmission phases, or both, are restricted in some way. It appears that this is the first time that shaped beam synthesis subject to the variety of transmission coefficient constraints has been reported, and certainly so for the phase-only synthesis of such shaped beams.

- In order to achieve the above-mentioned syntheses the projection method was implemented in both a serial and parallel form. In the present context (where we only use one pattern constraint operator and one transmission coefficient constraint operator in any synthesis process) these provide almost the same results. This is the first time a parallel version has been used in the projection synthesis of shaped beam antennas (albeit only using two projection operators, one for the pattern and the other for the transmission coefficient constraints). We believe it offers the advantage of performing a synthesis that provides an indication of what constraints can be tolerated without sacrificing too much as far as the pattern requirements are concerned, through judicious use of the multiplicative weights on the two operators. We saw in Section 2.7 that the parallel version can in fact incorporate several different projection operators; this might be used to good effect such as synthesizing a lens that simultaneously provides different beam types, one for each of two (or more) offset feeds, to name just one possibility.

- We have defined a new projection operator that constraints the transmission coefficient to values that must be selected from a set of available transmission coefficients. This allows what we have referred to as an "opportunistic synthesis". Transmission coefficient constraints of any kind can be effectively imposed by simply removing from the database transmission coefficient values that are not allowed.

- The development of an effective method to find sets of starting values of the transmission coefficients that will allow the projection synthesis algorithm to progress as it begins iterating. The method can be applied to any shaped beam pattern for which an ideal pattern shape is properly defined. Good starting values are crucial for the success of projection synthesis methods.

- We have also proposed and used what we have called the "trap navigation approach" to prevent the projection synthesis algorithm from stagnating at a trap.

There remain some issues whose investigation in the future would prove useful:

- Recently[65] a type of reflectarray antenna element has been devised where elements are selected not only for their correct reflection coefficient phases but also their geometrical similarity. If it were possible to use a similar approach to set up a database of printed lens elements (transmitarray elements), where more than one geometrical shape is available to give the same complex transmission coefficient value, then a projection synthesis method could be formulated to simultaneously synthesize the required shaped beam pattern and select elements so that each is surrounded by elements similar to it. We suspect that parallel form of the projection algorithm would be applicable.

- Another obvious suggestion for future work is to extend the synthesis procedure to apply to lens antennas which are not cylindrical (with a shaped beam in one pattern plane) but fully three-dimensional. This would require the forward operator to be derived for planar arrays of cells; this would be a relatively straightforward now that the form is know for

[65] J.Ethier, et al., "Reflectarray Design Using Similarity-Shaped Fragmented Sub-Wavelength Elements", *Electronics Letters*, Vol.48, No.15, pp.900-902, July 2012.

the cylindrical lens case from the present work. New starting value estimation details would be needed, but the method devised here can be so generalized.

- We have used the weight vector (in the reverse operator) in a simple fashion, namely by setting it equal to a higher value in the shaped beam region than the sidelobe region if necessary. It might be preferable to use it in an adaptive way, as follows : At the end of each iteration of the projection method search for only those sample angles where the pattern violates the shaped beam mask. During the next iteration set the weights corresponding to only these angles to values larger than unity.

- More general feed models could be incorporated that allow an offset feed to be used. The feed could then possibly be used to "help" the lens in providing a phase tilt when asymmetrical patterns such as the cosecant case, are desired, and perhaps achieve a pattern performance (when transmission coefficient amplitude and phase constraints are imposed) that are closer to that when no such constraints are imposed.

- In order to avoid large discontinuities in the printed lens conductor patterns we would want to constrain the smoothness of the amplitude and phase distributions. Projection operators should be sought to enforce such smoothness conditions within the projection synthesis framework. We suspect that this might be possible using a parallel version of the algorithm.

- A projection operator that could be used to minimise the tolerance sensitivity of a resulting synthesized excitation set would be useful to arrive at printed lens antennas for which a varying feed field incidence angle from element to element matters less as far as the element transmission coefficient value is concerned.